Spring 2010

# Investigation of local deformation of the median nerve in magnetic resonance images of the carpal tunnel

Nicole Marie Kunze
*University of Iowa*

# INVESTIGATION OF LOCAL DEFORMATION OF THE MEDIAN NERVE IN MAGNETIC RESONANCE IMAGES OF THE CARPAL TUNNEL

by

Nicole Marie Kunze

A thesis submitted in partial fulfillment
of the requirements for the Master of
Science degree in Biomedical Engineering
in the Graduate College of
The University of Iowa

May 2010

Thesis Supervisors: Assistant Research Engineer Jessica Goetz
Professor Thomas D. Brown

Graduate College
The University of Iowa
Iowa City, Iowa

CERTIFICATE OF APPROVAL

_____

MASTER'S THESIS

_____

This is to certify that the Master's thesis of

Nicole Marie Kunze

has been approved by the Examining Committee
for the thesis requirement for the Master of Science
degree in Biomedical Engineering at the May 2010 graduation.

Thesis Committee: _____
Jessica Goetz, Thesis Supervisor

_____
Thomas Brown, Thesis Supervisor

_____
Joseph Reinhardt

_____
Edwin Dove

_____
Daniel Thedens

_____
Ericka Lawler

ACKNOWLEDGMENTS

I would like to thank my advisors, Drs. Jessica Goetz and Thomas Brown for their invaluable guidance and assistance throughout the entirety of this project, as well as for providing me with an interesting topic for study. I am also grateful to Drs. Daniel Thedens and Ericka Lawler for their expertise along the way. Thanks also to my officemates and co-workers for their help and support. Finally, I would like to thank my family and friends – I would not have been able to make it through without their support and encouragement. Financial support was provided by NIH grant AR053899.

TABLE OF CONTENTS

LIST OF TABLES

LIST OF FIGURES

# CHAPTER I: INTRODUCTION

## 1.1 Carpal Tunnel Anatomy

The carpal tunnel (Figure 1) is a semi-rigid tunnel located at the base of the hand. It is bounded on the dorsal, radial, and ulnar sides by the carpal bones, and on the volar side by the transverse carpal ligament. This ligament extends from the tuberosities of the trapezium and scaphoid on the radial side, to the hook of the hamate and pisiform on the ulnar side.[1] Externally, the volar wrist crease approximates the proximal border of the transverse carpal ligament.[2] The deep and superficial flexor tendons of the fingers, the flexor pollicis longus (FPL) tendon of the thumb, and the median nerve course through the confines of the carpal tunnel and then diverge to the fingers.[3] The median nerve innervates the thumb, index, and long fingers as well as the radial side of the ring finger. The superficial tendons flex the proximal interphalangeal joint of each finger, and the deep tendons flex the distal interphalangeal joint.[4]

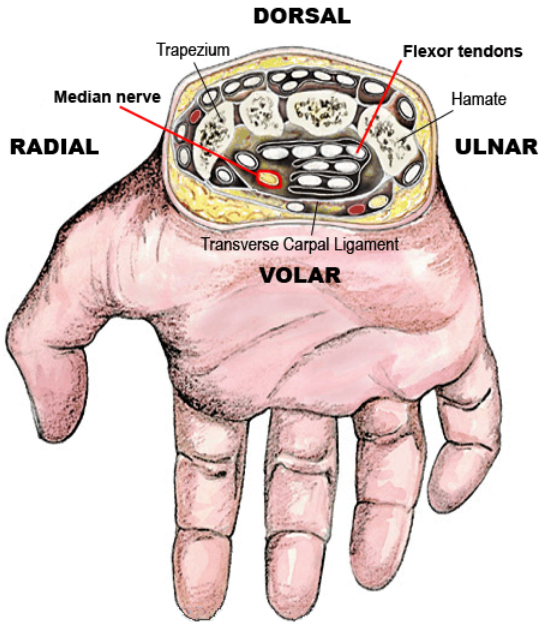


Figure 1. Anatomy of the carpal tunnel[5]

## 1.2 Overview of Carpal Tunnel Syndrome

Carpal tunnel syndrome (CTS) is the most common of a family of disorders described as peripheral compression neuropathies. Such disorders occur because some peripheral nerves are at higher risk of being compressed as a result of certain risk factors including superficial anatomic location, coursing through an area at higher risk of insult, or coursing along a narrow pathway through a bony canal.[6] Due to the anatomic position of the median nerve as it courses through the narrow carpal tunnel, it is at higher risk of insult than many other peripheral nerves. CTS has an estimated incidence of 1-3 cases per 1000 subjects per year in the United States[7] and an approximate prevalence of 50 cases per 1000 subjects in the general population.[8]

Symptoms include pain, numbness, muscle weakness, and paresthesia (tingling) through the region innervated by the median nerve.[6, 9] Generally, symptoms in less severe cases are intermittent and often seem to intensify at night, which may be due to flexion of the wrist during sleeping. However, symptoms in severe cases are unrelenting, and thenar (thumb) functional muscle loss occurs.[10] Certain occupational groups have been identified as having an increased risk of CTS, including farmers, construction workers, factory workers, drivers, typists, cashiers, and hairdressers.[11] Keogh *et al.* identified worker's compensation claimants in Maryland to examine the impact of CTS on the injured worker and their family. They reported that for the majority of claimants in their study, the impact of CTS symptoms were felt more at home than at work, and primarily involved difficulty with activities involving strength, such as pushing open a window or pushing up from an armchair, and activities involving grip strength, such as writing with a pen or pouring from a container to a glass.[12]

The full economic cost of CTS extends far beyond the direct medical costs, with financial losses being borne by patients and their families as well as

by employers. The workers and their families must cope with inability to perform social activities and activities of daily living due to pain, clinical depression, and most significantly the long-term loss of earnings. Employers must deal with indirect costs of production interruption, accident investigation, and the recruiting and training of a new worker to replace the impaired worker.[13] The full lifetime cost per injured worker, including medical bills and lost work time, averages approximately $30,000.[14] In 1995, the economic cost of CTS per year in the United States was estimated to exceed $2 billion.[4] According to the US Bureau of Labor Statistics, there were 11,950 formally reported cases of CTS involving lost work days in 2008 among government workers.[15] The study by Keogh *et al.* found that the number of lost work days was 5 times greater for employees with CTS than the average for all other illnesses and injuries.[12]

## 1.3 Diagnosis of Carpal Tunnel Syndrome

Diagnosis of CTS has increased sixfold since the 1980s.[16] Recently the American Academy of Orthopaedic Surgeons (AAOS)[17] released guidelines for diagnosing CTS. These guidelines state that a diagnosis should be made based on the history of the present illness, physical examination, and electrodiagnostic tests. History of present illness, such as the duration and severity of the symptoms, the location of pain/numbness, the rate of progression of the illness, any previous treatment, and the lifestyle of the patient may help in diagnosing CTS by ruling out other illnesses which can exhibit similar symptoms. Knowing when the symptoms occur (night-time or day-time), what ameliorates the symptoms (shaking the hand or putting it under warm water), and what exacerbates the symptoms (driving, vibrating tools, or holding a phone) can lead to a CTS diagnosis. As a part of the patient history, it is also useful to know if

any non-surgical treatments have been attempted, and their resulting impact on the CTS symptoms.

Physical examination may include personal characteristics (height, weight, etc.), range of motion of the hand, observations of the affected region (deformity, swelling, atrophy, etc.), pinch/grip strength, hand symptom diagram, sensory examination (two-point discrimination, vibrometry, texture discrimination, etc.), manual muscle testing (examination for muscle atrophy), provocative tests (Phalen's test, Tinel's sign, etc., see below), and discriminatory examination for alternative diagnoses (arthritis, tendonitis, etc.).[17] The results of these various physical examinations can help diagnose CTS. Hypalgesia (diminished sensitivity to pain) and classic or probable CTS symptoms as characterized in a Katz hand diagram are findings from physical examination indicative of CTS. The two provocative physical examinations most commonly used when a patient presents with symptoms associated with CTS are Tinel sign and Phalen maneuver.[6] The Tinel sign is elicited by tapping over the median nerve in the distal forearm and the Phalen sign is elicited by holding the wrist in a flexed position. These two tests indicate CTS if they produce dysesthesias (an abnormal sensation such as pain, burning, or tingling resulting from a normal stimulus). However, these two tests are only moderately sensitive and specific to the presence of CTS.[6, 10]

CTS cannot be diagnosed solely on the basis of physical examination; however in combination with symptoms and physical examination, electrodiagnostic tests can confirm a suspected CTS diagnosis. Electrodiagnostic tests are useful in differentiating between multiple diagnoses. Electrophysiologic studies have been the primary form of diagnostics used to confirm a suspected CTS diagnosis. These studies can be separated into two categories: electromyography (EMG) and nerve conduction studies (NCSs).

EMG measures muscle activity in response to stimulation using needle electrodes inserted into muscles. However, EMG has been found to be insensitive and non-specific for diagnosing CTS.[10] NCSs assess the functional integrity of nerves by measuring the velocity of conduction along a nerve using surface electrodes, and NCSs are more often used to diagnose CTS than is EMG. Generally, NCS results from the median nerve are compared to those from other nerves in the hand, which act as an internal control. Most often the ulnar nerve is used for comparison because it does not cross the carpal tunnel: any measured nerve potential slowing due to CTS will cause conduction delay of the median nerve and not the ulnar nerve.[10] NCSs have been shown to confirm CTS with a sensitivity of 85% and a specificity of 95%.[6]

While NCS has been shown to aid in confirming a CTS diagnosis, one study found that 25% of patients studied had normal NCS but clinically diagnosed CTS.[18] That study noted that patients with abnormal NCS were older and had a higher BMI than those with normal NCS. It was also observed that patients with a definite CTS diagnosis were more likely to have abnormal NCS. Imaging is a method which may help diagnose CTS when NCSs are inconclusive. Some authors have suggested using MRI as a tool for diagnosing CTS, since MRI may be able to distinguish between CTS and other wrist diseases which present similar symptoms.[19] However, the AAOS guidelines suggest not using MRI to routinely evaluate patients suspected of having CTS.[17] This recommendation was made on the basis of the changing appearance of the median nerve in MR images. Another study has shown that pressure-specified sensory (PSS) testing can be used in addition to NCS to diagnose CTS, and that PSS is especially useful when NCS appear normal. PSS assesses nerve function by quantifying the thresholds of pressure detected with static and moving touch, using probes and transducers to measure and record the

perceived pressure threshold.[20] Because there has not been sufficient evidence to support the use of PSS testing, AAOS also suggests not using it routinely to evaluate for CTS.[17]

## 1.4 Treatment of Carpal Tunnel Syndrome

AAOS has also recently released guidelines for the treatment of CTS. These guidelines recommend non-operative treatment as an option when a CTS diagnosis is made, unless there is evidence of median nerve denervation (loss of nerve electrical activity), or unless the patient elects to proceed directly to surgical treatment. In the guidelines, local steroid injection or splinting are specifically suggested prior to considering surgery. AAOS guidelines do not endorse heat therapy, as it has been seen to be less effective than placebo.[21] Short-term symptom relief has been seen during treatments with local and oral corticosteroids, ultrasound, yoga, carpal bone mobilization, and splinting in a slightly extended position at night and as tolerated during the day. Ergonomic keyboards, vitamins, diuretics, and anti-inflammatory drugs have been shown to generally not have any benefits.[6] The guidelines suggest that if a current treatment method fails to resolve symptoms within 2-7 weeks, another non-operative treatment should be considered, or the patient should proceed to surgical treatment.[21]

Carpal tunnel release by complete division of the transverse carpal ligament is the recommended surgical treatment for CTS, with the suggestion that the wrist should not be immobilized postoperatively.[21] Surgical treatment is often reserved for more severe cases, when other treatment methods have been ineffective. Surgery has proven to improve symptoms more than a well-defined non-surgical treatment plan.[22] Both open and endoscopic carpal tunnel release are widely used surgical treatments of CTS. Open carpal tunnel release is

performed by making an incision, typically 2 cm - 4 cm, beginning at the wrist crease and extending distally, such that the width of the carpal tunnel ligament is fully visible. The incision size is on the smaller side of the 2 cm - 4 cm range for "limited open" carpal tunnel release and on the larger side (or even larger than 4 cm) for extended carpal tunnel release. Endoscopic release is performed through one[23] or two[24] smaller (1 cm) incisions, and the transverse carpal ligament is divided from within the carpal tunnel, leaving the overlying skin and palmar aponeurosis (a sheet-like fibrous membrane beneath the skin in the palm) intact.[25] The first incision is made in the wrist crease, and the second incision (if one is used) is made in the palm.[26] The reported advantages of endoscopic release are less time away from work and less immediate post-operative pain.[27] However, endoscopic release has also been associated with higher incidence of complications such as lacerations of the median nerve and higher cost due to the need for special equipment and non-reusable instruments.[28, 29] Generally no statistical advantages of endoscopic over open release have been found in terms of amount of post-operative pain. Only slight differences have been found between time needed to return to work, which may be out-weighed by the increased cost.[28-30]

Complications have been reported for both open and endoscopic carpal tunnel release. Complete or partial nerve, tendon, and vessel lacerations can occur with either method of release. In addition to the median nerve, there have been reports of ulnar nerve and digital nerve lacerations. Incidences of superficial arch, ulnar artery, and radial artery lacerations have also been reported. Tendon laceration does occur, however, it appears to be the least common of these complications.[31] While complications do occur during carpal tunnel release, both open and endoscopic release have been reported to have

success rates between 90% and 95%, as indicated from patient questionnaires.[32-34]

## 1.5 Rationale for the Current Study

The development of CTS is often associated with workplace risk factors involving forceful or repetitive movements of the wrist, and exposure to vibration of the hands and arms. Additionally, it is also associated with non-occupational factors including female gender and certain medical conditions such as hypothyroidism, diabetes, rheumatoid arthritis, pregnancy, and obesity.[10, 35]

However, little is known about the actual mechanism of direct mechanical insult to the median nerve, which leads to the development of CTS. One theory, which CTS is often attributed to, is increased pressure within the tunnel due to a disproportion between the carpal tunnel contents and the available space.[36] Gelberman *et al.* were the first to quantify the pressure within the tunnel in patients diagnosed with CTS using catheters.[37] The results were compared to those obtained from normal subjects. In both groups, the pressure in flexed and extended wrist positions was increased from the pressure in the neutral wrist position. In all wrist positions, the pressure in the CTS group was elevated from the normal group.

While fluid pressure within the tunnel may play a role in eliciting CTS symptoms, others believe the primary mechanism of insult is direct impingement by the adjacent tendons and tunnel boundary. Flexion of the wrist and fingers has been observed to cause rearrangement of the tendons, forcing the nerve to become interposed between tendons. This rearrangement results in potential compression of the median nerve.[38] Using image-based carpal tunnel finite element models, Ko and Brown demonstrated that the stresses in the median nerve resulting from direct contact of neighboring structures were higher than the

stresses resulting from the fluid pressure surrounding the nerve.[39] It is plausible that multiple factors contribute to CTS, however, these results suggest that direct contact with other structures within the tunnel may be a major contributor of mechanical insult to the median nerve. The appearance, size, and shape of the median nerve in symptomatic and non-symptomatic patients may provide insight into median nerve insult.

# CHAPTER II. LITERATURE REVIEW

## 2.1 MRI of the Carpal Tunnel

MRI is often used to study the wrist and to diagnose wrist diseases because various pertinent tissues (bone, ligaments, nerves, tendons, cartilage, etc.) can all be visualized. For example, irregular cartilage loss resulting from osteoarthritis is apparent on MRI based on joint space narrowing and cartilage defects. It has also been reported that MRI is more sensitive than radiography in detecting bone erosion after the administration of a contrast agent.[40] Ligament tears can be seen on MRI since they are often associated with fluid traversing the region normally occupied by the disrupted ligament.[41]

Because of its excellent resolution of soft tissues, MRI has often been used in studying the anatomy of the carpal tunnel to assess possible abnormalities associated with CTS. The axial plane has been shown to be the best imaging plane for visualizing the contents of the carpal tunnel.[42] In T1-weighted images, both the transverse carpal ligament and the flexor tendons have low MR signal intensity, and thus appear black (Figure 2). The individual tendon boundaries are accentuated by the higher signal intensity of the surrounding tendon sheaths.[43] The median nerve typically appears as an intermediate signal intensity structure with a stippled texture.[44]

It has been suggested to use MRI prior to carpal tunnel release to determine whether bifurcation or trifurcation of the nerve exists within the tunnel, which would help the surgeons avoid lacerating the nerve during surgery.[45, 46] The median artery, which may also be present in the carpal tunnel, is the main source of blood supply to the forearm and hand in the embryo, but it is normally replaced by the radial and ulnar arteries and diminishes during development. However, in many individuals the median artery may persist as a sizeable vessel

for the entirety of life. Therefore, it has also been suggested to use MRI prior to carpal tunnel release to determine if this vessel is present within the tunnel.[45]

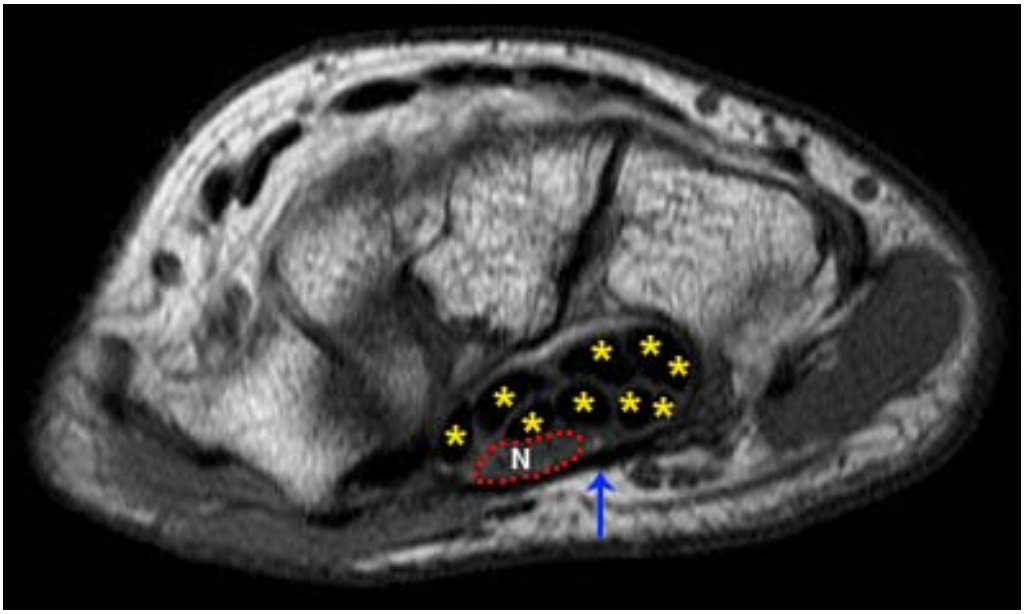


Figure 2. T1-weighted MR image through the carpal tunnel.[47] Dark tendons are indicated with yellow asterisks, the textured nerve (N) is outlined in a red dotted line, and the dark transverse carpal ligament is indicated by the blue arrow.

A challenge associated with MRI of regularly structured tissues, specifically tendons within the context of the carpal tunnel, is variation in signal intensity associated with the "magic-angle" effect. This image artifact occurs when the well-ordered collagen fibers of the tendons approach an angle of 55° relative to the orientation of the main magnetic field. The effect causes the signal intensity of the tendons to increase to a degree similar to that of the tissue surrounding the tendons, and in the most severe cases, the tendons appear indistinguishable from the surrounding tissue (Figure 3). When less pronounced, a slight increase in tendon signal can misleadingly indicate disease pathology.[48, 49]

Longitudinally oriented collagen fibers are also present within the nerve, which has also been observed to be affected by the magic angle effect when its fibers approach 55°. This increase in nerve signal intensity could erroneously be diagnosed as CTS.[50] Nerve signal intensity has also been shown to be increased or decreased from normal depending on the severity of the symptoms, which may cause additional confusion.[51-53] This should be kept in mind as a potential confounding factor when imaging a wrist with severe CTS symptoms. Therefore, care must be taken to place the wrist in an orientation in the MR scanner where the longitudinal fibers of the tendons and nerve are not oriented near 55° to the magnetic field.

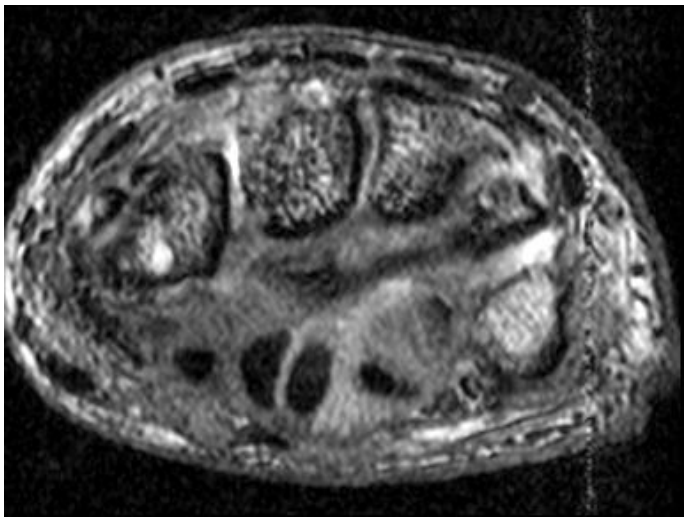

Figure 3. An axial MR image affected by the magic-angle effect. The signal intensity of the tendons on the right side of the carpal tunnel has increased to a similar intensity as that of the surrounding tissue.

## 2.2 Median Nerve Location within the Carpal Tunnel

Compared to other tissues in the carpal tunnel, the MRI visibility of the nerve is reduced. It is useful to know where the nerve is typically located in the carpal tunnel during various wrist positions. One study determined the location

of the nerve relative to specific tendons and the carpal tunnel boundary for 14 wrists of 7 normal volunteers.[38] The arrangements of the specific structures within the carpal tunnel were only observed at 6 mm intervals due to the difficulty of identifying specific tendons within the carpal tunnel. In this study, two nerve positions were observed in the neutral wrist. In the first position, long considered to be the 'standard' position, the median nerve was volar to the superficial index tendon. In the second position, a first variant of the standard position, the median nerve was interposed between the superficial index and thumb tendons. In the extended wrist, the nerve was observed in the standard position. While in flexion, the tendons shift volarly towards the transverse carpal ligament, and the nerve was observed in one of three positions (Figure 4): remaining in the volar position between the superficial index tendon and the transverse carpal ligament (the standard position), the first variant position, or a second variant position (interposed between the superficial tendons of the long and ring fingers).[38, 54, 55]

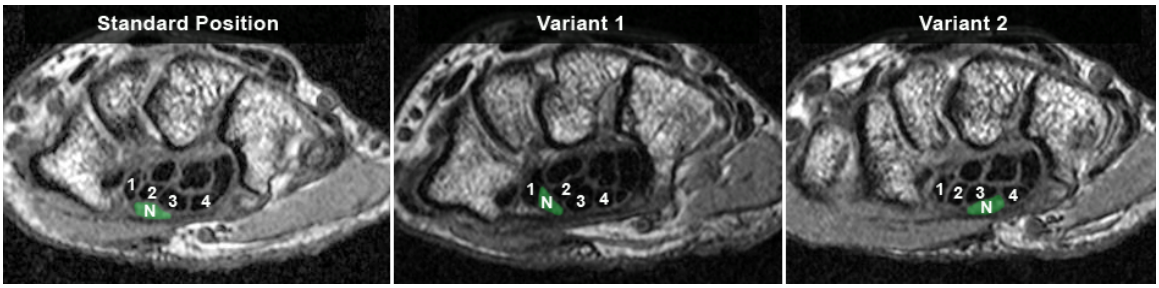


Figure 4. Three common median nerve positions: standard (left), variant 1 (middle), and variant 2 (right). The nerve (N) is highlighted in green, tendon 1 is the FPL of the thumb, and 2, 3, 4 are the superficial tendons of the index, long, and ring fingers, respectively.

The shifting of the tendons within the transverse plane through the tunnel as the wrist changes positions affects the amount of free space around the nerve, with that space being greatest during wrist extension and smallest during

wrist flexion. Additionally, flexing the fingers causes more of a volar shift of the tendons and thus further decreases the space available for the nerve. As the nerve shifts to a position interposed between tendons, it is probable that mechanical insult would occur during its extrusion between the loaded tendons.[38] Therefore, MRI can be useful for visualizing the position and movement of the nerve.

## 2.3 Quantifying Size and Shape

In addition to visualizing the location of the nerve, MRI is useful for studying the size and shape of the nerve and how these characteristics vary in normal subjects versus symptomatic patients. Numerous CTS studies have used MRI to quantify the size and shape of various structures within the carpal tunnel to identify pathological changes associated with CTS.[41, 56-62] Many studies have reported an enlargement and flattening of the median nerve, bowing of the transverse carpal ligament, and increased signal intensity of the median nerve in CTS.

### 2.3.1 Median Nerve Size

From an early study using a lower strength (1.5 Tesla) MRI scanner, the cross-sectional area, computed as the area of an ellipse fit of the median nerve, in a normal carpal tunnel was found to be 7 $mm^2$ at the level of the pisiform and 8 $mm^2$ at the level of the hook of the hamate.[56] However, another study, conducted using a higher strength (3.0 Tesla) MRI scanner, found the average cross-sectional area, calculated as the area within a traced boundary, of the median nerve in normal subjects to be 10 $mm^2$ at the pisiform and 11 $mm^2$ at the hook of the hamate.[59] More recently, a study of normal carpal tunnels by Yao and Gai found the average cross-sectional area of the median nerve, also calculated as

the area within a traced boundary, to be 10 $mm^2$ at the pisiform and 9 $mm^2$ at the hook of the hamate.[60]

In comparison to a normal carpal tunnel, patients with CTS appear to have enlarged median nerves.[41, 58, 62] Monagle *et al.* found that the cross-sectional area of the nerve in symptomatic patients was 50% larger than that of the normal subjects.[59] By quantifying these changes in cross-sectional area inside the carpal tunnel and correlating the findings with nerve conduction tests, one study demonstrated that the severity of CTS does have an effect on cross sectional area of the nerve, with the area increasing with increasing CTS severity.[61]

### 2.3.2 Median Nerve Flattening

The most frequently applied metric to evaluate median nerve shape in MR images is a nerve flattening ratio. Nerve flattening ratio is computed as the major axis length divided by the minor axis length of an ellipse fit to the nerve boundary, where a value of 1 indicates a perfectly circular shape. The nerve in normal carpal tunnels appears only slightly flattened, with ratios of 3.3 at the pisiform and 2.9 at the hook of the hamate.[57] Several studies have found that patients with CTS typically have significantly flatter median nerves at the hook of the hamate than normal carpal tunnels, with ratios of 3.4 at the pisiform and 3.8 at the hook of the hamate.[41, 58, 62] However, another study found that there was no significant difference between the nerve flattening ratio of normal and CTS patient groups.[59] This discrepancy may be due to the patients selected. The study by Monagle *et al.* compared only normal and CTS females, whereas prior studies included both females and males. Still another study has suggested that changes in the nerve profile, such as the flattening ratio, may be less reliable than total cross-sectional area, given that the nerve is frequently of a non-ovoid morphology.[60] Therefore, while the nerve flattening ratio may be an indication of

the overall shape of the nerve, it fails to fully describe the shape since two nerves may have completely different shapes visually (for example an ellipse and a crescent), but have very similar flattening ratios.

### 2.3.3 Transverse Carpal Ligament Bowing

Bowing is computed as the ratio of the maximum volar displacement of the transverse carpal ligament divided by the unbowed length (distance between its attachments). Normal carpal tunnels show only slight bowing of the transverse carpal ligament, with an average bowing of 6% of the unbowed length.[57, 63] In comparison, patients with CTS have more pronounced transverse carpal ligament bowing, especially at the level of the hook of the hamate, with an average of 18% of the unbowed length.[41, 58, 59, 62] This difference is statistically significant. Bowing may be best visualized at the hamate level because this is the region where the transverse carpal ligament is the thickest and most easily visualized.[63] It has also been demonstrated that the severity of CTS, defined in terms of NCSs, has an effect on the bowing of the transverse carpal ligament. Specifically, severe CTS has been associated with increased bowing.[61]

### 2.3.4 Median Nerve Signal Intensity

While many studies use visual inspection of MR images to determine when the nerve has increased signal intensity, some have quantified this increase using gray values. One method uses the percent difference between the signal intensity of the nerve and the signal intensity of the background.[58] With this type of method, many patients with CTS appear to have increased signal intensity of the median nerve on T2-weighted images, where the nerve generally appears as having intermediate signal intensity, similar to normal muscle.[41, 62] This increased signal intensity has been observed to decrease postoperatively.[58] Caution should be taken when making observations of the

signal intensity of the nerve, however, since this intensity can vary with the orientation of the fibers to the direction of the magnetic field (the magic-angle effect).

### 2.3.5 Carpal Tunnel Volume

Carpal tunnel volume has been used as an indirect way to determine how the pressure within the carpal tunnel may vary with wrist position, since increased pressure on the nerve could lead to injury. Increased hydrostatic pressure has been shown to occur in wrist positions deviated from neutral.[64] It has been observed that the bony landmarks used to define the ends of the tunnel can affect the calculated tunnel volume.[65] When landmarks defining the proximal and distal ends of the tunnel are chosen from medical images, it is inherently assumed that the ends of the tunnel are parallel and that the radial and ulnar lengths of the tunnel are equal. However, it has been shown that when only ulnar bony landmarks (proximal pisiform and distal hamate) are used to identify the proximal and distal ends of the tunnel, the resulting volume is overestimated. When radial and ulnar bony landmarks are used (proximal pisiform and scaphoid tubercle to distal hook of the hamate and ridge of the trapezium) the volume is underestimated. This overestimation and underestimation resulting from defining carpal tunnel ends from medical images is likely due to reported proximal-distal asymmetry.[66] The radial and ulnar lengths of the tunnel are not equal, and the tunnel end orientation varies with posture.[67]

Volumes thus defined have been compared to the volume found from a 3D model of the carpal tunnel that was reconstructed using modeled bone surfaces.[65] The transverse carpal ligament attachment sites were used to define the ends of the tunnel. These sites were essentially the same as the radial and ulnar landmarks used in other studies. However, they were defined anatomically

from the modeled bone surfaces; the carpal tunnel ends were not constrained to be parallel, nor were the two sides constrained to being equal length. Interpretations of the relationship between posture and carpal tunnel volume, and how volume relates to pressure on the median nerve, may be incorrect if the carpal tunnel volume is inaccurately estimated.

### 2.3.6 Carpal Tunnel Contents Ratio

Mechanical injury to the median nerve may arise due to increased crowding within the carpal tunnel. This would occur if the tendons enlarge or if the carpal tunnel boundary itself is small. A measure which has been used to study this issue is the carpal tunnel contents ratio, which is defined as the ratio of the nerve and tendon areas to carpal tunnel area. The remainder of the tunnel space is comprised of connective tissue and fluid and is not included in the ratio. A larger ratio would indicate either enlarged tunnel contents or a smaller tunnel, and thus there would be less space for the median nerve, which could lead to a higher propensity for insult.[68] The contents ratio has been found to be approximately 45% - 60% through the narrowest part of the tunnel.[19, 69] Because a small carpal tunnel could increase the risk of injury to the median nerve, the cross-sectional area of the tunnel is also of interest. The carpal tunnel is about 20% of the cross-sectional area of the wrist, approximately 185 $mm^2$.[2] The area is similar at both ends of the tunnel in neutral and extended wrists. In flexion, however, the area is smaller at the distal end than at the proximal end.[70, 71]

## 2.4 Correcting for Wrist Orientation

Some of the variation in the previously described measures may be attributable to these measures being evaluated on images taken with the hand in a variety of orientations within the scanner. It has previously been demonstrated that the potential error of imaging the carpal tunnel in non-neutral postures must

be corrected for[70] to ensure that the above-described measures are obtained from cross-sections which are perpendicular to the carpal tunnel.[72] Changing the orientation of the scanning plane through which images are acquired for different wrist positions may result in errors, since the finger flexor tendons appear to traverse the carpal tunnel at smaller flexion and extension angles than the overall wrist angle.[73] One study evaluated the effect of changing the orientation of the MR image acquisition plane on carpal tunnel cross-sectional area. Those results indicated that slices taken both perpendicular to the axial orientation of the scanner, and perpendicular to the external wrist (measured using the radius and third metacarpal), overestimated the cross-sectional area of the tunnel in all of the wrist positions analyzed (30° flexion, neutral, and 30° extension). The cross-sectional area from the slice oriented perpendicular to the external wrist was only 1.8% larger than the area from the slice oriented perpendicular to the tunnel in extension, but it was 24.3% larger in flexion. The cross-sectional area from the slice perpendicular to the axial orientation of the scanner was 9.1% larger than the cross-sectional area perpendicular to the tunnel in extension and 0.6% larger in flexion.[67] To account for these differences, measures should be made on cross-sections which are perpendicular to the carpal tunnel.

## 2.5 Initial Attempt at Tracking the Tendons

Because CTS is a nerve entrapment disorder, MRI studies of the carpal tunnel have understandably focused primarily on characterizing abnormalities of the median nerve. Few attempts have been made to characterize any abnormalities in the digital flexor tendons, despite the fact that the tendons may be responsible for direct mechanical insult to the median nerve. Only one study has been conducted to track the digital flexor tendons through the carpal tunnel by connecting tendon centroids through an MR image series.[73] In that work,

three participants were scanned with the wrist splinted in four positions (straight, 20° extension, 20° flexion, and 45° flexion) under both loaded (three finger pinch) and unloaded conditions. Images were acquired at 4 mm intervals from approximately 20 mm proximal to the distal wrist crease to 20 mm distal to the hook of the hamate, resulting in about 20-25 axial images. The tendon centroids were manually digitized and transformed into an anatomic reference system, thus defining three dimensional trajectories of each tendon. These data were then used to determine the radii of curvature of the tendon paths around the wrist joint, rather than to determine any potential interaction of those tendons with the median nerve.[68]

The difficulty in identifying which tendon is which within the carpal tunnel has hindered studying specific tendon-nerve interactions. Therefore, creating a method which automatically identifies each tendon within the carpal tunnel holds appeal, since this would facilitate further investigation of specific tendon interactions with the nerve that may lead to the development of CTS.

# CHAPTER III. IMAGE PROCESSING METHODS

Image analysis algorithms were developed to create models of the carpal tunnel contents of both normal and symptomatic CTS subjects, from which specific nerve interactions could be analyzed. Three-dimensional MR images of the wrists of 12 subjects (8 male, 4 female) were acquired. Seven of the subjects had clinically-diagnosed CTS, whereas the other five subjects had no history of wrist pain and were considered to have normal wrists (Table 1). For the CTS patients, the symptomatic hand, which in all but one case coincided with the dominant hand, was chosen for scanning. The non-dominant hand of one CTS subject was scanned because the patient had already had carpal tunnel release surgery performed on the dominant hand. The dominant hand was scanned for all of the normal subjects.

Table 1. Subject demographics.

| Subject | Gender | Age | Height (m) | Weight (kg) | BMI (kg/m^2) | Motor Nerve Conduction Data Latency (ms) | Sensory Nerve Conduction Data Latency (ms) | CTS Severity |
|---|---|---|---|---|---|---|---|---|
| CTS - 1 | M | 35 | 1.85 | 82.40 | 24.08 | 4.1 | 3.3 | Mild |
| CTS - 2 | M | 67 | 1.93 | 89.80 | 24.10 | 6.0 | Not Reported | Severe |
| CTS - 3 | F | 64 | 1.61 | 82.80 | 31.94 | 5.4 | 5.2 | Moderate |
| CTS - 4 | M | 50 | 1.77 | 145.60 | 46.70 | 4.4 | 4.1 | Mild |
| CTS - 5 | M | 35 | 1.70 | 91.50 | 31.66 | 5.6 | 2.4 | Moderate |
| CTS - 6 | F | 46 | 1.66 | 56.16 | 20.29 | 5.5 | 3.7 | Severe |
| CTS - 7 | F | 49 | 1.68 | 94.17 | 33.51 | 10.4 | Not Reported | Severe |
| Norm - 1 | M | 60 | 1.88 | 98.88 | 28.01 | -- | -- | Normal |
| Norm - 2 | M | 29 | 1.73 | 95.30 | 31.95 | -- | -- | Normal |
| Norm - 3 | F | 24 | 1.70 | 70.30 | 24.27 | -- | -- | Normal |
| Norm - 4 | M | 43 | 1.75 | 64.00 | 20.90 | -- | -- | Normal |
| Norm - 5 | M | 62 | 1.80 | 73.48 | 22.68 | -- | -- | Normal |

CTS severity was assigned by each clinician who performed the NCS based on resulting NCS latencies and amplitudes using established guidelines.[74]

MRI scans were performed on a Siemens TIM Trio 3T (Siemens Medical, Malvern, PA, USA) scanner using a ninety-second Dual Echo Steady State (DESS) pulse sequence (TR/TE = 13.0/4.3 ms), with water excitation to suppress signal from fat tissue. The acquired resolution was 0.2 mm x 0.2 mm x 1.0 mm voxels over an 8 cm x 6 cm x 7.5 cm field of view. A transmit/receive lower extremity coil was used for imaging because it provided the clearance necessary to accommodate both flexed and straight wrist angles and the isometric loading devices which were required for imaging the hand while functionally loaded.

Subjects were scanned in the prone position, with the arm extended overhead and with the wrist splinted in the desired position (Figure 5). Eight different wrist position/loading activity combinations were studied for each subject. During four of the eight scans, the wrist was splinted in a neutral position (zero degrees of wrist flexion). Scans were acquired first with straight fingers and no load, second with a straight four-finger flat press, third with a curled finger power grip, and fourth with a curled finger index-thumb pinch. These same four loading activities were then repeated with the wrist splinted in 35 degrees of flexion.

These three specific loading activities were chosen because they have been observed to result in median nerve impingement by the flexor tendons. The isometric loading devices used for the activities were fabricated from non-ferromagnetic materials (brass, acrylic, nylon, and polypropylene) specifically for this study (Figure 6). This ensured the safety of the subjects during scanning and made certain that image quality would not be degraded due to metal artifact. A loud beeping noise was used as audible feedback to assure subjects that they were applying appropriate load during the scan. The beeper, powered by a 9-volt battery, was wired to the each device and remained outside of the scanner. The beep was constant if the applied load was appropriate, but the beep stopped

if not enough load was being applied. A total of 88 scan volumes from the 12 subjects were utilized for analysis.

Figure 5. A normal volunteer subject in the scanning position. Towels and foam were used to pack the subject's arm in the coil to reduce motion.

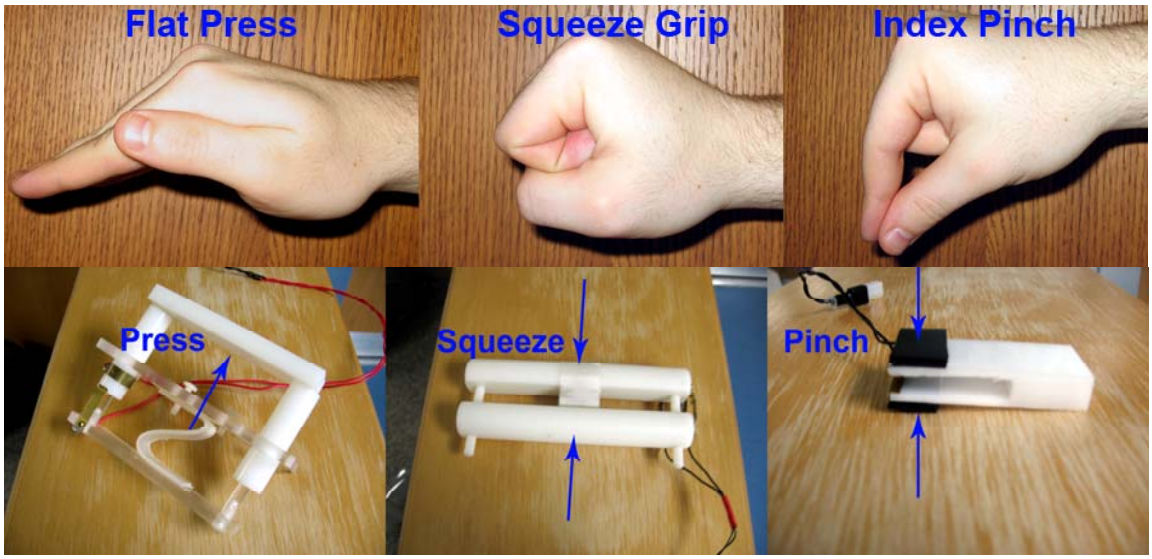


Figure 6. The three loading activities are shown in the top row and the devices used for the loading are shown in the bottom row: flat press (left), squeeze grip (middle), and pinch (right). The arrows on each device indicate the direction in which the load is applied by the fingers.

## 3.1 Carpal Tunnel Contents Segmentation

The carpal tunnel boundary (carpal bones and transverse carpal ligament), median nerve, tendons, and the sub-synovial connective tissue (SSCT) surrounding the tunnel contents are visible on axial MR sections through the wrist. Tendon boundaries were determined by finding and tracing the boundary where the greatest contrast appeared between the (dark) tendon and (lighter) SSCT. The median nerve appeared as a textured, fascicular region within the carpal tunnel. Thus, the median nerve boundary was determined by tracing between the light gray-textured region and the typical band of encircling low signal intensity attributable to the epineurium surrounding the nerve. The carpal tunnel boundary was determined by finding the (low-signal-intensity) transverse carpal ligament on the volar side of the tunnel, and the dark cortical shell of the carpal bones on the dorsal side of the tunnel (Figure 7).

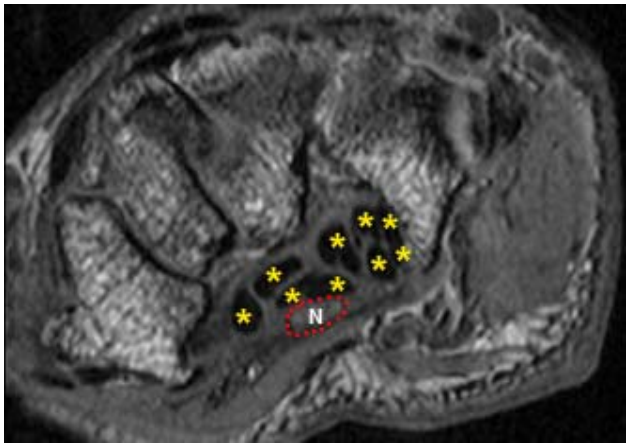


Figure 7. MR image through the carpal tunnel. Dark tendons are indicated with yellow asterisks and the nerve (N) is outlined by a red dotted line.

For each acquired scan, MR sections containing the proximal edge of the pisiform and the distal hook of the hamate were used to define the proximal and

distal ends of the carpal tunnel, respectively. A set of Matlab (The Mathworks, Natick, MA, USA) programs was developed specifically to segment the median nerve, the nine digital flexor tendons, and the carpal tunnel boundary on a set of axial MR images spanning the length (typically 25 to 30 mm) of the carpal tunnel. To better visualize the region of interest, the axial MR images were cropped to the carpal tunnel. Segmentation was initialized on the proximal-most image of the carpal tunnel, and then proceeded semi-automatically to the distal end of the carpal tunnel. Briefly, tendon boundaries on each 2D MR image spanning the carpal tunnel were automatically identified using active contouring. Segmentations resulting from active contouring were visually checked and manually edited (if needed) in each 2D MR image, prior to moving on to the next distal image.

### 3.1.1 Segmentation Initialization

To begin, the previously identified proximal-most carpal tunnel image was automatically presented to the user, allowing each tendon to be manually segmented by selecting points on the boundary of the tendon. The median nerve and tunnel boundary were also manually traced in the same manner as the tendons. The initial tendon segmentations were then available for use to automate tendon boundary segmentation on the subsequent distal image using active contours.

### 3.1.2 Active Contour Growing

Active contouring was used to automatically generate tendon boundaries. This method was chosen because edge detectors and threshold-based methods resulted in boundaries surrounding low signal intensity regions other than tendons, such as portions of cortical bone and the transverse carpal ligament. The goal of active contouring is to automatically grow a contour on an MR image

from an initial contour. For illustration purposes, a simple surrogate MR image was created with tendon and background regions (Figure 8) and active contouring is shown here using this surrogate MR image. A contour was grown on this surrogate MR image beginning from a simple triangular mask.

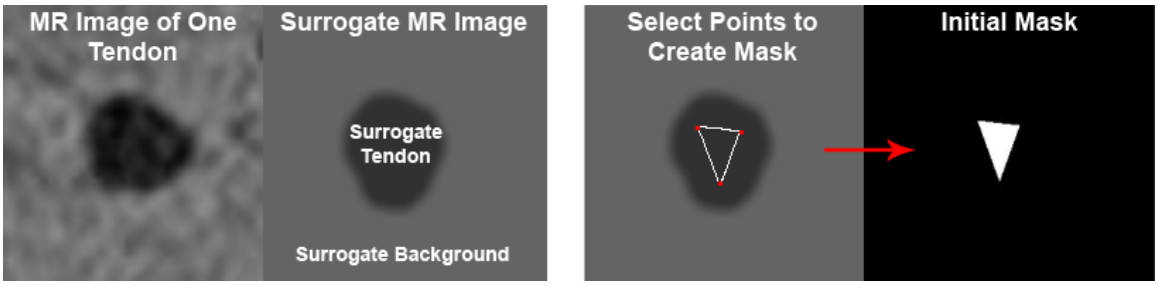


Figure 8. An MR image of a tendon (far left) and the surrogate MR image (middle left) from which a contour was grown. The initial mask (far right) was defined by connecting 3 user-selected points (middle right) on the tendon region of the surrogate MR image.

Active contouring used previous information about each tendon boundary to generate a new boundary on the next distal image, and therefore it did not result in boundaries surrounding structures other than tendons. Each tendon's segmentation was then used to help grow tendon boundaries on the next image, using the Chan-Vese active contour method.[75] This method of active contouring was used because it separates the image into regions based on grayscale intensities, but unlike many other active contour methods, the Chan-Vese method is not dependent on the gradient of the image (as is the case with edge functions) to terminate the contour growing.

Active contouring was done one tendon at a time within a 2D image, and all nine tendons were actively contoured on the working 2D image before moving on to process the next MR image. A tendon boundary on a given 2D MR image undergoing analysis was grown beginning from that tendon's segmentation on

the previously-analyzed next-proximal image. A working tendon's segmentation on the previously-analyzed next-proximal section was isolated from the other tendon regions and used to create a binary mask. Initially, the new growing contour was equal to the boundary of the binary mask (Figure 9). From this mask, a signed distance map was generated by assigning each pixel a number that was equal to the Euclidean distance between that pixel and the nearest boundary pixel in the mask (Figure 9). In the signed distance map, pixels lying on the boundary of the mask image were assigned a value of zero, those lying outside of the boundary were assigned a positive distance, and those within the boundary were assigned the negative of the distance.

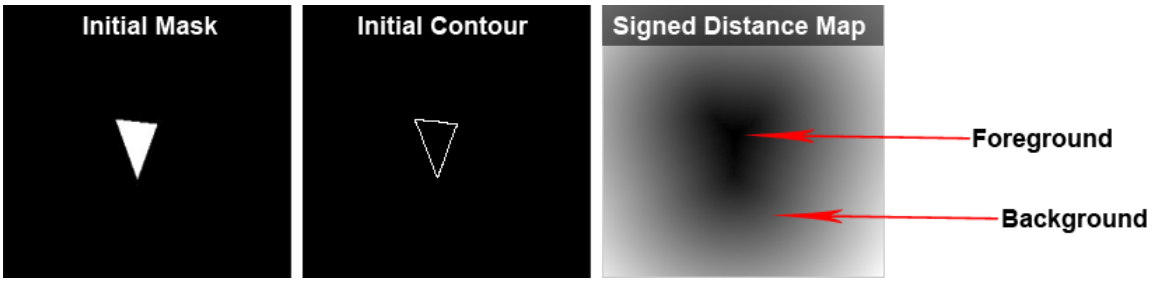


Figure 9. Simple binary mask (left), and its boundary (middle) and signed distance map (right) with the foreground and background regions indicated by arrows. Gray values in the signed distance map represent the distance of that pixel location from the boundary of the mask image. The boundary of the mask is the initial growing contour.

The first step in growing the contour was to define the foreground and the background regions within the signed distance map. These regions were defined by assigning any pixel with a distance value less than or equal to zero in the signed distance map to the foreground (inside the mask), and any pixel with a distance value greater than zero in the signed distance map to the background (outside the mask).

Means were computed from these two regions. The first ($mean_1$) was a mean of pixel gray values in the MR image corresponding to locations considered to be foreground in the signed distance map. The second ($mean_2$) was a mean of the pixel gray values in the MR image corresponding to locations considered to be background in the signed distance map. Using the MR image ($I$) and these two means ($mean_1$ and $mean_2$), a "force" from the MR image (*Image Force*) was computed as:

$$\textit{Image Force} = -(I - mean_1)^2 + (I - mean_2)^2$$

Image Force (Figure 10) is an image the same size as the MR image used to compute it.

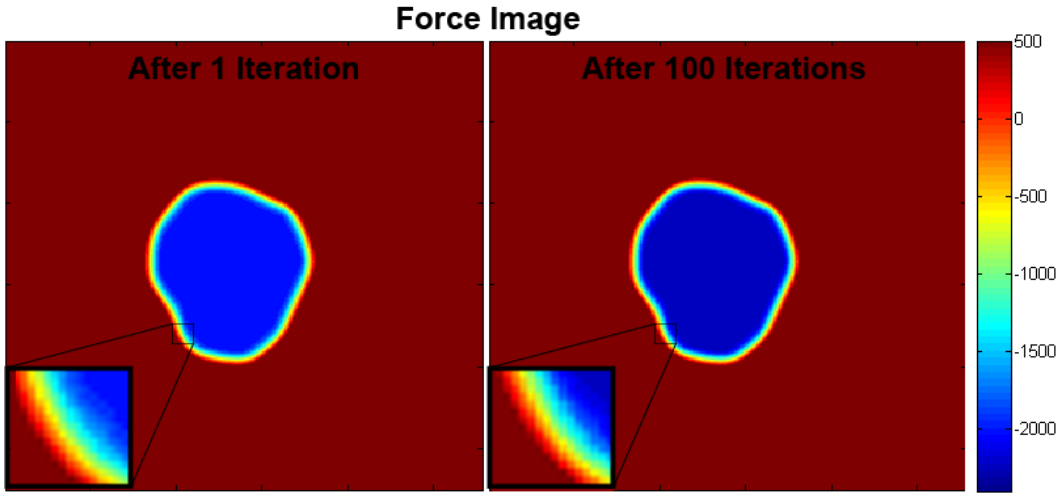


Figure 10. The Force Image shown in the first iteration (left) and after 100 iterations. The images have the same maximum pixel value (2500), but the Force Image after 100 iterations has a lower minimum pixel value. It is apparent in the insert images that with more iterations the gradient across the boundary increases.

This force can be considered a "fitting" term of the growing contour. The further the contour is inside the object (large negative force), the stronger it is being pushed out towards the object boundary (zero force). On the other hand,

the further the contour is outside of the object (large positive force), the stronger it is being pushed in towards the object boundary. It is therefore apparent that the force is minimized when the growing contour lies exactly on the boundary of the object, and this force drives the evolving contour to the object boundary.

Curvature information (*kappa*) of the signed distance map was found using finite differences of the pixels and their 8 neighbors. To find these finite differences, the signed distance map was first padded with ones on all sides, thus increasing each dimension of the image by two. This padded image (*P*) was then used to compute the finite difference images ($f_x$, $f_y$, $f_{xx}$, $f_{yy}$, and $f_{xy}$) of the signed distance map. These finite difference images were found by subtracting the padded image (*P*) from the padded image (*P*) shifted either up or left by 2 pixels, depending on the difference being computed. For example, $f_x$ was computed as *P_shifted_left* – *P*, and $f_y$ was computed in the same way but with the image shifted up. To find $f_{xx}$ and $f_{yy}$, the original signed distance map multiplied by two was subtracted from $f_x$ or $f_y$, respectively. Lastly, $f_{xy}$ was found by subtracting an image shifted in both directions (Figure 11).

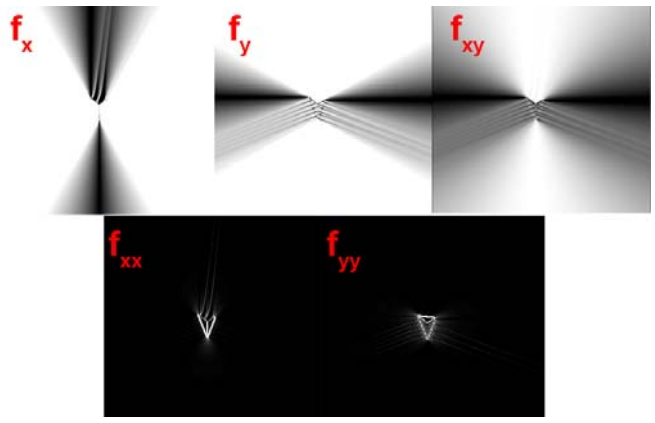


Figure 11. Finite differences of the signed distance map of the triangle mask. The absolute value of each finite difference is displayed so pixels of maximum change are all displayed as white. The original $f_x$ and $f_y$ values range from -200 to 200, $f_{xx}$ and $f_{yy}$ values range from -200 to 4, and $f_{xy}$ values ranges from -100 to 100.

These individual finite differences approximate partial derivatives of the signed distance map, where a large number indicates a large change resulting from the directional shift. The finite differences were then combined to obtain the total curvature information (*kappa*) of the growing contour (Figure 12):

$$kappa = \frac{f_{xx} * f_y^{\,2} - 2 * f_{xy} * f_x * f_y + f_{yy} * f_x^{\,2}}{(f_x^{\,2} + f_y^{\,2})^{3/2}} \sqrt{f_x^{\,2} + f_y^{\,2}}$$

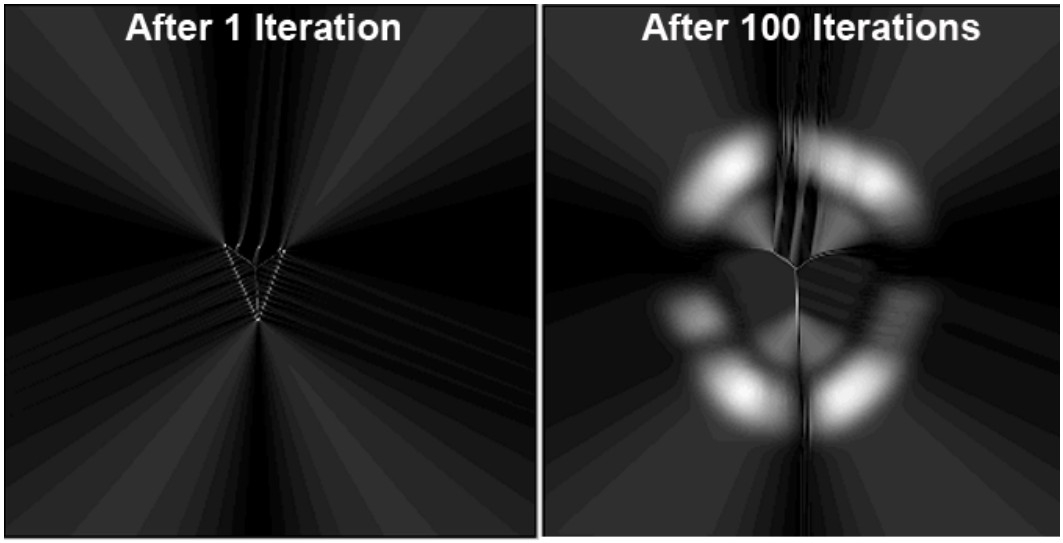


Figure 12. The curvature information image (kappa) of the original mask (left) and again after 100 iterations of contour growth (right) using the simple image shown in Figure 9. The gray values in these kappa images represent approximations of their derivatives. The absolute value of the curvature information image is shown so that areas of high curvature are displayed as white. The actual kappa values range from -0.79 to 1.0 (left) and -0.96 to 1.0 (right), respectively.

This curvature information was used in conjunction with the previously computed Image Force to compute the External Force of the contour:

$$\textit{External Force} = mu * kappa / \max(\max(|kappa|)) + \textit{Image Force}$$

The External Force, an image itself (Figure 13), was normalized by the absolute value of the maximum pixel value in the external force. It is apparent from Figure

13 that the Image Force is more dominant than the curvature information in the External Force.

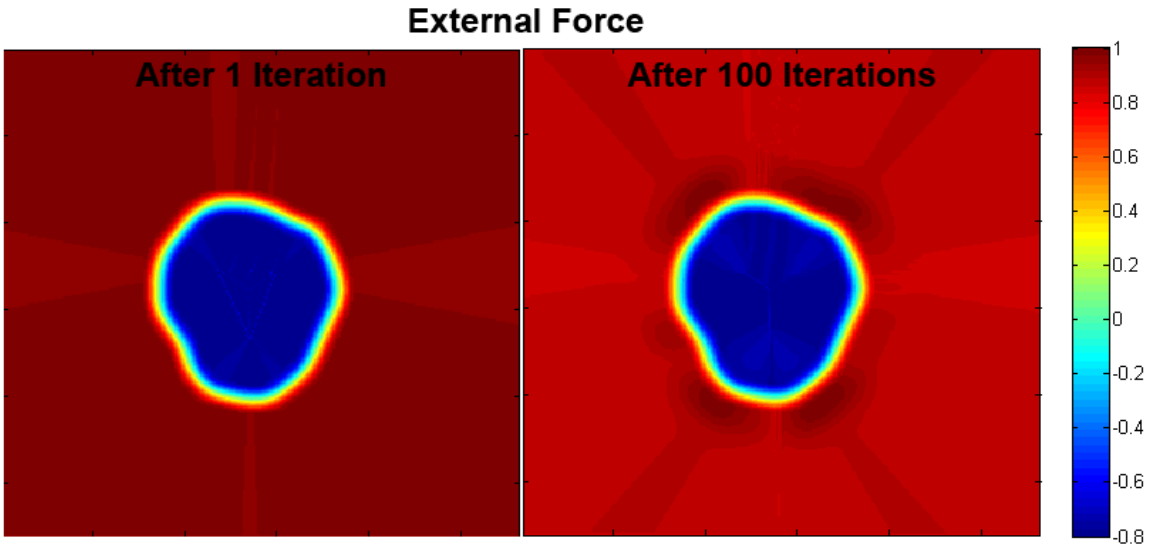


Figure 13. The normalized External Force images shown in the first iteration (left) and after 100 iterations (right). The images have the same maximum pixel value, but the External Force after 100 iterations has a lower minimum pixel value. The non-normalized values range from -2180 to 2480 after 1 iteration and -2500 to 2480 after 100 iterations.

In the External Force equation, *mu* is a scalar weight term corresponding to the length of the perimeter of the growing contour. When *mu* is set to a large number, the curvature apparent in kappa is emphasized, which serves to ignore any forcing effects generated from image noise. For this work *mu* was set to 0.1 * 255^1.5, where the base 255 is used because in this case 8-bit integer data were used. The multiplier (0.1) and power (1.5) were selected based on judgment of what values resulted in a boundary unaffected by the particular noise of the carpal tunnel MR images. A new signed distance map was determined by multiplying the normalized external force image by a step size of 0.5 and adding this to the previous signed distance map. At this point, the area of the negative

region of the new signed distance map was calculated. This negative region corresponded to the growing tendon region and provided a new mask used to continue the contour growth. Therefore, the new contour was the boundary of the new mask. Figure 14 shows examples of the new signed distance map, mask, and contour after iteratively growing a tendon-like contour from the triangular mask in Figure 9.

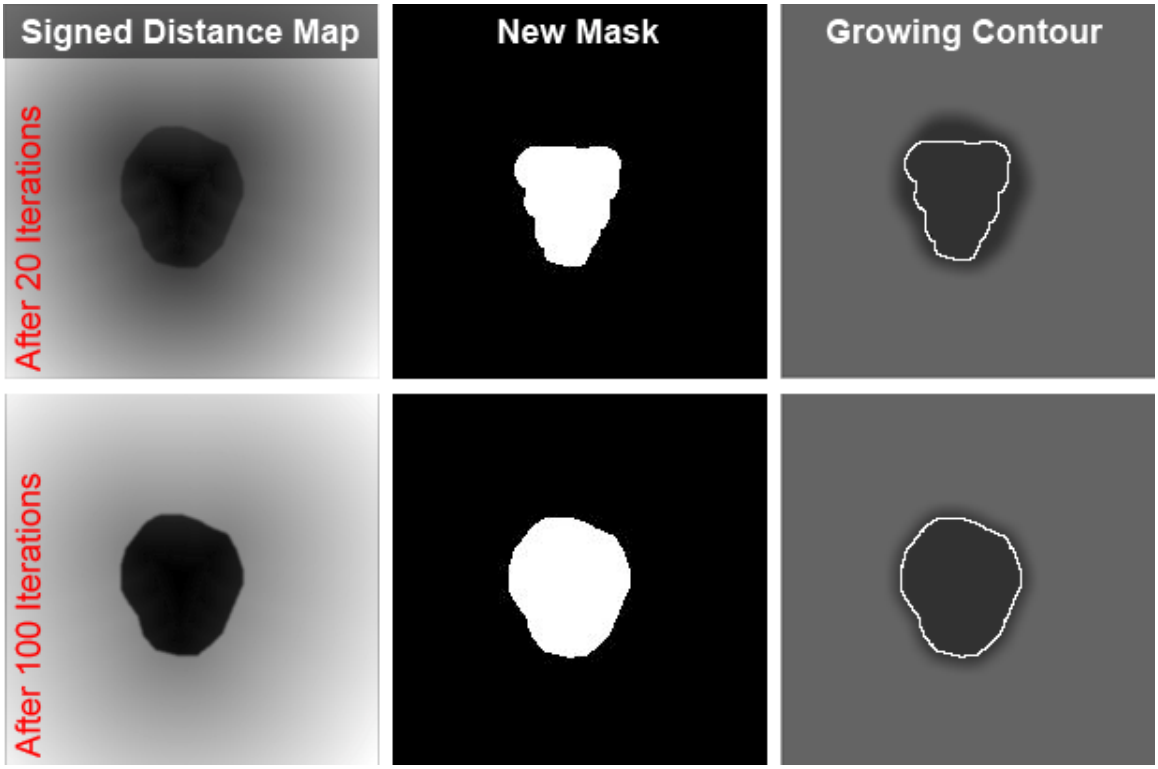


Figure 14. Signed distance map and the corresponding new mask and contour after 20 (top row) and 100 (bottom row) iterations. The growing contour is shown overlaid on the surrogate MR image from which the contour is being grown.

The process to actively grow a contour continued through 100 iterations. This number of iterations was selected purely on the empirical basis that accurate contours were grown without taking an excessive amount of time.

Growth limitations were established to ensure that the region did not grow too much larger or shrink too much smaller than the previously segmented tendon region. The growth was terminated if the region area was less than the minimum area limit, which was set equal to 80% of the previously segmented tendon region area. Similarly, the growth was terminated if the growing area was greater than the maximum area limit, which was set equal to 120% of the previously segmented tendon region area. If the area was within the area limits and 100 iterations had not yet been performed, the contour growth was performed again. Active contour growing terminated if the area was outside of the limits or if all 100 iterations had been performed. The algorithm for active contour growing is summarized schematically in Figure A-1.

After a tendon region was grown, checks were performed to ensure that this new region would not overlap neighboring boundaries that were already completed in the 2D section that was being analyzed. An overgrown tendon region sometimes occurred in cases where there was not a clear tendon boundary, either because of a close neighboring tendon (where the two tendons might appear as one), or if the magic-angle effect was present in the image. Overlaps would indicate that one or more of the overlapped tendon regions had overgrown during contouring. The overlap check was performed by determining pixel locations where the newly-completed tendon region would be placed in the master segmentation image containing other tendon regions that had already been grown. Overlap was indicated if any of the pixels in the new region would be placed in a location whose value was already non-zero. This would indicate that another structure had already been identified in that location.

In cases where neighboring boundaries would overlap, both boundaries were flagged for additional processing. This processing consisted of comparing each boundary flagged as overgrown to the boundary of the corresponding

tendon region on the previously-segmented next-proximal slice. Each pixel in the overgrown boundary was compared to the closest pixel in the previous boundary. If the pixel in the overgrown boundary was greater than three pixels away from the previous boundary, the closest pixel in the previous boundary was used in its place. However, if the pixel in the overgrown boundary was three or fewer pixels away from the previous boundary, the pixel in the overgrown boundary was kept (Figure 15).

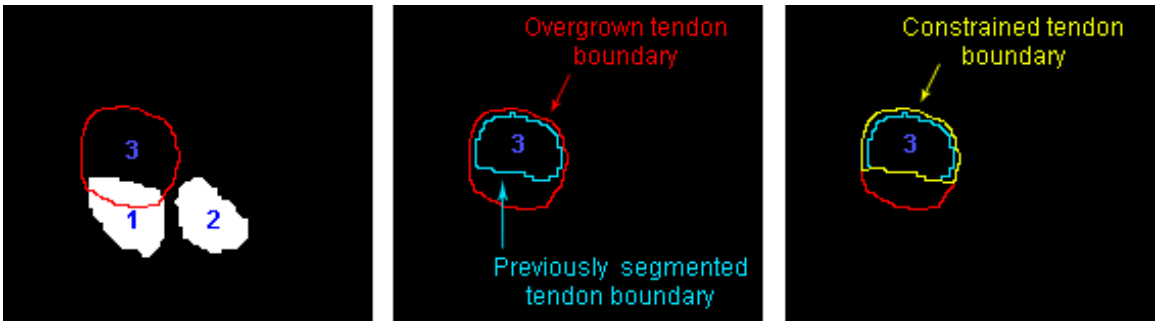


Figure 15. It is apparent that the boundary of tendon 3 will overlap tendon 1 when placed in the master segmentation image (left). Both tendons (1 & 3) are flagged for additional processing. Each pixel in a flagged boundary is compared to the nearest pixel in its previously segmented boundary (middle). The overgrown boundary is constrained by replacing any pixel greater than 3 pixels away from the previously segmented boundary with the nearest pixel in that previously segmented boundary. This results in a constrained boundary which is not overgrown (right).

### 3.1.3 Segmentation Editing

All of the new tendon boundaries were overlaid on the MR image and presented to the user along with a custom-developed four push-button graphical user interface (GUI) which allowed the user to edit any of the tendon boundaries and to segment the nerve and carpal tunnel boundaries (Figure 16). The first button (“Segment Tendons”) leads to a secondary custom-developed push-button GUI which allowed tendon boundaries to be deleted and traced. Deleting

could be done either by tracing the area to be deleted - for instance if only a small mistake in the boundary needed to be removed - or by clicking to delete an entire boundary if the user desired to re-trace that entire boundary. Tendon tracing was done by manually selecting points along the boundary of the tendon. The second and third buttons on the main GUI allowed the nerve and tunnel boundaries, respectively, to be traced in the same manner as the tendons. The fourth button indicated that editing of the tendons and the segmenting of the median nerve and tunnel boundary on the MR image was complete.

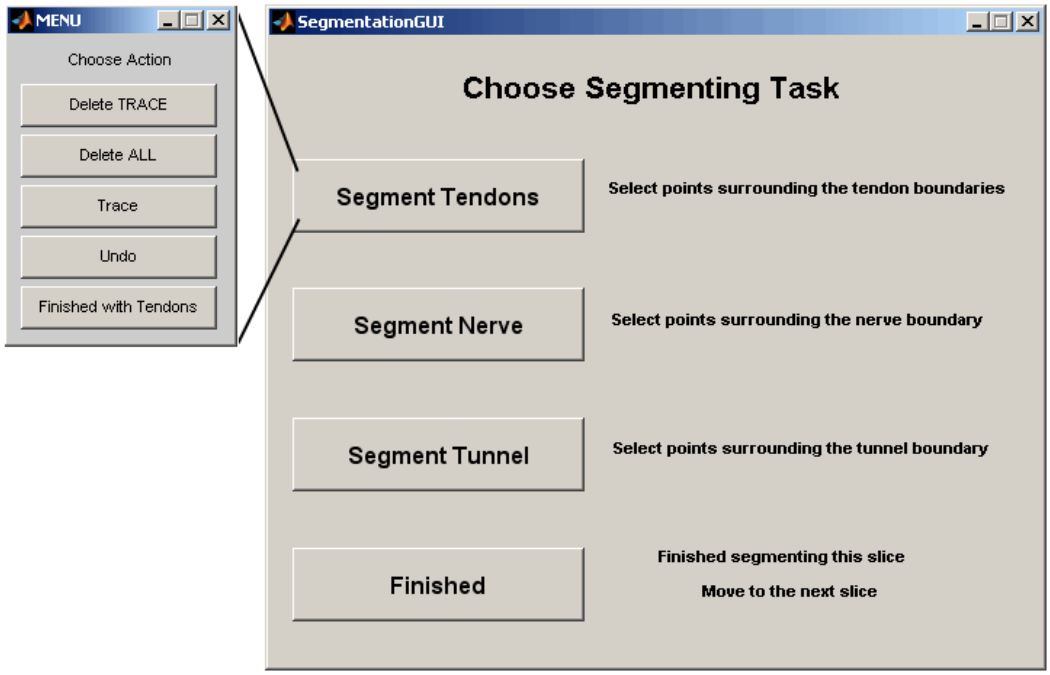


Figure 16. Segmentation GUI (right). When the top button, 'Segment Tendons', was selected, the tendon menu (left) was presented.

Typically, the tendon boundaries of the ring and little fingers required editing due to the close proximity of these tendons on the ulnar side of the tunnel. Generally the deep tendons of these fingers were directly adjacent with minimal SSCT between to distinguish between the two boundaries. Often the superficial

little finger tendon, the smallest of the flexor tendons, was directly adjacent to the superficial ring finger tendon or the deep little finger tendon, making its boundaries equally difficult to distinguish.

The nerve and carpal tunnel boundaries were manually segmented on each image. Neither boundary could be segmented automatically due to variations in the appearance of these boundaries. The nerve was often difficult to distinguish on a single image due to its low contrast of signal intensity with the surrounding SSCT. While the nerve did tend to have more of a textured appearance, the level of texture present varied between images within the same MR image sequence, and between the MR image sequences. Additionally, to locate the nerve in an image, often the user needed to scroll through the image series to watch for movement in the regions of intermediate signal intensity. The tunnel boundary on a given image was formed by pixels of various intensities. It was often difficult to distinguish on a single image; in which case, the user was again required to scroll through the images in the series to find where the boundary was well defined and observe changes in the boundary in other images.

Once editing was complete, those segmentations were then used to grow the tendon regions on the next-distal image using the above-described active contouring method. This segmentation process was performed 2D slice by 2D slice, with the automatically generated segmentations of each section being evaluated prior to moving on to process the next-distal image. This process was repeated for all of the images spanning the carpal tunnel. On average, approximately 30 MRI sections through the carpal tunnel were segmented per wrist. These segmentations were stored as a 3D image stack in a Matlab data file.

## 3.2 Tendon Identification

### 3.2.1 Tendon Tracking Algorithm

After the segmentation of images spanning the carpal tunnel was complete, the boundaries of all the tissue structures were demarcated. However, the identities of each specific tendon were ambiguous through the length of the carpal tunnel. This ambiguity of the tendon identities is due to the close proximity of the tendons within the carpal tunnel, to variations in stacking arrangements between loading activities and subjects, and to large transverse movements of the tendons with wrist motion. Therefore, each tendon was individually identified after segmentation using a region-growing technique that tracked the tendon identities from a more distal hand location where the identity was unambiguous (Figure 17).

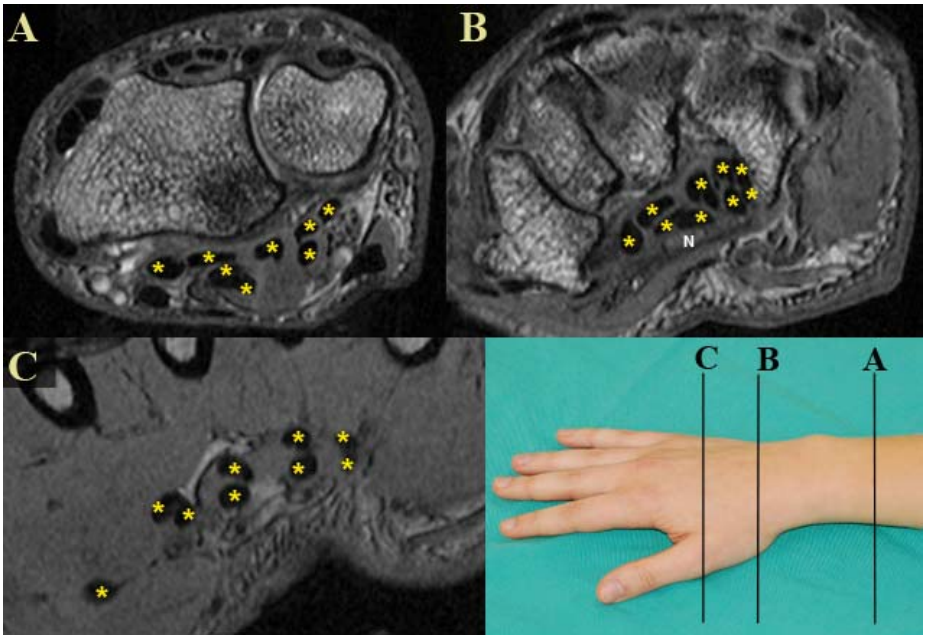


Figure 17. MR images with flexor tendons identified (*) within (B), and on either side of (A&C) the carpal tunnel. Only in the distal image from the hand (C), where the tendons align in pairs going to each finger (one to the thumb) and in two layers (deep and superficial), was unambiguous tendon identification possible.

A distal MRI section from within the hand, in which each tendon could be easily distinguished, was manually selected and used as the starting image for the region-growing technique. To initiate the automatic region-growing, each of the nine tendons on the starting image was manually identified and outlined in the same order: thumb, superficial index, deep index, superficial long, deep long, superficial ring, deep ring, superficial little, and deep little (Figure 18). This tracing order ensured each tendon received the same identifier in every scan, regardless of arrangement once the tendons reached the tunnel.

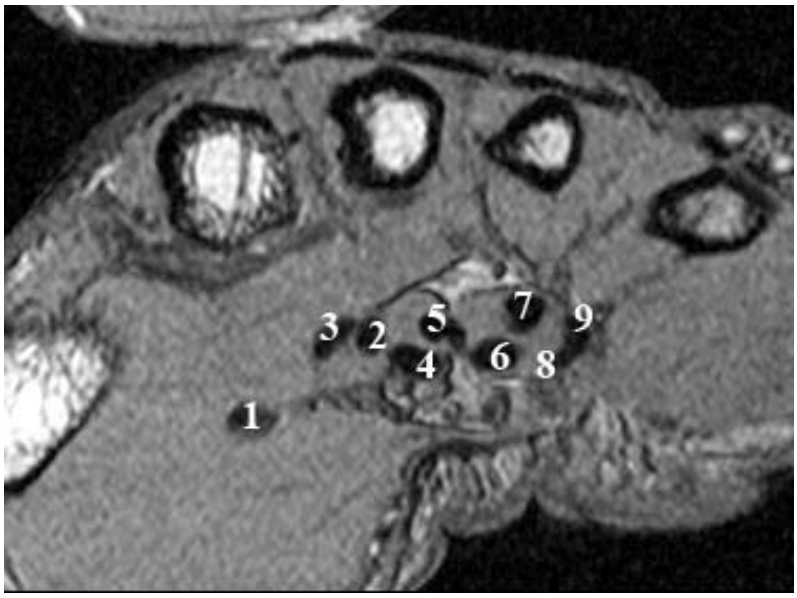


Figure 18. In order to ensure that each tendon received the same numeric label (shown above) in any scan, tendons were always outlined in the same order. 1 corresponds to the thumb, 2 the superficial index, 3 the deep index, 4 the superficial long, 5 the deep long, 6 the superficial ring, 7 the deep ring, 8 the superficial little, and 9 the deep little tendon.

The centroid of the initially-outlined tendon cross-sectional area was used as the center of a 3x3 seed region from which to grow the tendon region on the next-proximal MR image in the series. Within a given 2D image, the mean of the

9 pixel intensities in the 3x3 seed region was computed ($I_{mean\_of\_seed}$). The tendon region within the working image was grown using a 4-connected neighborhood comparison scheme, with a candidate pixel being added to the provisional tendon cross-section if its intensity ($I_{candidate}$) was in the appropriate grayscale range for the overall tendon cross-section:

$$\left| I_{candidate} - I_{mean\_of\_seed} \right| \leq 0.8 * I_{mean\_of\_seed}$$

In a 2D MRI section, a tendon region continued to grow until either there were no remaining candidate boundary pixels, or until its area had reached the area growth limitation threshold. The cross-sectional area within each initially traced tendon boundary was calculated and used as the growth limitation threshold. This threshold ensured that during region growing, one tendon region did not grow so large as to merge into another, and its implementation prevented the necessity of establishing a set size threshold within the algorithm.

The centroid of the resulting grown region was then used to define the 3x3 seed region from which to grow the tendon region on the next-proximal image, and so forth. The tendon tracking process, performed on one tendon at a time, was complete once the section-by-section region growing for all nine tendons had propagated to the image delimiting the distal margin of the carpal tunnel (Figure 19).

The result of this region-growing and tracking process was a labeled image, which corresponded to the distal-most carpal tunnel image, and contained the identities of each tendon region. According to the initial tracing order, each grown tendon region was identified with a number 1 through 9, corresponding to each of the digital flexor tendons (thumb=1, superficial tendons=even digits, and deep tendons=odd digits). To most reliably obtain the labeled image, region-growing was performed on each MR section (1 mm intervals) between the

starting and ending sections. Because all of the images through which the identities were tracked were distal to the carpal tunnel, region growing did not need to result in perfect structure boundaries. Rather, it just needed the ability to rapidly track the tendon identities longitudinally through a set of axial slices. The algorithm for tracking individual tendon identities is summarized schematically in Figure A-2.

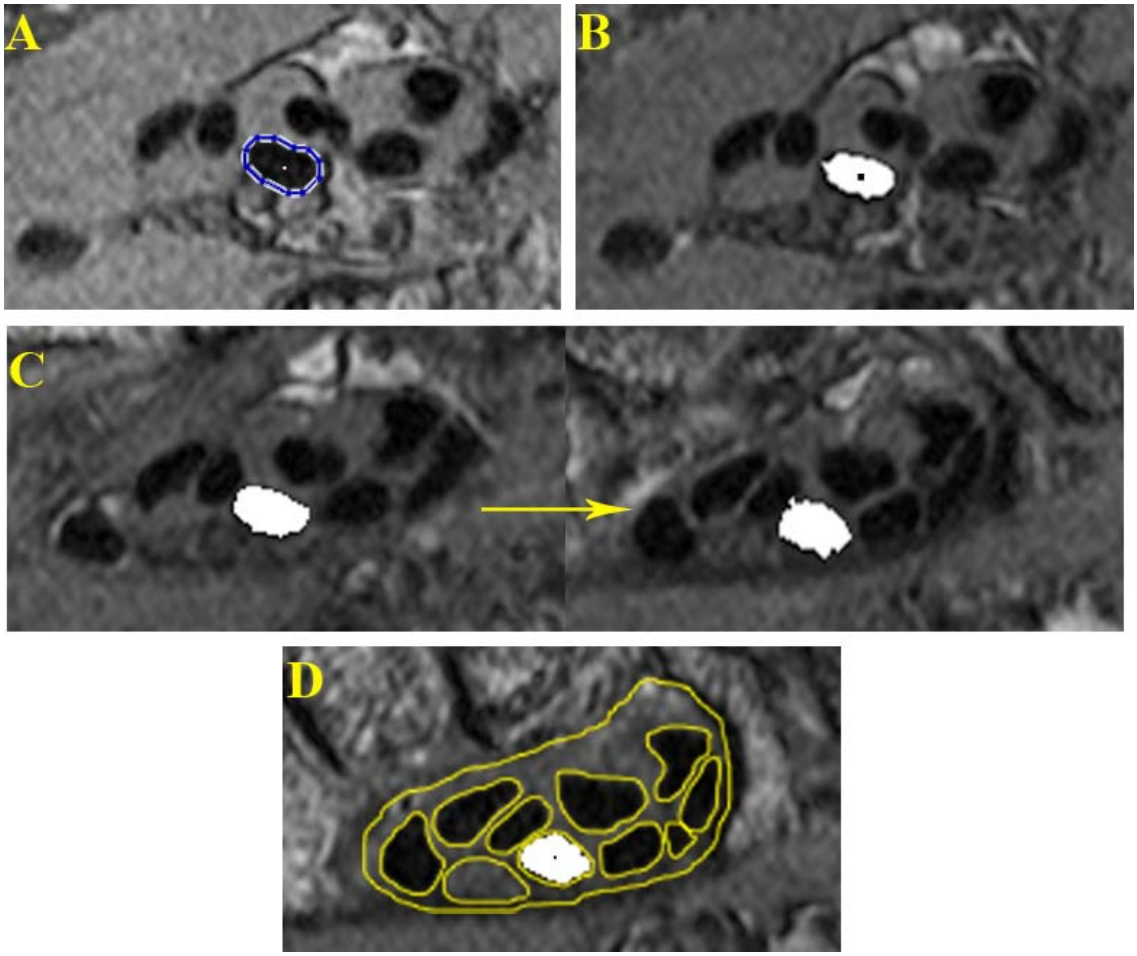


Figure 19. Progressive automatic tracking of the long finger superficial tendon, beginning from the starting distal image. The centroid of the outlined tendon boundary (A) was used to establish the seed region (B) from which the next tendon region was grown. Additional cross-sections of this tendon at six-section increments, moving proximally toward the distal end of the carpal tunnel are shown in C. Tracking continues until the image of the distal carpal tunnel is reached, which coincides with the distal-most segmentations (D).

### 3.2.2 Tendon Identity Propagation

The labeled image resulting from the region-growing and tracking process was then used to conclusively identify each of the pre-segmented tendons within the carpal tunnel. Tendon identities were automatically propagated from the labeled image through the segmentations by determining in which region on the label image the centroids of the unknown tendons on the distal end of the carpal tunnel segmentations were located. The centroids of the unknown tendons on the next proximal segmented image were then compared to the labeled neighboring image to determine in which region each was located, and so forth. The arbitrary labels in the 3D image stack of segmentations were changed to reflect the known tendon identities in the labeled image.

Most of the time, tendon identity propagation was simple and straightforward. However, there were some cases in which the centroid propagation method proved insufficient. In cases where the tendon had a small cross-sectional minor axis (a long narrow shape) and a high degree of curvature through the tunnel, the unknown structure centroid was occasionally not located within any tendon region on the adjacent labeled image. In such cases, the distance from the unknown tendon centroid to each of the regions on the neighboring labeled image was calculated. Since the unknown segmented region would still lie closest to the labeled region of the same tendon, the unknown segmented region was given the label corresponding to the known region on the labeled image with the shortest distance to the unknown tendon centroid.

Similarly, in the case of highly concave tendons, the centroid of the unknown structure did not fall within its perimeter, and once the concave part of the tendon was reached during identity propagation, the label would be tracked through the empty space surrounding all of the structures. In this case, rather

than working from the centroid, identification was performed using a substitute point that was defined specifically to fall within the tendon boundary. This substitute point was defined by determining the upper and lower row of the centroid column, finding their midpoint, and moving the centroid coordinate vertically until it reached the center of the tendon along that line. Once the substitute point was defined, the identity label was tracked properly through the tendons.

In this manner, the segmented tendons in the carpal tunnel were given the same identifier as the corresponding region in the labeled image. It was not necessary to track the identity of the nerve since its identity is unambiguous in the carpal tunnel, and therefore always received the same unique label in the 3D image stack of segmentations. The same numeric identifier was assigned to the same tendon in all image series processed with this method, thereby allowing for assessment of specific tendon-nerve interactions which result in deformation of the nerve. It also allows inter-subject comparisons of tendon stacking arrangement to be made.

### 3.2.3 Three Dimensional Model Generation

The identified segmentations were used to create 3D triangulated surface models of the carpal tunnel, illustrating the median nerve, the nine flexor tendons, and the tunnel boundary (Figure 20). This was done by enclosing each identified tissue region within an isosurface generated using Matlab. Direct comparisons of the tissues in the different models allowed for observations to be made about specific tendon-nerve interactions occurring during the different wrist positions and loading activities.

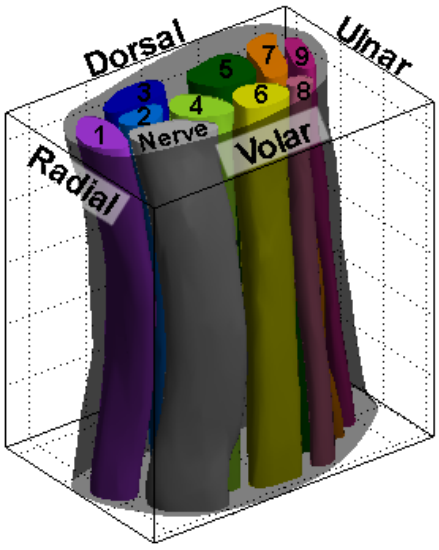


Figure 20. 3D surface model of a carpal tunnel boundary, the median nerve, and the nine tendons. Tendon labels correspond to those in Figure 18.

## 3.3 Forearm Bone Segmentation

To ensure accuracy of comparisons of tissues in the different models at specific locations within the tunnel, it was necessary to make certain that all of the models were in a similar orientation. This was necessary due to the discrepancy in tissue appearance which could result from an oblique view through one scan compared to a true cross-sectional view in another scan. These different views result from the variations of wrist orientation within the scanner during MR imaging (Figure 21).

To accommodate the variations in wrist orientation, the carpal tunnel models were registered to a subject-specific anatomic coordinate system. The coordinate system was established from each subject's neutral unloaded scan, since the wrist is straightest in this position. Axes were established using landmarks of the forearm bones, including the long axis of the radius and the ulnar styloid process. To obtain the bony geometry needed to establish the coordinate system, two different scan regions were required. The wrist scan of

the carpal tunnel contained the required distal ends of the forearm bones. Additionally, an arm scan was acquired to obtain the shafts of the forearm bones.

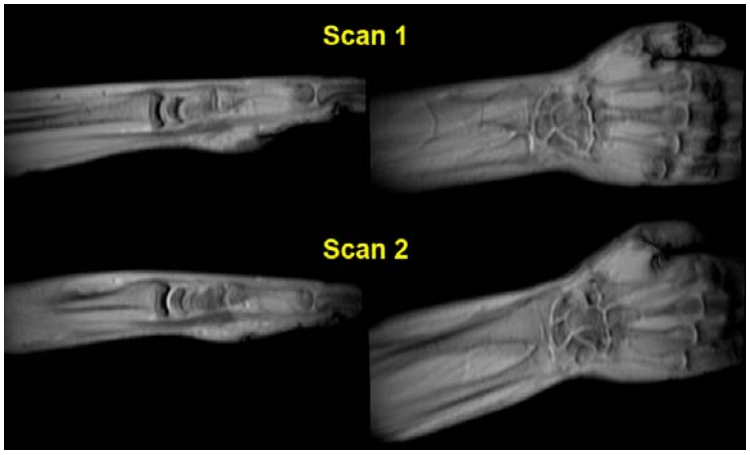


Figure 21. MR scout images of one subject's varied wrist positions for two different neutral scans with sagittal (left) and coronal (right) views shown.

### 3.3.1 Wrist Scan Bone Segmentation

The radius and ulna were segmented from each MRI scan containing the carpal tunnel specifically for registration purposes. Bony segmentation began on the first MR image in the stack and continued through the last image where either bone appeared. Segmentation was performed manually using another purpose-written Matlab program. Similar to the tendon segmentation program, this version sequentially opened all images spanning the radius and ulna, and automatically presented those images to the user, along with a series of push-button menus (Figure 22). The first menu contained three buttons, one each to segment the radius and ulna, and a third to indicate that bone segmenting on the image was complete, bringing up the next image in the series. Separate menus were presented when either of the buttons to segment the bones was selected. These menus contained options to either trace or delete a structure boundary,

and to indicate that segmenting of the bone was complete. It was possible to outline multiple boundaries for each bone in the case when regions of the same bone were disjoined. For example, an axial image through the distal end of the radius may result in disjoined regions due to the concavity of the articular surface (Figure 23).

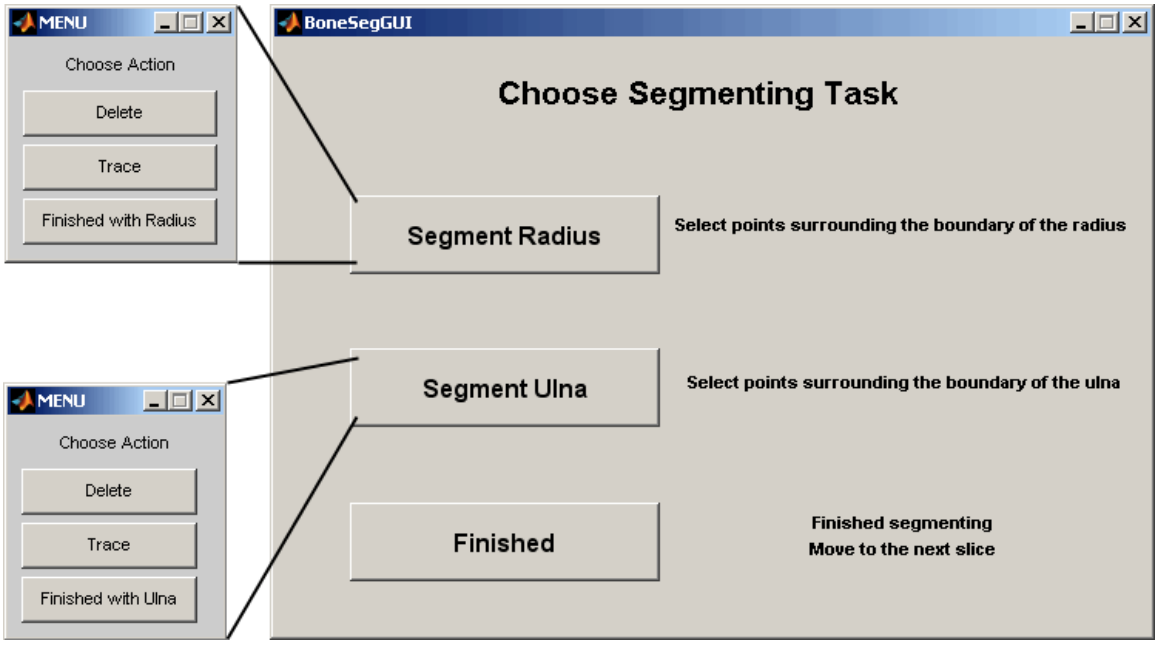


Figure 22. Bone segmentation GUI (right). When either button to segment the bones is selected, the corresponding menu (left) is presented.

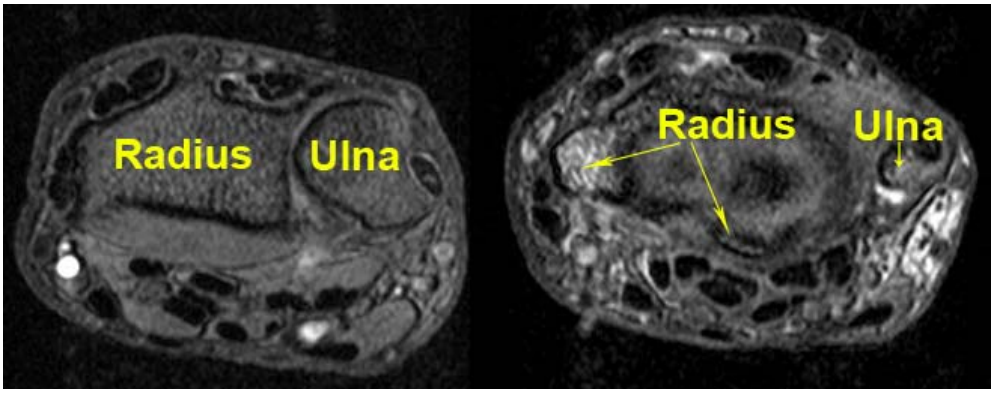


Figure 23. Forearm bones, as they appear in the carpal tunnel scans, shown proximal (left) and distal (right) to the radial articular surface.

### 3.3.2 Arm Scan Bone Segmentation and Alignment

To establish an axis coincident with the long axis of the radius on the neutral, unloaded scan, more images of the bones in the forearm were needed. Because the field of view of the wrist scan was not large enough to obtain proximal images in the forearm, a separate scan was performed specifically to obtain these images. A multi-slice fast spin echo scan sequence was used to acquire these images. The resolution of the forearm scan was 0.8 mm x 0.8 mm x 10 mm over a 16 cm x 12 cm x 14 cm field of view. The two separate scan regions (wrist and forearm) then had to be aligned because the field of view and image size of the forearm scan were different from those of the wrist scan. Because the wrist is most straight in the neutral unloaded position, the orientations of the wrist scan and the arm scan were always parallel. So, orientation between these two scans did not require adjustment.

To relate these two different scanning fields of view, a normal to the wrist imaging plane was found using the wrist scan orientation information contained in the DICOM header data, specifically the x- and y-axis data. The normal (z-axis) was found by computing the cross product of the x- and y-axes. This z-axis unit vector was used to find the scalar distance between the wrist and forearm imaging planes by multiplying the z-axis vector by the difference between the wrist and forearm image position coordinates from each scan's DICOM header. A projection point of the upper left hand corner of the wrist image into the forearm image along the z-axis was found by subtracting the z-axis vector multiplied by the distance between imaging planes from the wrist image position. The pixel location within the arm image where this projection point should appear was computed by subtracting the projection point from the forearm image position coordinate, dividing this difference by the forearm pixel spacing to obtain a unit of

pixels, then multiplying by the negative of either the x-axis or y-axis to obtain the x and y pixel locations.

The arm image was then cropped to match the physical size of the wrist image. The crop width was determined by multiplying the number of columns in the wrist scan by the quotient of the wrist scan pixel spacing and the forearm scan pixel spacing. Similarly, the crop height was determined by multiplying the number of rows in the wrist scan by the pixel spacing quotient. The forearm image was then cropped using the x and y crop locations and the crop width and height. Finally, the cropped image was rescaled to match the pixel dimensions of the wrist image. This process resulted in a forearm image being displayed the same as it would have been if the set of wrist slices had continued down to the forearm. After aligning the wrist and forearm scan regions, the radius and ulna in the forearm images were segmented using the same push-button menus used to segment these bones in the wrist scan.

## 3.4 Model Registration

An anatomy-based coordinate system was established for each subject using the segmented radius and ulna from the neutral, unloaded scan. First, a local z-axis through the radial shaft was defined by performing principal component analysis using the centroids of the radius on the first and last images in the forearm scan and the articulation image in the wrist scan (the last image aligned with the shaft of the radius, and prior to images containing the radial styloid process). These centroid locations were selected because they best represented a series of images containing the more regularly shaped radial diaphysis. An initial local x-axis was defined from the distal end of the z-axis through the centroid of the distal-most segmentation of the ulnar styloid process. The local y-axis was calculated from the cross product of the z- and x-axes, and

was directed volarly. A final orthogonal x-axis was calculated from the cross product of the y- and z-axes, and was directed towards the ulna. The origin of this local coordinate system (Figure 24) was defined as the intersection of the local z-axis with the distal radial articular surface.

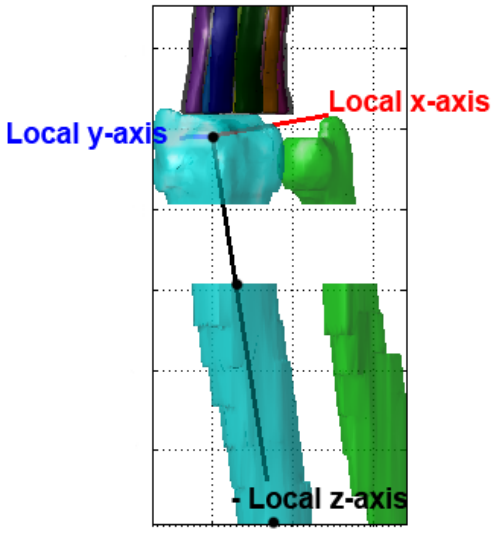


Figure 24. Subject-specific local anatomic coordinate system, shown prior to rotation. The negative z-axis is displayed to visualize how the shaft of the radius was used to obtain this axis. The black dots through the radius correspond to the three centroids used to obtain the z-axis.

The neutral, unloaded model for each subject was rotated using this subject-specific coordinate system. To perform this registration, first, the rotation angle between the local z-axis and the global z-axis was calculated, using the Matlab function *vrrotvec*, which returned an axis-angle rotation vector. The arbitrary axis of this rotation vector was computed as the normalized cross product of the local and global z-axes. The angle of the rotation vector was computed as the inverse cosine of the dot product of the local and global z-axes. This rotation vector was converted to a transformation matrix using the Matlab function *vrrotvec2mat*, and this matrix was used to transform the carpal tunnel

model. The same was then done using the local y-axis and the global y-axis, causing the x-axes to also align. Using the radial shaft to establish the z-axis was preferable to using the irregularly shaped distal radial styloid process, which tended to skew the axis laterally.

To ensure that all other models of the various wrist positions and loading activities of a given subject were rotated to the same reference coordinate system, iterative closest point registration was performed. The vertices of the radius in the neutral, unloaded scan were used as the fixed vertices, and registration was performed on the vertices (moving vertices) of the radius of the other wrist position/loading activity scans to align the bones. The iterative closest point function used a rigid registration, since no scaling of the bones was needed. The registration was deemed complete once the distance between the two groups of vertices, computed as the difference between the fixed vertices and moving vertices, had been minimized. A transformation matrix containing the translation and rotation parameters which minimized the distance was output from the iterative closest point function. These translation and rotation parameters were determined using a Broyden-Fletcher-Goldfarb-Shanno (BFGS) optimization method. This transformation matrix was then used to translate and rotate the 3D tunnel, nerve, and tendon isosurfaces.

Following registration, all of the models were appropriately aligned, allowing comparisons of the structures to be made at specific sections through the models.

## 3.5 Model Post-Processing

### 3.5.1 Ensuring that Structures Did Not Intersect

The slight smoothing which was required to eliminate the stair-step effect of piecing together the discrete slice segmentations caused occasional

overlapping of closely neighboring structures. When these regions were enclosed within an isosurface generated in Matlab, the resulting vertices of some tissue structures were sometimes contained inside the boundary of other structures. These overlaps needed to be removed to obtain separate structures. When encountered, overlaps were removed by translating the overlapped vertices in the direction normal to the structure surface, thereby driving the tissue boundaries apart by the distance of the overlap. Additionally, a minimum 0.2 mm gap between all tissue boundaries was created to ensure the structures were actually separated and not sharing common points in their boundaries.

The first step to check for overlap required obtaining surface normals that were all directed away from the surface of the tendon. Surface normals of each triangular face in a structure's isosurface were obtained by performing the cross-product of two vectors from the face's centroid to two of its vertices, and normalizing this cross-product by its magnitude. Each surface normal was checked to determine if it was directed into or out from the tissue structure body. This check was done by computing the signed distance from the plane perpendicular to the face normal and through the face centroid to the closest reference centroid within the isosurface:

$$\textit{signed distance} = normal * closest\_referenceCentroid + perpendicular\_plane$$

The reference centroids were established every 2 mm through the structure to provide points known to be inside the structure, for comparison when determining the surface normal directions (Figure 25). A positive signed distance – a distance in the same direction as the normal – indicated that the normal was pointed into the structure center. A negative signed distance indicated the normal was pointed away from the structure center. Any normal pointing towards

the structure center was then negated, to ensure that all normals were pointing away from the center.

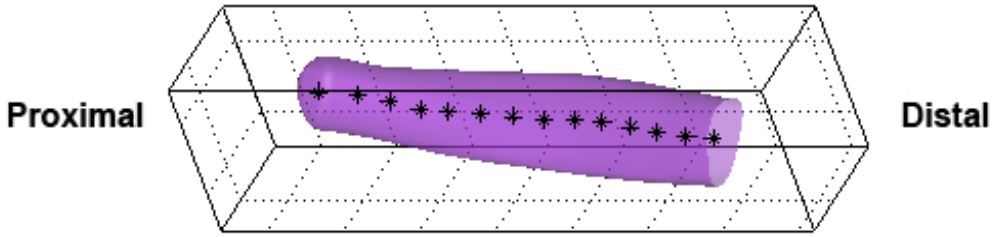


Figure 25. Thumb tendon with reference centroids (black asterisks) every 2 mm through the center.

The outward directed surface normals were then used to determine whether vertices of other carpal tunnel structures were contained within the working isosurface. This was done by again computing the signed distances from other structures' vertices to the closest perpendicular plane, where the perpendicular planes are planes of each face perpendicular to the face normal. To ensure each structure had a slight gap between it and any neighboring structures, a minimum separation distance of 0.2 mm was defined. Therefore, any of the other structures' vertices being checked with a signed distance less than 0.2 mm from the working structure was moved in the direction of the working structure's normal to a distance of 0.2 mm from the face. This check was performed for each isosurface.

To reduce the time needed to perform this check, each structure's isosurface was compared to each of the other structures' isosurfaces only once. This was done in the order of the label received for the tendons (1 - 9), the nerve (10), and the tunnel (11), with the number of comparisons performed being reduced by one for each subsequent structure. All of the structures were

compared to the FPL (label = 1) to determine whether any of the vertices composing their isosurfaces were contained within the FPL. Next, all structures except the FPL were compared to the superficial index tendon (label = 2). This method of reducing comparisons continued for all of the tendons, except the superficial little tendon, which was never used as the working structure due to its small size, and instead was included in the comparison to all other structures. Additionally, only structure vertices within 2 mm of any of the vertices in the working structure were checked to further reduce the number of comparisons required.

### 3.5.2 Anatomic Cross-Section Selection

Two cross-sections of the rotated models were then selected for analysis of each structure within the carpal tunnel boundary. This was done by selecting a 0.7 mm range of z-values from the rotated models (Figure 26). The cross-sections selected for analysis were at levels of the most bony incursion into the carpal tunnel: the hook of the hamate and the pisiform. MR images containing each of these landmarks were identified manually, and within these images, the user selected a single point representing the location where the pisiform or hook of the hamate most intruded into the carpal tunnel. These two locations were each saved as three-dimensional coordinate points, which were then rotated in the same manner as the bones and carpal tunnel contents, using the transformation matrices established from the anatomic coordinate system. The resulting z-value for each rotated landmark was used as the center of the range of z-values needed to isolate a cross-section of the carpal tunnel model at each level. These levels represented locations near the proximal and distal ends of the carpal tunnel.

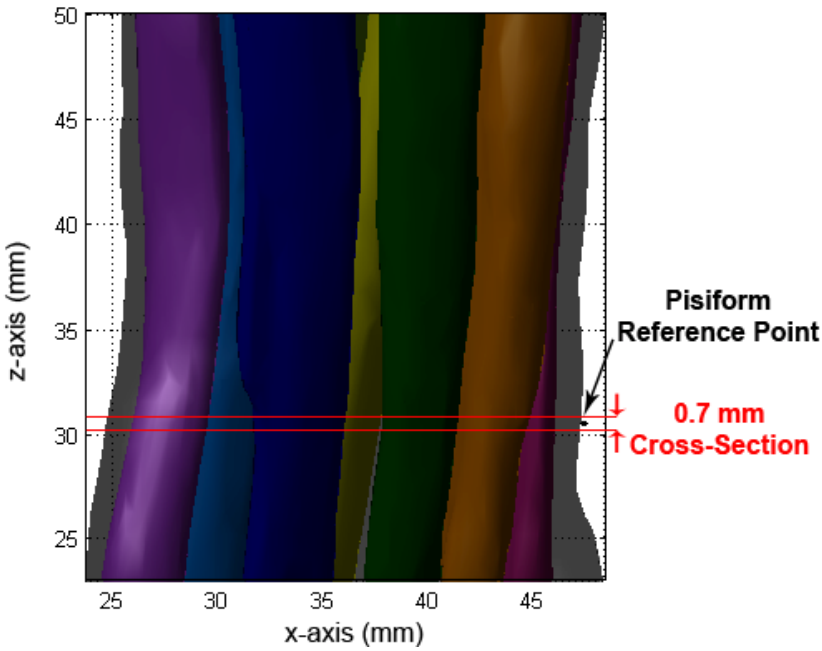


Figure 26. Longitudinal view of the carpal tunnel isosurfaces, with the pisiform reference point (black) centered in the 0.7 mm range of z-values for the cross-section selection (red lines).

Because the models were rotated into the anatomic coordinate system, the boundaries of each structure needed to be isolated from the vertex point cloud composing each isosurface, as opposed to using the individual slice segmentation. A 0.7 mm range of z-values was selected for this isolation, to guarantee that each boundary had a sufficient number of vertices to form a closed boundary curve. A smaller range of z-values empirically sometimes resulted in non-closed boundary curves, which would have left the overall size and shape of the structure indeterminable. To ensure isolation of closed tendon, nerve, and tunnel boundaries during cross-section isolation, the number of points defining a surface had to be increased. This is because Matlab's isosurface command did not generate equal size triangular faces. Therefore, if the needed cross-section passed through edges of the triangular faces and not through

vertices, the resulting structure boundaries were composed of very sparse vertices.

To ensure enough vertices to sufficiently enclose each region on the selected section, the number of vertices needed to be increased. This was performed on a structure-by-structure basis. First, the area of each triangular face of an isosurface was computed using Heron's formula.[76] An area threshold for each structure was defined as 20% of the largest triangle's area. Any triangle with an area larger than the area threshold was divided into six new triangles, by dividing each edge at its midpoint, and connecting the midpoints to the centroid of the original triangle (Figure 27). The area of each of these new triangles was then computed, and if they were still larger than the area threshold, they underwent another level of refinement. This process was iterated up to 20 times for each structure.

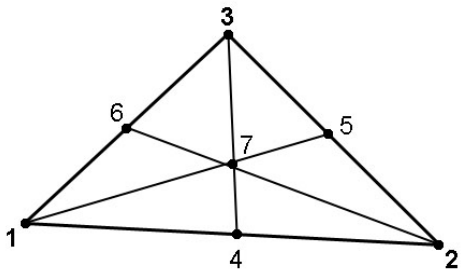


Figure 27. Vertices 4,5,6 correspond to the midpoints of the edges of the large triangle and 7 to the centroid. Breaking a large triangle at these points resulted in 6 smaller triangles, and added 4 new vertices to the surface definition.

In order to ensure that true cross-sections were obtained even with the normal curvature of the carpal tunnel that was present in the flexed models, additional processing was necessary prior to selecting the cross-section

containing the hook of the hamate. No additional processing was needed prior to selecting the pisiform cross-section, since this reference point was in the proximal third of the carpal tunnel, and by inspection, prior to where the structures begin to curve. The additional processing required obtaining the tunnel centroids 1 mm in both z-directions from the tunnel centroid closest to the hook-of-the-hamate reference point. A 3D trendline was fit to these three centroids using principal component analysis. A curve could have been fit to these three centroids, but because they were only 2 mm apart, the result would have been very similar. A rotation vector needed to rotate the 3D trendline to align with the z-axis was then obtained using the Matlab function *vrrotvec*, which was converted to a rotation matrix using the Matlab function *vrrotvec2mat* and then used to rotate the 3D isosurfaces of the tendons, nerve, and carpal tunnel boundary. Following this rotation, the hook-of-the-hamate slice was isolated in the same manner as the pisiform slice. This additional rotation enabled true tunnel cross-sections to be obtained in the presence of tunnel curvature.

## 3.6 Obtaining Shape Measures

Observations were made of how the overall size and shape of the carpal tunnel structures changed from one end of the tunnel to the other, and in various wrist positions/ loading activities. Additional observations were made of specific tendon-nerve interactions and the resulting nerve deformations which may be associated with CTS. Making use of the known tendon identities, traditional CTS-related size (cross-sectional area) and shape (flattening ratio) measurements were tabulated for all carpal tunnel structures (nerve, tunnel, and each tendon) in each of the two cross-sections selected. The cross-sectional area and the major/minor axis lengths were extracted from the slices taken from the rotated models using code developed in Matlab. Additionally, two localized

measures were developed specifically to examine interactions involving the nerve. The first of these was a nerve adjacency measure, which registered the specific tendons neighboring the nerve, and the amount of the nerve boundary that was closely neighbored by another carpal tunnel structure (tendon or tunnel boundary). The second localized measure registered local deformations (pinches and impingements) in the nerve boundary.

### 3.6.1 Traditional Size and Shape Measures

The traditional shape measure – the flattening ratio – approximates the shape of a structure as an ellipse. Therefore, an ellipse was fit to the coordinates forming the boundary of each tissue structure, using a non-weighted least squares method. From each ellipse, the major and minor axis lengths were obtained. The flattening ratio was calculated as the structure's major axis length divided by its minor axis length.[57, 59, 67] The cross-sectional area of each structure was found by calculating the area inside each structure boundary. A carpal tunnel contents ratio was also calculated, defined as the sum of the cross-sectional areas of the tendons and nerve, divided by the cross-sectional area of the carpal tunnel. Because the identities of each structure in the tunnel were known from the tendon tracking algorithm, the size/shape results were automatically catalogued, by structure, in Microsoft Excel spreadsheets for inter- and intra-subject comparisons.

### 3.6.2 Nerve Adjacency Measures

In addition to the more traditional size and shape measures employed to evaluate CTS, a new MRI evaluation metric was developed which utilized the tendon identity information in a manner that might be a potential indicator of CTS. First, the coordinates of the tendon, nerve, and carpal tunnel boundaries were determined relative to the centroid of the nerve. These structure boundary

coordinates were then converted to polar coordinates, and the identity and distance of the closest adjacent structure to the nerve boundary (tendon or transverse carpal ligament) was determined in 5 degree increments around the nerve. A given structure was considered to be adjacent to the nerve if it was within 1 mm of the boundary of the nerve. From these adjacency data, a percentage of the nerve boundary adjacent to neighboring structures, the amount of nerve boundary shared with each individual flexor tendon, and the approximate location angle from the centroid of the nerve to where each adjacent tendon was located were measured. The location angle was additionally manually converted to an anatomic direction (dorsal, ulnar, volar, radial, or a combination of these).

By comparing the total percent adjacency of a subject's nerve during various wrist positions and loading activities, it was inferred which positions and activities might have a more pronounced effect on the nerve in terms of deformation. This inference was based on increased nerve adjacency, which would indicate an increase in tendon/nerve contact interactions potentially leading to CTS. The anatomic directions of the adjacent structures were used to find when the nerve changed position relative to the other structures in the tunnel, by observing the changes in these directions with the various positions and activities. This provided information as to the transverse movement (or rearrangement) of the structures within the carpal tunnel as the wrist moved or the hand was loaded.

### 3.6.3 Local Deformation Shape Measure

The flattening ratio is most often used to describe the shapes of structures within the carpal tunnel. However, the ellipse fit needed to calculate this ratio is insufficient for describing local deformations. For example, an oval and a

crescent shape may have similar flattening ratios, but these are clearly not equivalent shapes. There is a localized feature in the crescent that is not well defined by measures of the ellipse major and minor axes. Therefore, a second new metric was developed to consistently identify local deformations in a tissue structure's boundary. This metric included implementing shape numbers of each structure to indicate changes in shape along the structure's boundary.[77]

First, the boundary of each tissue structure was discretized into equal-length line segments. This was done by automatically sorting through the points surrounding the boundary on each model cross-section (approximately 200 for each tendon and nerve and 600 for the tunnel) and reporting points every 0.5 mm. This value was contingent upon the smallest tendon still being composed of enough points to accurately represent its boundary, while sufficiently down-sampling the number of points on large boundaries. Using equal-length line segments also facilitated calculating the physical length (mm) of strings of shape numbers. The interior angle between all adjacent line segments was calculated.

Shape numbers were assigned to each such angle using 20 degree slope change increments (Figure 28). Specifically, each shape number was assigned to a 20 degree range, with each multiple of 20 degrees being the average of the range. For example, a shape number of 1 corresponds to an angle of 160 degrees, and thus would be assigned to any angle between 150 and 170 degrees. Larger numbers (closer to 8) represent large slope changes, and therefore a more severe change in direction of the shape boundary, whereas smaller numbers (closer to 0) represent more gradual changes in the direction of the boundary.

For example, if two line segments formed a 180 degree angle, the corresponding shape number would be zero, because there was no change in direction of the boundary. If two line segments formed a 160 degree angle, the

shape number would be 1, indicating that the change in direction of the boundary was slight. However, if two line segments formed a 20 degree angle, the corresponding shape number would be 8, indicating that the change in the direction of the boundary was severe. Negative numbers represented locations where the shape boundary intrudes towards the center of the structure. For example, if the interior angle was 140, the shape number was 2. However, if it was the exterior angle that was 140 (the interior angle was 220), the shape number was -2 (Figure 28).

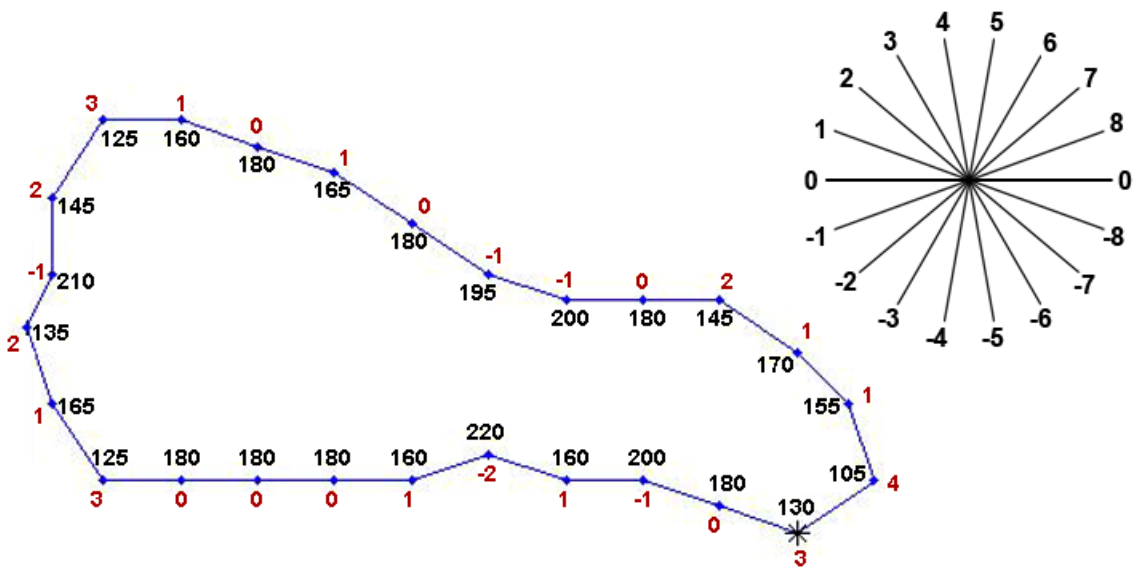


Figure 28. Shape number example. Interior angles (black) shown inside the boundary, and corresponding shape numbers (red) shown outside the boundary at each point. The insert image (upper right corner) shows the slope changes of 20 degrees starting from line 0, with the corresponding assigned number used in the chain.

The shape number chain was assembled starting from the point closest to the reference point (pisiform or hook-of-the-hamate) defining the cross-sectional location. Similarly to the traditional carpal tunnel measures, nerve adjacency and

shape number data were automatically catalogued by structure in Microsoft Excel spreadsheets for inter- and intra- subject comparisons.

Analysis of the shape number chains provided information about local deformations in the shape boundary, which may correspond to occurrences of impingement (negative shape numbers) or pinch (shape numbers greater than 2). The average numbers of pinch and impingement instances in the nerve boundary were determined for the different wrist positions and loading activities, for both the CTS patient and normal subject groups. This facilitated the investigation of whether differences existed between the two groups, or if specific loading activities increased nerve deformation. The average numbers of deformation incidences were also compared to the average percent adjacency for each wrist position and activity, to determine the effect the surrounding structures had on nerve deformation. To visualize the deformations, the location of local pinches and impingements were highlighted in red on a plot of the data points where shape numbers were calculated. These plots were then compared to the adjacency plots to determine when an adjacent structure was the cause of the nerve deformation.

# CHAPTER IV. RESULTS

Model rotation, slice selection, and shape measure acquisition were successfully performed for all 88 of the scans which were segmented. This allowed for comparisons of shape measures and stacking arrangements in CTS versus normal subjects.

## 4.1 Image Processing Times

Segmenting the 9 digital flexor tendons, median nerve, and carpal tunnel boundary on images spanning the carpal tunnel took on average 4 minutes per cross-sectional image, depending on the image quality (Figure 29). Generally, the tendon boundaries were successfully grown using active contouring, and were automatically checked for overlap in approximately 1.5 minutes (total time for all nine boundaries). If necessary, manual editing by the user took approximately 1-3 minutes per image, again depending on the image quality. Depending on the size of the tunnel, this segmentation rate resulted in a total of 1.5-2 hours to segment the entire carpal tunnel.

Images with well-defined tendon boundaries, resulting from larger amounts of space between tendons and no blur due to subject motion, were segmented faster. Since such images were easily separated into regions based on pixel intensity, the boundaries were straightforwardly grown by the active contour method, and very little manual editing was required to obtain accurate structure boundaries. Images affected by the magic-angle effect or by subject motion took longer to segment because the tendon boundaries were not well-defined, and thus required much more user-editing to eliminate overlapping contours. The time needed for manual editing was on the longer end of the 1-3 minute range in cases where the user needed to scroll through the MR images to

track tendons lost due to the magic-angle effect, or to determine boundaries which had no visible tissue between adjacent tendons.

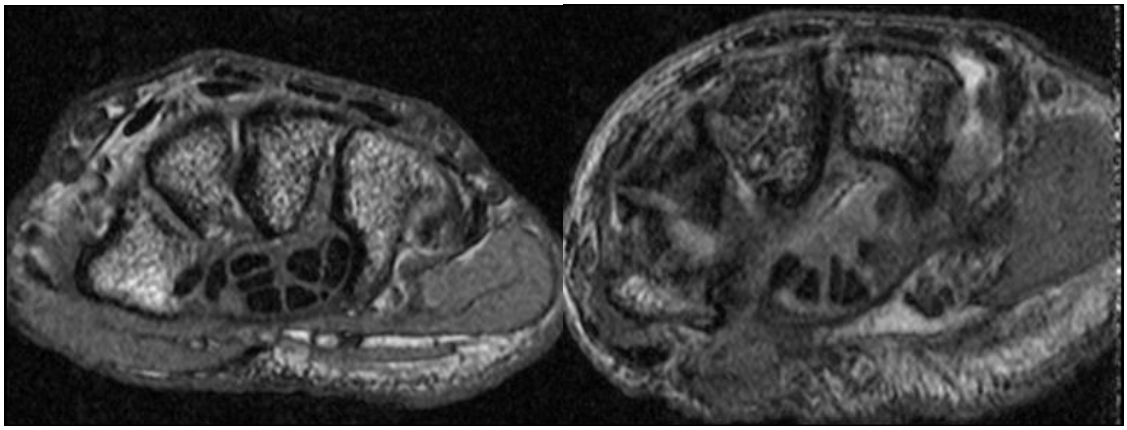

Figure 29. Two MR images within the carpal tunnel. The left image would be fast to segment because nearly all of the tendon boundaries are well defined. The image on the right is affected by the magic-angle effect in half of the tendons so this image would take longer to segment due to the necessary manual editing.

Segmenting the radius and ulna in the wrist and arm scans required approximately 1 minute per image, for a total of 20-30 minutes depending on the number of images containing these bones. Even though the bone segmentation was performed manually, segmenting the bones took much less time than the soft tissues because there were fewer boundaries to segment, and no editing of active contour was necessary.

Tracking the nine flexor tendons' identities from the distal image in the hand using region-growing, and propagating the identifiers through the segmentations, was very fast, usually requiring less than one minute for an entire scan. Typically, the tendon identities were tracked from the hand back to the carpal tunnel through approximately 20 MR images. Rotating the models into the anatomic coordinate system and removing overlaps of the structures each took

approximately 2 – 3 minutes for the entire model, depending on the number of vertices composing each structure (2 minutes for a model containing 4000 vertices and 3 minutes for a model containing 7000 vertices). Resampling to ensure that a sufficient number of vertices surrounded the boundary of each structure on the selected 2D model sections (pisiform and hook-of-the-hamate) required anywhere from 10 – 45 minutes for the entire model. This larger variation in the amount of time needed depended on the number of large faces needing to be resampled. The size of the triangles could not be prescribed in advance and thus the number and size of the triangles depended on how the Matlab function isosurfaced each structure. Computing and tabulating the size, shape, and location measures of the carpal tunnel structures in the selected slices took approximately 2 minutes. To go through the entire image process from MR images to full data tables required approximately 2.5 – 3 hours per scan.

## 4.2 Comparing Size and Shape Measures at the Pisiform and Hook-of-the-Hamate Cross-Sections of the Tunnel

Carpal tunnel contents ratios in the sections through the pisiform and the hook of the hamate were calculated as a validation measure using the cross-sectional areas of the structures on each section. This ratio ranged from 35-66% at the pisiform and 42-65% at the hamate. These values closely overlap the range typically reported (45-60%) at the narrowest part of the tunnel (the hamate)[19, 69], indicating the resulting models were realistic and consistent with prior work. Near-100% contents ratios are precluded by the subsynovial connective tissue which surrounds the tendons and the nerve in the carpal tunnel.

Comparison of the segmented tunnel length for corresponding neutral and flexed models was also performed. The number of MR images segmented from scans acquired while the wrist was in the flexed position was fewer than the number segmented for the neutral position, due to the curvature of the tunnel when the wrist is flexed. However, the tunnel lengths, as computed by summing the distance between tunnel centroids at each MR image level, were only slightly different. The segmented tunnel length in the neutral models was at most 4 mm longer than that in the flexed models. This discrepancy may be due to the respective definitions of the ends of the tunnel with axial MR images. It is probable that the true tunnel ends extend slightly beyond these image positions, and it is likely that the true ends are not parallel, and therefore would not coincide with the axial images deemed to constitute the proximal and distal carpal tunnel ends.

Conventional size and shape measures were obtained from the pisiform and hook-of-the-hamate locations of each model, allowing for changes in cross-sectional area and flattening ratio to be quantified as a function of longitudinal location within the tunnel. The percent change in cross-sectional area from a location near the proximal end of the tunnel (the pisiform) to a location near the distal end of the tunnel (the hook of the hamate) was calculated (Table A-1 and Table A-2). The change in cross-sectional area was investigated to determine if structures generally become smaller or larger as they traversed the length of the tunnel, as the wrist moves from neutral to flexion, or with different loading activities. From the data in Table A-1 and Table A-2 it can be concluded that the tunnel showed a clear trend in cross-sectional area being consistently smaller at the hook of the hamate than at the pisiform for all subjects in all wrist positions and loading activities. This was confirmed by statistical analysis comparing the cross-sectional areas at the two levels, using a paired t-test and a significance

level of 0.05. The resulting p-value for the difference in cross-sectional area of the tunnel between the two levels was 0.0001. The difference in cross-sectional area between the two tunnel levels of the superficial little tendon and nerve were also significant (p-values = 0.01 and 0.04, respectively). The p-values of the other tendons ranged from 0.2 to 0.8. Therefore, no specific trends in cross-sectional area for any of the other tendons were found with respect to longitudinal location in the tunnel, wrist position, or loading activity.

A similar second comparison was made between the flattening ratios for each of the tissue structures in the sections at the levels of the pisiform and the hook of the hamate (Table A-3 and Table A-4). A positive percent increase in the flattening ratio indicated the structure was flatter at the distal end compared to the proximal end of the tunnel. These values were investigated to determine if there was a proximal to distal trend in the flattening ratio of any structures between a neutral and a flexed wrist, or with different hand loading activities. A statistical analysis was performed using a paired t-test and a significance level of 0.05. Two of the tendons (deep long and deep little) showed significant differences in flatness with p-values of 0.03 and 0.015, respectively. The p-values of the other structures ranged from 0.06 to 0.98. Thus, there was no broad trend in flattening ratio for the other tendons, nerve, or tunnel.

## 4.3 Conventional Shape Measures

The flattening ratio is often used to describe the shape of the nerve in the carpal tunnel, but this ratio can only give a general indication of the overall flatness of a structure. Dramatic changes in carpal tunnel soft tissue shapes could sometimes be observed when visualizing the carpal tunnel models, but these changes often were not reflected in the flattening ratio values. For example, in one CTS patient, the nerve flattening ratios calculated at the level of

the pisiform for a neutral wrist and a flexed wrist with no loading activity were nearly equal, with values of 2.0 and 1.9, respectively. However, upon visual examination of the 2D model sections from which those flattening ratios were calculated (Figure 30), the nerve appeared to have extruded between the thumb and index tendons from the volar side to the dorsal side of the tunnel as the wrist moved from neutral to 35 degrees of flexion. The lack of a difference between nerve flattening ratios associated with the wrist motion gave no indication of the probable deformation the nerve underwent during this dramatic change in position.

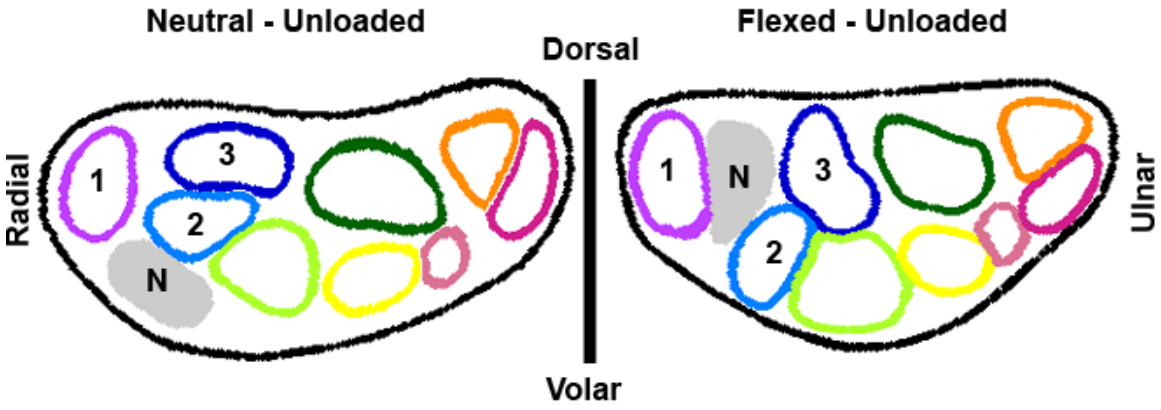


Figure 30. Comparison of CTS Patient 4, neutral (left) and flexed (right) wrist, unloaded, at the pisiform. The nerve (N) appears as the gray structure, which extruded between the thumb (1) and index (2 and 3) tendons, presumably undergoing deformation as it moved. However this associated deformation was not reflected in the flattening ratios (2.0 vs. 1.9).

Similarly, in another CTS subject imaged in both neutral and flexed wrist positions with a squeeze grip loading activity, the nerve flattening ratios were 1.3 and 1.6, respectively (at the level of the pisiform). While there is a slightly larger difference between these two values - reflecting a flattening of the nerve in the

flexed wrist - these ratios still give only a slight indication about the deformation of the median nerve associated with the change in nerve position evident in the 2D model sections (Figure 31). It is evident from visual inspection of the model sections that the nerve extruded between the thumb and index tendons, that the tunnel became significantly rounder, and that there were large transverse movements of the tendons. These large tendon movements (changes in stacking arrangement) presumably caused deformation of the median nerve. However, there was minimal indication of this resulting nerve deformation from the flattening ratios.

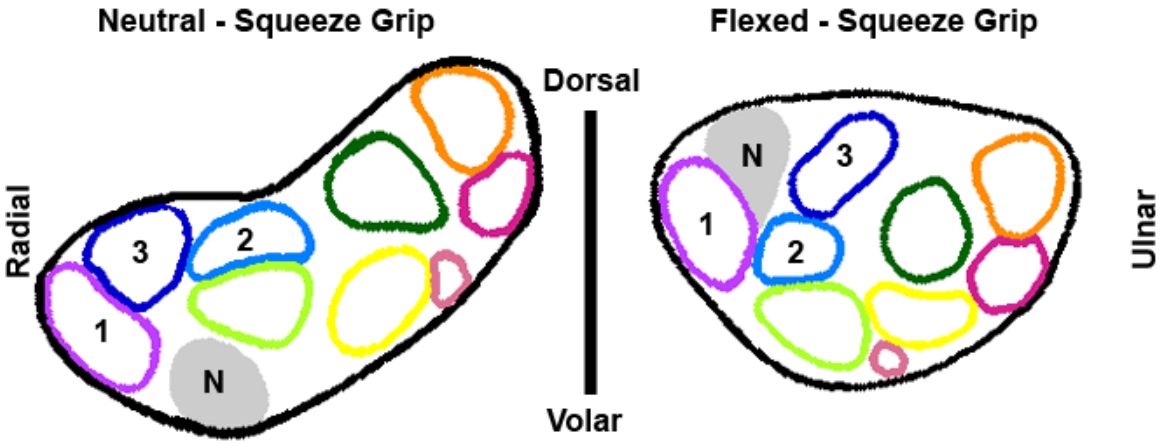


Figure 31. Comparison of CTS Patient 1, neutral (left) and flexed (right) wrist, squeeze grip at the pisiform. The nerve (N) appears as the gray structure. The nerve extruded between the thumb (1) and index (2 and 3) tendons, and there were also large transverse movements of the tendons. This large amount of movement of the carpal tunnel contents during wrist flexion presumably caused deformation to the nerve, which was not evident from the flattening ratios (1.3 vs. 1.6).

The discrepancy between nerve flattening ratio and resulting deformation from the visually apparent nerve position change was also true for normal subjects. For example, one normal subject's neutral wrist with no load had a flattening ratio of 1.8 and the same subject's flexed wrist with no load had a

flattening ratio of 1.75. These flattening ratios were only marginally different, but from the model sections (Figure 32) it is evident that the nerve extruded between the superficial long and ring finger tendons. This slight change in nerve flattening ratio reflected a slight change in shape. There was an evident change in nerve position, indicating the nerve underwent deformation by extruding between tendons.

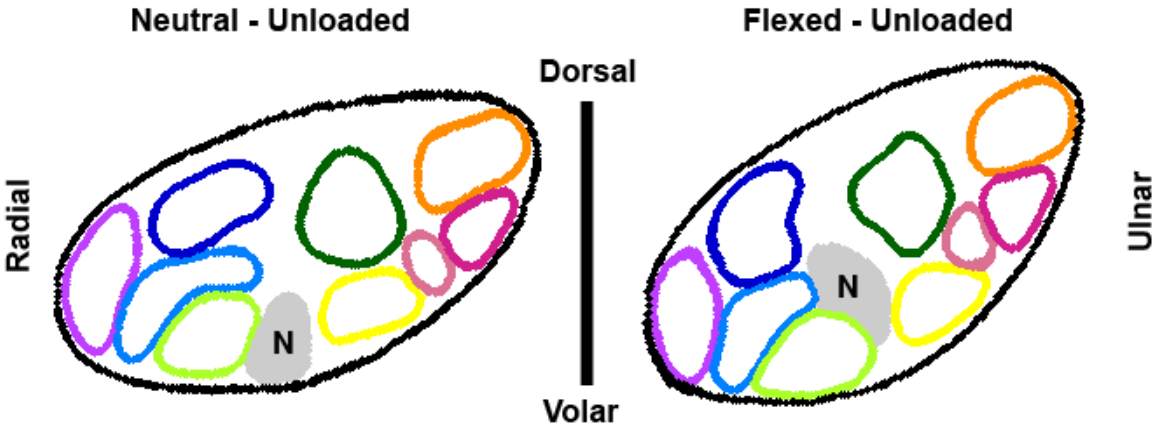


Figure 32. Comparison of Normal Subject 1, neutral (left) and flexed (right) wrist, unloaded, at the level of the hook of the hamate. The flattening ratios are nearly the same (1.8 vs. 1.75), which is not reflective of the nerve deformation. This ambiguity was true for normal subjects and CTS patients.

The often dramatic nerve position and tendon configuration changes were suggestive of noticeable tendon-nerve interaction during wrist motion, but these interactions were not reflected in the conventional flattening ratio. It was apparent that tendons and the nerve markedly shift in position as the wrist flexes. In order to assume a new stacking arrangement, the structures involved needed to slide past one another until the new configuration was reached. During this sliding and transverse movement, multiple tendons may have contacted and impinged upon the nerve. The nerve flattening ratio is too insensitive to register

local deformations, and would never be able to describe rearrangement. Therefore, more descriptive metrics were needed to identify when tendon-nerve interactions occurred, and to identify which of these interactions might have caused appreciable deformation and impingement of the nerve during various loading activities and wrist positions.

## 4.4 Nerve Adjacency Measures

In order to register the shifts in position of the nerve and its neighboring tendons which occurred as the wrist position changed, the identity of each structure adjacent to the nerve (i.e., within 1 mm of the nerve boundary) was determined. From this adjacency information, a total percentage of adjacency was computed, which was defined as the percentage of the nerve boundary adjacent to any structure (tendon or tunnel boundary). A higher percent adjacency indicated that more of the nerve boundary was contacting or closely neighbored by a tendon or by the tunnel boundary. The approximate anatomic direction of each adjacent tendon or the tunnel boundary relative to the nerve was also determined. This nerve adjacency measure was evaluated for the nerve at both the pisiform (Table A-5 and Table A-6) and hook-of-the-hamate (Table A-7 and Table A-8) levels for each of the models processed.

The total percent adjacency of the subjects' nerves at the pisiform ranged from 4% to 90%, versus 24% to 93% at the hook of the hamate. The thumb and tunnel boundary were the structures most commonly adjacent to the nerve at both levels, often in concert with the superficial and deep index and superficial long tendons. It is apparent from Table A-5 through Table A-8 that the deep ring and deep little finger tendons never engaged the nerve in any wrist position or activity, for any of the subjects. The deep long and superficial little finger tendons only rarely engaged the nerve at either level.

Generally, at both the level of the pisiform and of the hook of the hamate, the total percent adjacency increased with the wrist in flexion compared to neutral during all loading activities. Often in wrist flexion, the tendons were shifted volarly and the tunnel became more round, both of which could be responsible for the observed increase in the percent adjacency. However, for the pinch activity, the percent adjacency decreased with the wrist in flexion for most subjects. In subjects where this was most apparent, the nerve was adjacent to the thumb and index finger tendons in the neutral position. Then, while performing the thumb-index pinch activity with the wrist flexed, the nerve was extruded dorsally while the tendons shifted volarly, with the greatest shift observed in the thumb and index finger tendons, which are the tendons involved in the pinch activity. This increased shift caused the percent nerve adjacency to decrease in flexion for the pinch activity.

For all CTS subjects, the total percent nerve adjacency tended to increase from the pisiform level to the hook of the hamate (proximal to distal). This is most likely due to the narrowing of the cross-sectional area of the tunnel at the hook of the hamate compared to the pisiform, as previously discussed (Table A-1 and Table A-2). For normal subjects, there were more cases of a slight decrease in the percent of nerve adjacency when moving proximal to distal compared to the CTS subjects. However these percent adjacencies were only marginally different (for example, 30% at the pisiform versus 23% at the hook of the hamate) compared to the dramatic differences seen in the CTS subjects (58% at the pisiform and 85% at the hook of the hamate). Upon comparing the overall percent adjacencies of the nerve both at the level of the pisiform and at the hook of the hamate, normal Subject 4 was an outlier, whose nerve showed substantially more variation in the amount of adjacency to other structures during the various wrist poses and activities, ranging from 15% to 81% (65% span) at

the pisiform and 25% to 86% (61% span) at the hook of the hamate. Ranges of adjacency for the wrist positions and activities for the other subjects typically spanned at most 40% at both levels.

Nerve adjacency is a useful measure for determining which wrist positions and activities increase the risk of impingement to the median nerve, since this increased risk would most likely occur when the nerve adjacency increases. It was observed, based on the amount of adjacency, that for most activities (excluding the thumb-index pinch), the nerve was at higher risk of impingement in the flexed wrist position as opposed to the neutral position. For all loading activities and for wrist flexion, this risk was also higher at the narrowest part of the tunnel (the hook of the hamate) than at the pisiform.

In addition to knowing which structures were adjacent to the nerve and the amount of the nerve boundary that was adjacent to other structures, it was informative to have the locations of these adjacencies. Changes in adjacency locations indicated structure rearrangement within the carpal tunnel, likely affecting the median nerve. Table A-9 though Table A-12 show the approximate anatomic direction of each tissue structure that was determined to be adjacent to the nerve. Locations in these tables are specified as radial (R), ulnar (U), dorsal (D), volar (V), or a combination of two directions.

Often the tunnel was volarly adjacent to the nerve in a neutral wrist, but became dorsally adjacent in the flexed position. The thumb tendon was generally radially adjacent in the neutral position and volarly (or volar-radially) adjacent in the flexed wrist position. The directions of the superficial and deep index and superficial long tendons were more variable. By comparing the locations of each structure between different wrist positions, it was readily apparent when the nerve had changed its relative position.

For example, considering one of the CTS subjects at the level of the pisiform with no load, moving from neutral to flexion, the position change of the nerve visible in Figure 33 was also apparent when comparing the relative locations of adjacent structures cataloged in Table A-9 (CTS – 1).

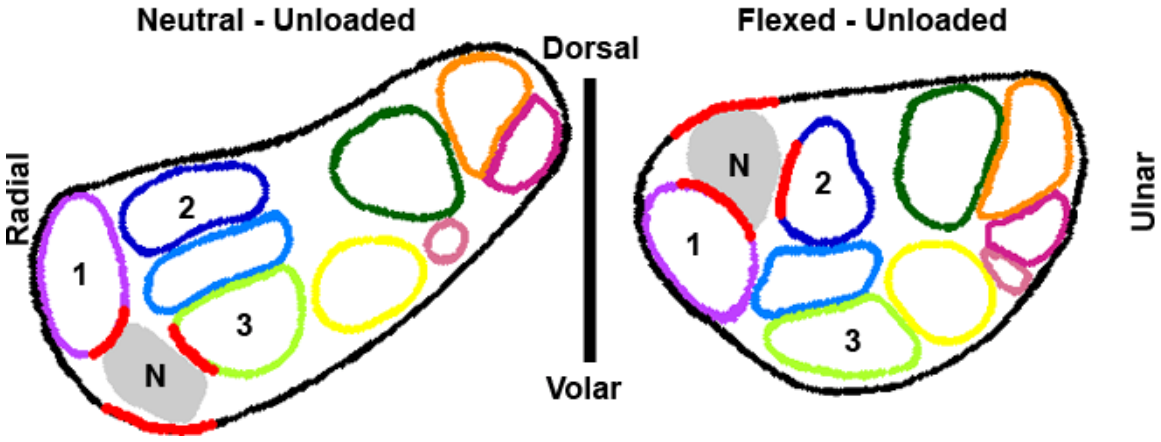


Figure 33. CTS Subject 1, neutral (left) and flexed (right) wrist, unloaded, at the level of pisiform. Red points indicate locations where the structure is adjacent (within 1mm) to the nerve. A nerve (N) extrusion from the volar to the dorsal side is apparent. The thumb tendon (1) appears on a different side of the nerve and the deep index (2) and superficial long (3) tendons move into and out of adjacency, respectively.

The position change was especially evident in the different location of the tunnel boundary relative to the nerve. In the neutral wrist position, the tunnel boundary was located volarly, while in the flexed wrist position the tunnel boundary was located dorsally. This difference in location indicates that the nerve was extruded through the tendons from the volar side of the tunnel to the dorsal side during wrist flexion. In this same pair of scans, the superficial long tendon, which was dorsal-ulnarly adjacent to the nerve in the neutral position, was no longer within 1 mm of the nerve in the flexed position.

Similarly, the deep index tendon, which did not engage the nerve in the neutral wrist position, became ulnarly adjacent to the nerve in the flexed wrist position. Additionally, the thumb tendon appeared on a different side of the nerve when the wrist moved from neutral to flexion (dorsal-radially and volar-radially, respectively). These changes in direction of the adjacencies of tissue structures to the nerve are fully consistent with the drastic movement apparent in Figure 33, and indicate probable nerve deformation during its change of relative position. This information was not available from the conventional nerve flattening ratios of 1.8 versus 1.4 for the neutral and flexed wrist positions, respectively.

The adjacency metric worked equally well for the normal subjects. For example, at the level of the hook of the hamate, a normal wrist with a flat press activity demonstrated an apparent change in nerve position, as cataloged in Table A-12 (Norm – 4), as the wrist moved from neutral to flexion (Figure 34).

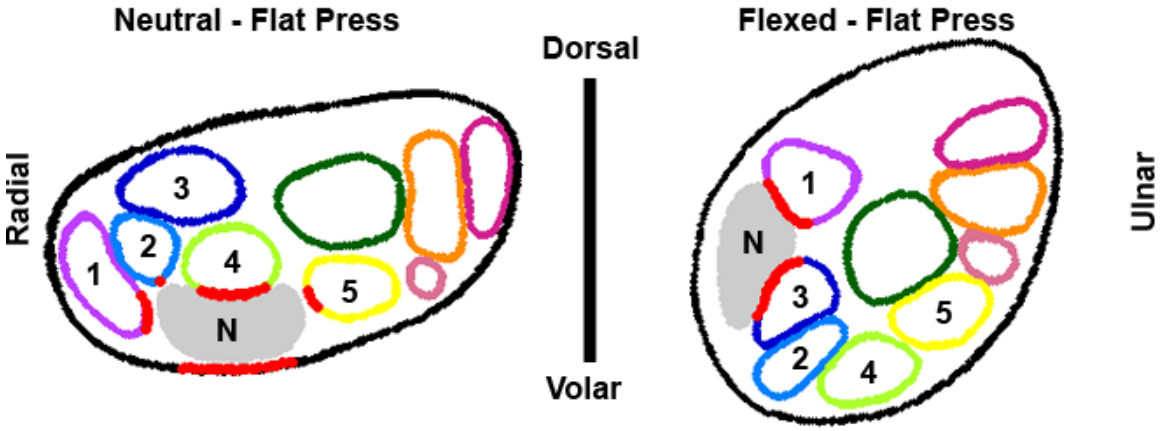


Figure 34. Comparison of Normal Subject 4's neutral (left) and flexed (right) wrist at the level of the hook of the hamate during a flat press activity. Red points indicate locations where the structure is adjacent (within 1 mm) to the nerve. The nerve (N) moves from the volar side of the tunnel to the radial side with wrist flexion. The thumb tendon (1) appears on a different side of the nerve. The tunnel and superficial index (2), long (4), and ring (5) tendons move out of adjacency, while the deep index tendon (3) moves into adjacency.

In the neutral wrist position, the tunnel boundary was volarly adjacent to the nerve, while in the flexed wrist position the tunnel boundary was no longer within 1 mm of the nerve. The thumb tendon appeared on a different side of the nerve in the flexed position (dorsal-ulnarly) than in the neutral position (radially). Additionally, the superficial index, long, and ring finger tendons and the tunnel boundary, which were adjacent to the nerve in the neutral wrist position (dorsal-radially, dorsally, ulnarly, and volarly, respectively), were no longer within 1 mm of the nerve in the flexed wrist position. However, the deep index tendon moved into adjacency with the nerve in the flexed wrist position (volar-ulnarly).

Based on such observations, these novel measures of adjacency hold attraction for meaningfully describing abnormalities and variants of relative positions of carpal tunnel soft tissue structures, information which is not available from the conventional nerve flattening ratio. For the purpose of comparison, an extrusion event was implicit when tissue structures adjacent to the nerve appeared on a different side of the nerve in the flexed position than in the neutral position, for a given loading activity. Based on this definition, every subject but one had a nerve extrusion for at least two of the loading activities. It was not possible to determine extrusion events for CTS Subject 3, because this individual had only one successful MRI segmented in flexion (unloaded), and no nerve extrusion occurred in that instance. The difference in nerve flattening ratios of the models at the level of the hook of the hamate was less than 1.0 for all but three of the extrusion events. For these three, the difference was less than 1.75. Thus, in general, the nerve flattening ratios gave indication of minor changes in the flatness of the nerve, but no indication that these differences were associated with nerve extrusion events.

## 4.5 Shape Number Coding Measure

While the nerve adjacency measures gave indication of which neighboring structure(s) may have caused insult to the nerve, this measure did not quantify the degree of insult, as indicated by local tissue deformations. Nerve flattening ratios were found by fitting a single ellipse to the boundary, making these ratios insensitive to local deformation in the nerve boundary. Thus, in order to assess what compressive insults might have occurred, the shape number coding measure was employed. The shape numbers assigned to the boundary showed the occurrence of local deformations. A chain of shape numbers for a nerve was composed of 20 or more individual numbers effectively representing the local contour of the boundary at specific intervals. Thus, there were many samplings to represent the shape of the entire boundary, whereas the flattening ratio combined all boundary information into one single number representing the overall shape. An elliptical boundary with no severe local changes would have a shape number chain composed of low numbers (0-2), whereas a chain containing higher numbers would indicate a more pronounced curvature, or a pinch, distorting the shape of the boundary from a smooth ellipse. Negative shape numbers indicated a portion of the boundary which was compressed inward, or indented, toward the center of the structure. Analyzing chains of shape numbers calculated for the nerve boundary can thus indicate that a neighboring structure might be impinging inwardly on the nerve, or that the nerve was being pinched between two neighboring structures.

Severe local distortions in the nerve boundary were considered to be at points where the shape number was greater than or equal to a 3, which corresponded to a boundary angle change of at least 50-70 degrees over a boundary length of 1 mm. Since smooth, elliptically shaped boundaries have shape numbers of 0-2, a 3 was selected as the lower end of more drastic

boundary changes. The largest shape number measured in this work was an 8, resulting from a squeeze grip activity. Because each line segment was 0.5 mm in length, the length of the pinched or impinged region could be calculated. Such lengths in a loaded or flexed wrist position were compared to those in the neutral unloaded wrist, to gain a sense of whether these features actually were pinches or indentations, or if the shape number anomaly resulted merely from the intrinsic shape of the individual's nerve. Visual comparison of the shape number values versus adjacency location information indicated which neighboring structures might be directly affecting the nerve, causing pinch or impingement instances in the local nerve boundary. Shape number chains at the pisiform and hook of the hamate are provided in Table A-13 through Table A-16.

As described in the Methods section, the locations of local pinches and impingements were highlighted in red on a plot of the data points where shape numbers were calculated. By comparing these locations of more severe local deformation with the nerve adjacency plot, it was possible to determine which neighboring structures were affecting the nerve. For example, a section at the hook of the hamate from a CTS subject performing a flat press activity with a neutral wrist position (Figure 35) showed a pinch on the dorsal side of the nerve, where the corresponding shape number chain value was 3 (representing an angle change between 50 and 70 degrees). The nerve at this point was radially adjacent to the thumb tendon and dorsally adjacent to the superficial index tendon (Table A-11, CTS - 3). Based on chain and adjacency data, it is clear that these two tendons were causing a local pinch on the nerve boundary. On the ulnar side of the nerve there were two shape numbers equal to 3. The nerve was not immediately adjacent to any structures at these points. However the pinch may have been caused by the dorsal-ulnarly adjacent superficial long tendon and the volarly adjacent tunnel boundary. On the side of the nerve

adjacent to the superficial index tendon, there were negative shape number values, indicating that this tendon was impinging on the nerve.

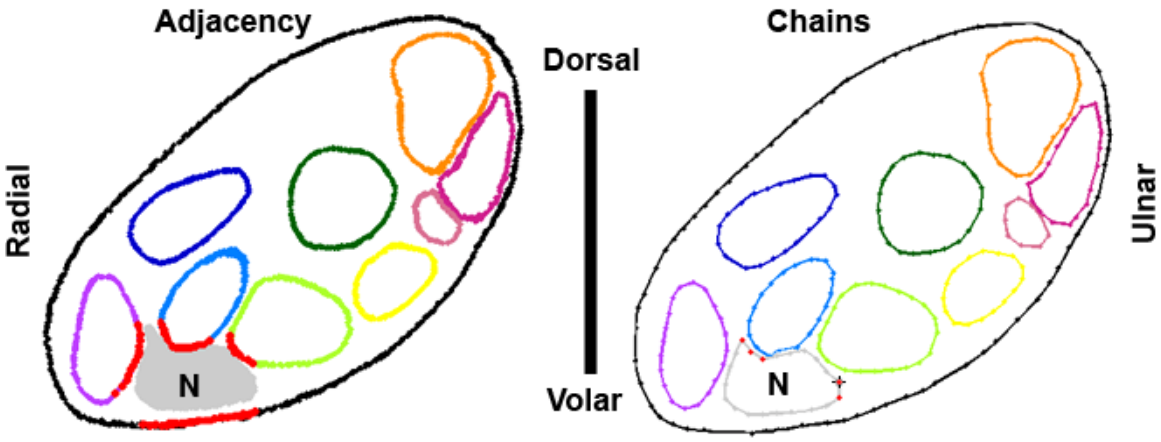


Figure 35. Comparison of adjacency (left) and chain (right) measures for CTS Patient 3, neutral wrist, flat press, at the hook of the hamate. Red points on the adjacency plot indicate locations where the structure is adjacent (within 1 mm) to the nerve. Nerve shape number values begin from the black asterisk and continue clockwise around the boundary. Chain values in bold correspond to points plotted in red: **3**, **3**, 1, 0, 0, 0, 0, 1, 1, 2, 1, 0, 0, **3**, **-1**, **-2**, 0, 0, 2, 1, 0

In another CTS subject performing the squeeze grip activity in a neutral wrist position, an example of a tendon impinging on the nerve can be seen in the comparison of the shape number and adjacency location plots (Figure 36). On the dorsal side of the nerve, there was a string of -1 shape number values at the same location where the nerve was adjacent to the superficial long tendon (Table A-11, CTS - 6). This chain of shape numbers indicates that the superficial long tendon was impinging heavily on the median nerve boundary. Because there were four -1 shape number values in the string (which was formed by 5 line segments each 0.5 mm in length), the length of this impingement region was 2.5 mm. These two examples, the pinch and the impingement, illustrate the

usefulness of these novel measures of adjacency and chain values for meaningfully describing local deformations of carpal tunnel structures.

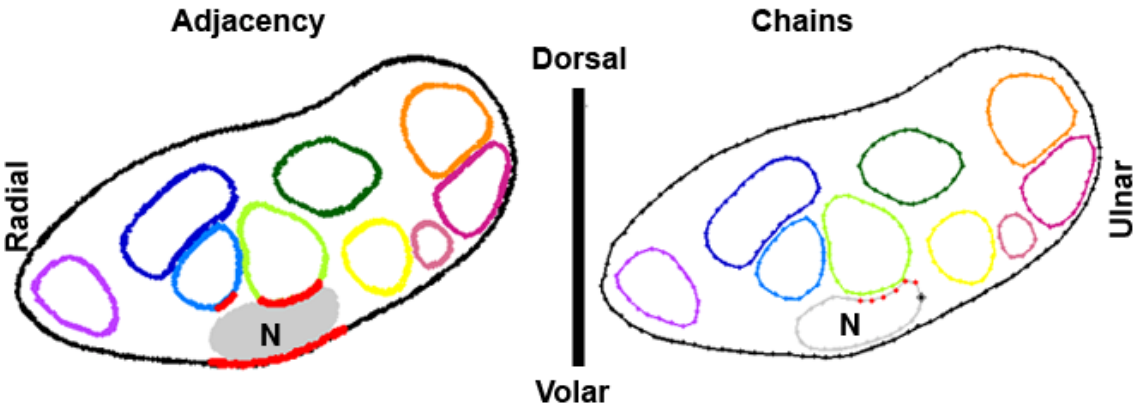


Figure 36. Comparison of adjacency (left) and chain (right) measures for CTS Patient 6, neutral wrist position, squeeze grip, at the hook of the hamate. Red points on the adjacency plot indicate locations where the structure is adjacent (within 1 mm) to the nerve. Nerve chain values begin from the black asterisk and progress clockwise around the boundary. Chain values in bold represent pinch and impingement instances, and they correspond to locations on the plot highlighted in red: 1, 1, 1, 0, 1, 0, 0, 0, 0, 0, 1, 2, 2, 2, 1, 0, 2, 0, **-1**, **-1**, **-1**, **-1**, **3**, **3**

## 4.6 Comparison of CTS and Normal Subjects

The localized deformation of the nerve was quantified in terms of numbers of pinch and impingement instances in the nerve shape number chains. The average numbers of these occurrences were calculated to facilitate various comparisons between the subject groups, activities, and wrist positions. Table 2 shows the average number of impingement and pinch instances at the level of the pisiform and hook of the hamate for the CTS and normal groups for the two wrist positions. The average numbers of pinch and impingement instances were added to determine the total average number of instances of local deformation around the nerve boundary. Because CTS arises due to mechanical insult of the

median nerve, it was expected that the CTS subjects would have more pinch and impingement instances than the normal subjects. From Table 2 it is apparent that the total number of localized deformation instances was indeed higher for the CTS patient group than for the normal subjects group. This was true for both the neutral and the flexed wrist positions, at both the level of the pisiform and of the hook of the hamate. However, the difference between the two groups reached statistical significance only at the level of the hook of the hamate in the neutral wrist position (p-value = 0.0002).

Table 2. Comparison of average number of pinch and impingement instances between the CTS patient and normal subject groups at the pisiform and hook of the hamate for both wrist positions.

| Level | Group | Wrist Position | Average # of Pinch Instances | Average # of Impingement Instances | Total Average # of Instances | Average % Adjacency |
|---|---|---|---|---|---|---|
| Pisiform | CTS | Neu | 0.7 | 0.6 | 1.2 | 49 |
| | | 35F | 1.0 | 0.8 | 1.8 | 53 |
| | Norm | Neu | 0.9 | 0.3 | 1.1 | 60 |
| | | 35F | 1.0 | 0.6 | 1.6 | 53 |
| Hook of the Hamate | CTS | Neu | 1.4 | 1.4 | 2.9 | 64 |
| | | 35F | 1.2 | 1.1 | 2.3 | 61 |
| | Norm | Neu | 0.8 | 0.7 | 1.5 | 61 |
| | | 35F | 1.0 | 0.9 | 1.9 | 57 |

Because of the decreased carpal tunnel cross-sectional area at the level of the hook of the hamate, it was expected there would be more pinch and impingement instances for both groups at the hook of the hamate compared to the level of the pisiform. This expectation was in fact borne out in both the neutral and the flexed wrist positions in the CTS group. The largest increase in the number of local deformation instances (from 1.3 to 2.8), occurred with a neutral wrist position moving from the level of the pisiform to the hook of the hamate, which corresponded to the largest change in the percent adjacency of

the nerve (from 49% to 64%). By comparison, the average number of instances in the nerve boundary for the normal group showed only slight changes for the different levels and wrist positions.

Table 3 shows the average number of pinch and impingement instances at the proximal (pisiform) and distal (hook of the hamate) carpal tunnel levels for both groups in the loaded (average of instances for all loading activities) versus unloaded neutral wrist position. Only slight changes were observed for both the CTS patients and normal subject groups at both the level of the pisiform and the level of the hook of the hamate. A slight decrease in the number of deformation instances occurred in the CTS group at the hook of the hamate upon loading, however, there were still many more instances in the CTS group than in the normal group. A large increase in the number of localized deformation instances is again apparent in the CTS group at the hook of the hamate compared to the pisiform.

Table 3. Comparison of average number of pinch and impingement instances between the CTS patient and normal subject groups at the pisiform and hook of the hamate for the loaded and unloaded neutral wrist position.

| Level | Group | Load | Average # of Pinch Instances | Average # of Impingement Instances | Total Average # of Instances | Average % Adjacency |
|---|---|---|---|---|---|---|
| Pisiform | CTS | Unloaded | 0.6 | 0.3 | 0.9 | 44 |
| | | Loaded | 0.7 | 0.7 | 1.4 | 51 |
| | Norm | Unloaded | 1.0 | 0.0 | 1.0 | 55 |
| | | Loaded | 0.8 | 0.3 | 1.1 | 61 |
| Hook of the Hamate | CTS | Unloaded | 1.7 | 1.1 | 2.9 | 59 |
| | | Loaded | 1.3 | 1.6 | 2.9 | 66 |
| | Norm | Unloaded | 0.4 | 0.4 | 0.8 | 59 |
| | | Loaded | 0.9 | 0.8 | 1.7 | 61 |

Table 4 shows the average number of pinch and impingement instances at both the proximal and distal carpal tunnel levels for both groups in the neutral

wrist position, for each of the hand loading activities. The activity which resulted in the fewest pinch and impingement instances for the CTS patient group was the squeeze grip and for the normal subject group was the flat press. Additionally, the index-thumb pinch generally resulted in the most pinch and impingement instances for both groups. For the CTS group, the index-thumb pinch activity had the highest number of deformation instances at the both the level of the pisiform (2.2, vs. 2.0 for the normals) and hook of the hamate (3.0, vs. 2.0 for the normals). For the normal group, the index-thumb pinch activity also had the highest number of instances at the pisiform; however, the squeeze grip activity had a slightly higher number at the hook of the hamate (2.2, vs. 2.5 in the CTS patient group). At the level of the hook of the hamate, the lowest number of deformation instances in the CTS group was 2.5 (occurring with the squeeze grip activity). This value was still larger than the largest number of deformation instances in the normal group (2.2 with the squeeze grip activity).

Table 4. Comparison of average number of pinch and impingement instances at the pisiform and hook of the hamate for each loading activity in the neutral wrist position of the CTS patient and normal subject groups.

| Level | Group | Activity | Average # of Pinch Instances | Average # of Impingement Instances | Total Average # of Instances | Average % Adjacency |
|---|---|---|---|---|---|---|
| Pisiform | CTS | NL | 0.6 | 0.3 | 0.9 | 44 |
| | | FP | 0.8 | 0.7 | 1.5 | 55 |
| | | SG | 0.2 | 0.3 | 0.5 | 48 |
| | | IP | 1.2 | 1.0 | 2.2 | 50 |
| | Norm | NL | 1.0 | 0.0 | 1.0 | 55 |
| | | FP | 0.4 | 0.0 | 0.4 | 52 |
| | | SG | 1.0 | 0.6 | 1.6 | 66 |
| | | IP | 1.0 | 1.0 | 2.0 | 66 |
| Hook of the Hamate | CTS | NL | 1.7 | 1.1 | 2.9 | 59 |
| | | FP | 1.5 | 1.5 | 3.0 | 66 |
| | | SG | 0.7 | 1.8 | 2.5 | 72 |
| | | IP | 1.8 | 1.3 | 3.2 | 61 |
| | Norm | NL | 0.4 | 0.4 | 0.8 | 59 |
| | | FP | 0.6 | 0.4 | 1.0 | 54 |
| | | SG | 1.2 | 1.0 | 2.2 | 67 |
| | | IP | 1.0 | 1.0 | 2.0 | 63 |

Table 5 shows the average number of pinch and impingement instances at both the proximal and distal carpal tunnel levels for both groups in a flexed wrist position with various hand loading activities. With a flexed wrist, the CTS group showed the fewest pinch and impingement instances during the flat press activity, while the normal group had its fewest instances for the index-thumb pinch activity. The CTS group had its most instances of localized deformation for the index-thumb pinch and squeeze grip activities, and the normal group had its most for the squeeze grip (at the pisiform) and index-thumb pinch (at the hook of the hamate) activities.

Table 5. Comparison of average number of pinch and impingement instances at the pisiform and hook of the hamate for each loading activity in the flexed wrist position of the CTS patient and normal subject groups.

| Level | Group | Activity | Average # of Pinch Instances | Average # of Impingement Instances | Total Average # of Instances | Average % Adjacency |
|---|---|---|---|---|---|---|
| Pisiform | CTS | NL | 0.6 | 0.6 | 1.1 | 59 |
| | | FP | 1.0 | 0.7 | 1.7 | 49 |
| | | SG | 1.5 | 1.0 | 2.5 | 57 |
| | | IP | 1.3 | 1.0 | 2.3 | 44 |
| | Norm | NL | 1.0 | 0.4 | 1.4 | 54 |
| | | FP | 1.0 | 0.6 | 1.6 | 50 |
| | | SG | 1.2 | 1.0 | 2.2 | 64 |
| | | IP | 0.8 | 0.4 | 1.2 | 43 |
| Hook of the Hamate | CTS | NL | 1.4 | 1.0 | 2.4 | 68 |
| | | FP | 1.2 | 0.7 | 1.8 | 57 |
| | | SG | 0.8 | 1.7 | 2.5 | 63 |
| | | IP | 1.5 | 1.3 | 2.8 | 52 |
| | Norm | NL | 1.2 | 1.0 | 2.2 | 55 |
| | | FP | 0.6 | 1.0 | 1.6 | 51 |
| | | SG | 1.6 | 1.0 | 2.6 | 66 |
| | | IP | 0.4 | 0.6 | 1.0 | 55 |

In general, there was no consistent trend evident for either group in terms of a specific number of local deformation instances resulting from any given activity when it was performed in either of the wrist positions. However, the

activities and the wrist positions which resulted in the highest number of localized deformation instances were usually the ones which showed the highest average percent adjacency of the nerve. It was generally true that the activities which resulted in the fewest instances of deformation were the activities which showed the lowest average percent adjacency of the nerve.

Overall, a higher incidence of local deformation instances was associated with the CTS patients. This was especially evident at the hook of the hamate, compared to the pisiform. Table 6 shows a summary of the expected relationships, the actual observed relationships, the resulting p-values, and whether or not the expectation was met. Fulfillment of the expectation was based on a significance level of 0.05, however, some of the expectations would be nearly fulfilled at the 0.1 significance level. Only the expectation that the CTS group would have a higher number of deformations with a squeeze grip activity than the normal group performing a squeeze grip activity had an observed relationship that was opposite from the expected relationship. In summary, the two new metrics (nerve adjacency and shape numbers) showed the CTS patient group had higher levels of nerve percent adjacency and more local nerve deformations than the normal subject group. Both of these observations have implications for CTS.

Table 6. Summary of the expected and the actual observed relationships at the hook of the hamate section.

| | Expected Relationship | Observed Relationship | p-value | Expectation Fulfilled? |
|---|---|---|---|---|
| **Nerve Percent Adjacency** | Average CTS % Adjacency > Average Normal % Adjacency | Average CTS % Adjacency > Average Normal % Adjacency | 0.12 | ~ |
| **Deformation Instances in a Neutral Wrist** | Average Neutral CTS Deformations > Average Neutral Normal Deformations | Average Neutral CTS Deformations > Average Neutral Normal Deformations | 0.0002 | ++ |
| **Deformation Instances in a Flexed Wrist** | Average Flexed CTS Deformations > Average Flexed Normal Deformations | Average Flexed CTS Deformations > Average Flexed Normal Deformations | 0.12 | ~ |
| **Deformation Instances in a Loaded Hand** | Average Loaded CTS Deformations > Average Loaded Normal Deformations | Average Loaded CTS Deformations > Average Loaded Normal Deformations | 0.009 | ++ |
| *Flat Press* | Average Flat Press CTS Deformations > Average Flat Press Normal Deformations | Average Flat Press CTS Deformations > Average Flat Press Normal Deformations | 0.02 | + |
| *Squeeze Grip* | Average Squeeze Grip CTS Deformations > Average Squeeze Grip Normal Deformations | Average Squeeze Grip CTS Deformations < Average Squeeze Grip Normal Deformations | 0.4 | - - |
| *Index-Thumb Pinch* | Average Pinch CTS Deformations > Average Pinch Normal Deformations | Average Pinch CTS Deformations > Average Pinch Normal Deformations | 0.075 | ~ |

# CHAPTER V. DISCUSSION

As the diagnosis of carpal tunnel syndrome increases, an understanding of the mechanisms of insult to the median nerve which lead to its development becomes ever more imperative. Knowledge of the exact cause of CTS could lead to improved diagnostic and treatment methods, or more importantly, to better preventative measures. The goal of this study was to investigate interactions of structures within the carpal tunnel during wrist flexion and hand loading, in order to obtain information about one specific mechanism of insult to the median nerve. Symptomatic and normal subjects were compared to observe differences in the interactions of the median nerve with its surrounding structures. New methodology was developed to facilitate the evaluation of these populations.

This work describes a new approach to obtain shape and location information about the individual digital flexor tendons, the median nerve, and the carpal tunnel. This information was obtained after semi-automatically segmenting the carpal tunnel structures through a series of MR images, automatically tracking the individual identities of the digital flexor tendons into the carpal tunnel, and registering these segmentations to an anatomic coordinate system. This method is not dependent on the size of anatomic structures, the position of the wrist, or the loading activity used during scanning. Registering the segmentations to the same coordinate system afforded inter- and intra-subject comparisons of changes in the transverse location and shape of each of the individual tendons/nerve within the carpal tunnel during various hand loading activities. Knowing the individual tendon locations and shapes relative to the nerve location and shape for both of the subject populations has provided information about interactions which may potentially contribute to CTS.

From this work, it is evident that there is interaction between the nerve and the adjacent tendons which results in local pinches and impingements in the nerve boundary. These deformations were observed in both subject groups, but there were more in the CTS patients. No significant change in the number of pinch and impingement instances was found for the normal subject group between the two wrist positions or at the two tunnel levels (pisiform and hook of the hamate). However, large changes in the number of such instances were apparent in the CTS subject group between the two tunnel levels. The use of a hand/finger loading activity and/or wrist flexion caused the number of pinch and impingement instances in the nerve boundaries of both groups to increase relative to the unloaded, neutral wrist position. All of the loading activities elicited increased pinch and impingement in the nerve boundaries, although no one activity stood out as causing more of an effect than the others. The increase in the number of deformation instances was especially evident at the hook of the hamate for the CTS subject group.

## 5.1 Image Processing Challenges and Limitations

The first limitation of this work is a classic one in image processing: how to fully automate segmentation of boundaries which are relatively imperceptible to the human eye. This was overcome by allowing manual editing of each image by a user. Thus, the developed segmentation method was a semi-automated process. Boundaries which could not be accurately segmented automatically occurred when there was little distinction between tendon regions, or when the visibility of the tendon region on the image faded, as with the magic-angle effect. In both of these situations, the tendon boundary was difficult for the user to distinguish while only looking at just the one image. Often the boundary became

more apparent by scrolling through the series of adjacent images and observing how the location, size, and shape of the tendon changed from image to image.

Occasionally, when selecting a distal image in the hand for the tendon identity tracking algorithm (the image which best displayed the tendons as pairs of superficial and deep tendons running to each finger), the FPL (thumb) tendon had faded due to magic-angle effect as it wrapped around the trapezium. However, because this tendon was always located on the radial side of the carpal tunnel, it was the easiest tendon to distinguish in all of the image series. In cases where the FPL was not visible in the selected starting image, the remaining eight tendons were identified on the distal image in the hand, and then were tracked back to the distal carpal tunnel image. The remaining unidentified tendon was then identified as the FPL tendon. There were also some situations in the tendon tracking algorithm when tendon regions grew together due to a lack of definition between the two structure boundaries on an image. However, once the majority of the tendons on the distal carpal tunnel image were identified by the tracking algorithm, it became easy to manually identify any remaining tendons using process of elimination.

Agreement between resulting carpal tunnel contents ratios and those found in previous work served as the primary means of validation of segmentation accuracy for this study. If one wanted to definitively evaluate accuracy of the segmentations, more extensive validation using a cadaver wrist could be performed. This wrist would first need to be fixed in a known position prior to MR imaging, and would then need to be imaged at known slice locations. The resulting images would be processed using the present new methodology, and measures of the structures from each MRI slice would be obtained. The wrist could then be dissected through the imaging axis at the exact slices where images were obtained. Physical measures (cross-sectional area and flattening

ratio) of the structures in these sections could be obtained and compared to those found using the image processing method.

A number of critical parameter values were used in the image processing method. The first was the number of iterations through the active contour algorithm. One hundred iterations was selected as the maximum number of iterations, purely on the empirical basis that accurate contours were grown without taking a disproportionate amount of time. Because the stopping criteria for the active contour growing were also based on the area within the growing contour, the algorithm did not always progress through 100 iterations. A substantial change in the resulting segmentation would not have been observed if more than 100 iterations had been allowed, because the initial contour used to grow the new contour was very similar to the new contour that was needed, since it was from the same tendon on an image only 1 mm away. The area limits were selected as being 20% greater than or less than the initial area within a boundary. This was also selected on the basis of the initial contour being similar to what the new contour should be, as well as the fact that the cross-sectional area of the tendon would not be expected to grow or shrink considerably in just 1 mm. If smaller area limits had been used, the contours might not have fully reached the region boundary; if larger area limits had been used more region overgrowth would most likely have occurred.

In the active contour algorithm, the parameter *mu* was set to 0.1* 255^1.5, approximately 400. This parameter must be greater than zero, and often ranges from 0.2 to 3000. A small value is used when fine details in the object boundary need to be detected, resulting in a jagged contour – especially when noise is present in the image. A large value of *mu* (on the order of 130,000) is used in situations where the contour must enclosed an object formed by grouping, for example, enclosing multiple dark circles on a light background in only one

contour. For this work, *mu* was set to an intermediate value since the tendon boundaries should be relatively smooth and unaffected by noise, but are not formed by a grouping of discrete objects. A smaller value of *mu* (for example 0.2) was observed to result in more jagged boundaries. A much larger value of *mu* was not evaluated since it would be expected to smooth away some of the anatomic detail in the tendon boundaries, perhaps resulting in perfectly smooth or even circular boundaries.

A separation gap of 0.2 mm was specified in the algorithm to ensure neighboring structures did not overlap and to reinforce that no structure would be closer than 0.2 mm from the nerve boundary, which facilitated finite element meshing for stress analysis studies. A value of 0.2 mm was selected because it was equal to the minimum length of an edge of the elements used to create a fluid mesh between the carpal tunnel structures. It is also important to note that when an overlap existed, the accommodation was made by modification of only one structure's surface rather than by splitting the difference between the two structures' surfaces, which would also remove the overlap. Fortunately, the observed overlap distances were small; therefore these two methods would have nearly the same results.

In the model cross-section selection algorithm, the range of z-values used to isolate a cross-section of the model was 0.7 mm. This range was necessarily a judgment based on what resulted in a sufficient number of vertices composing each boundary for the purpose of making adjacency, area, and shape number chain measures. A smaller range resulted in too few vertices surrounding a boundary, and a larger range resulted in a thick, blurred boundary, especially when the structures had highly curved or tortuous trajectories, such as at the hook of the hamate in the flexed models.

For the nerve adjacency measure, adjacent structures were determined in 5 degree increments around the nerve boundary. This value resulted in adjacency being determined at 72 points around the nerve boundary, which was deemed sufficient considering the relatively small size of the nerve (on the order of 10 $mm^2$). Points along a structure boundary which were adjacent to the nerve would have been missed if the increment had been increased, as a result of which the percent adjacency of each structure to the nerve would not have been as accurate a reflection of the actual adjacency. The choice of 1 mm proximity as the condition for constituting adjacency was also a judgment, based on image resolution, segmentation precision, and 3D model generation. The pixel spacing was 0.2 mm, which was equal to the separation gap, so this constituted the lower limit of what might be considered adjacent. Visualization of the adjacency radius around nerve boundaries were used to determine that 1 mm reasonably captured the adjacent structures. Smaller values (such as 0.5 mm) missed boundary points which appeared to be adjacent, and larger values (such as 2 mm) included boundary points which appeared too far from the nerve to be considered adjacent.

In developing the chains of shape numbers, the length of the line segments used to surround the boundary was 0.5 mm, which was determined by visual inspection of a number of different lengths. Line segments less than 0.5 mm in length resulted in longer chains of shape numbers, but did not detect any changes in the boundary which were not equally reflected by the 0.5 mm line segments. As the length of the line segment increased from 0.5 mm, important variations in the boundary were increasingly omitted.

Shape numbers were assigned to each angle using 20 degree slope change increments. This value was selected because it resulted in a reasonable number (17) of different shape numbers (-8 through 8) to describe a boundary.

Had a smaller increment been used, the differences in the slope changes would have become more difficult to distinguish, and had a larger increment been used, the shape numbers would have represented too large a difference in the slope change of the boundary, such that pinches would no longer be easily distinguished in the chains. Severe local deformations in the nerve boundary were considered to be at points where the shape number was greater than or equal to a 3, which corresponded to a boundary angle change of at least 50-70 degrees over 1 mm of nerve boundary. This value was selected on the basis that shape numbers composing regularly shaped boundaries (circular and ellipsoidal) ranged from 0 to 2. Therefore, 3 was selected as the lower shape number limit of more drastic changes in the boundary.

Because each line segment composing the shape number chains was of a known length, the length of a pinched or impinged region could be calculated and compared for different wrist positions and hand loading activities. The boundaries could have instead been composed of an equal number of line segments, which would have allowed comparison of chains number-by-number. However, this type of comparison would require that the starting points of the chains be identical in each and every data set. Also, the number of line segments needed to accurately reflect all of the changes in the boundary would depend on the length of the perimeter, which could be different for a given cross-sectional area depending on the flatness of the structure. It would be difficult to determine the number of line segments needed to compose each of the different sized tendon, nerve, and tunnel boundaries, while ensuring that local deformation information in the boundary was not being lost.

It is important to note the apparent tilt in the models at the level of the hamate. It seems logical that upon rotation of the models to an anatomic coordinate system, any tilt in the model would be removed. However, this tilt was

apparent at the level of the hamate in each model, although not at the level of the pisiform (Figure 37). This tilted tunnel appearance may be due to the taping of the fingers to the splint during MR imaging, a procedure in which the ring and little fingers were pulled dorsally when taping them to the splint near the knuckles.

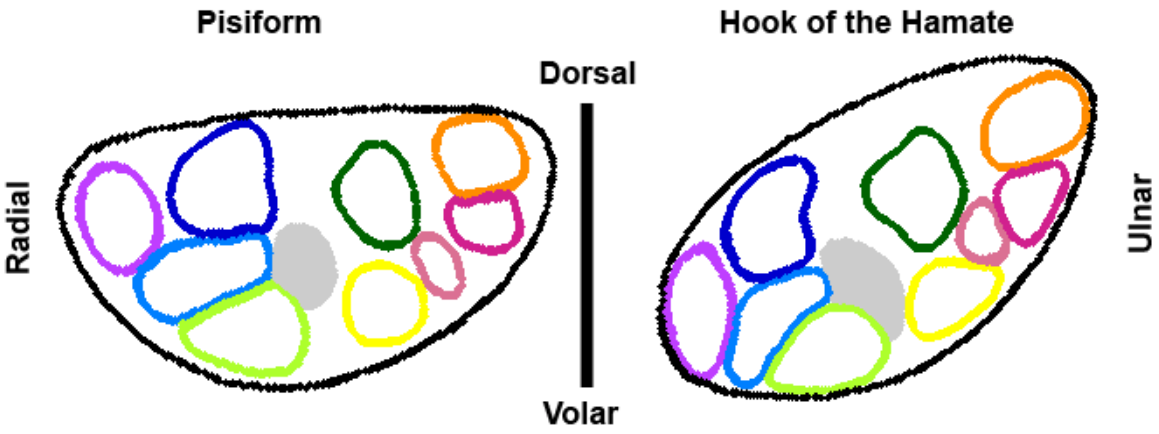


Figure 37. Comparison of sections at the pisiform (left) and hook of the hamate (right). Tilt is apparent at the hook of the hamate but not at the pisiform.

## 5.2 Subject MR Images

Another limitation in this work was the quality of the acquired MR images. Images with a higher signal-to-noise ratio might have been obtained using a different scan sequence or a coil specifically intended for the wrist. However, the selection of the coil was limited to one which would allow the various hand loading devices to be used during the scan, while keeping the carpal tunnel centered in the coil. A wrist coil was initially tried, but was abandoned because the space inside the coil for the hand was inadequate for the flat press and squeeze grip activity devices, as well as for a large hand in a flexed position. The scan sequence was limited by a compromise between acquisition time and

sufficient image contrast. To reduce subject motion and its attendant image artifact, a sequence was selected which would obtain closely spaced slices through the carpal tunnel, with adequate image contrast for segmenting, in a relatively short amount of time (90 seconds).

Despite the specific MRI protocol that was used, not all CTS subjects had a full set of eight scans that could be segmented. All of the CTS subjects experienced symptoms to varying degrees of severity while scanning. The presence of pain/numbness in the hand increased the difficulty of remaining motionless during scanning, and therefore, some of the resulting CTS patient images were affected by motion artifact. This was not an issue for any of the CTS patients imaged in either wrist position with an unloaded hand, but it did affect some of the scans with loading activities in both wrist positions. Additionally, one CTS subject experienced numbness to the extent of no longer being able to feel the loading device, so scanning of this subject was terminated before all of the scans were acquired. Segmentability of the resulting images depended on the amount of motion artifact present. Figure 38 shows examples (from the same CTS patient) of an image from a scan which was easily segmentable, and an image from a different scan which was not segmentable.

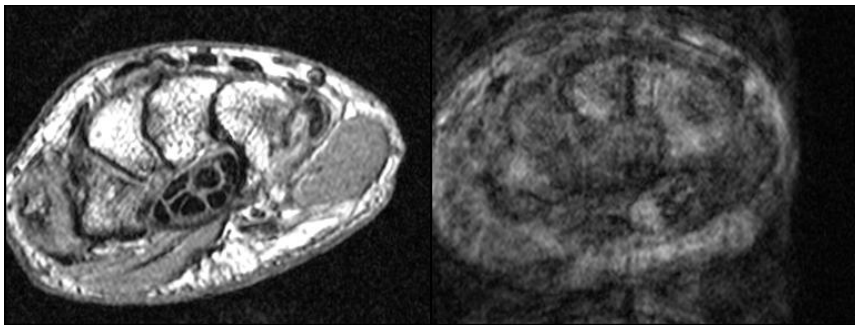

Figure 38. An image from CTS Subject 3 in an unloaded, neutral wrist position which was easily segmentable (left). An image from the same subject, performing the squeeze grip activity in a flexed wrist position which was not segmentable due to motion artifact (right).

All of the scans from CTS Subject 2 exhibited a magic-angle effect to various degrees of severity within the carpal tunnel. Specifically, the tendons of the ring and little fingers disappeared approximately 10 slices into the carpal tunnel and reappeared 10-15 slices later. The presence of the magic-angle effect in all of the scans, including the neutral wrist position, was unexpected because this subject's arm was no more obviously mis-aligned with respect to the scanner orientation than any of the other subjects. Rather this patient's distal carpal bones seemed to be shifted dorsally and the carpal tunnel structures were wrapping around that additional tunnel curvature. Analyzing scans from this subject required appreciable user editing and manual segmentation, as there frequently was not a low intensity tendon region apparent on the image from which to grow a boundary contour. In the case of magic angle effect, the user was required to scroll through the MR image stack and estimate the trajectories of the tendons from where they disappeared to where they again reappeared. For CTS Subject 2, the tendons which were affected by the magic-angle effect never contacted the nerve; therefore this approximation method of tendon segmentation was not of concern when viewing the incidence of tendon/nerve interactions.

One important factor to note when interpreting nerve location within the tunnel is the potential day-to-day variability in a given subject's nerve position. This variability was observed in a study of nerve position in normal wrists over a three-day time period.[78] Contrary to expectations, preconditioning of the carpal tunnel contents by prescribed hand activities and repetitive flexion/extension did not reduce nerve position variability. Therefore, this day-to-day variability should be considered before making any direct conclusions involving nerve position.

While 88 scans from the 12 subjects was not always adequate to reach statistical significance, it was more than sufficient to verify the robustness of the

image processing methodology on scans with a wide range of image quality and hand poses, as well as under both normal and pathological conditions. Though the number of subjects was modest, comparisons between the two groups could still be made. Having a larger number of subjects would help accentuate differences between the two groups.

Despite the above-noted limitations, this new methodology has yielded novel observations regarding geometric relationships of structures within the carpal tunnel and specific tendon/nerve interactions. This information is not available from conventional shape measures, which in this study proved to leave many questions unanswered.

## 5.3 Potential Extension of the Developed Methodology

An inviting extension of this work is to use the described methodology to complement other investigative tools, such as finite element analysis (FEA), which offer means to provide kinetic information about the associated mechanical insult to the median nerve. Knowing the exact identity of each tendon within the tunnel allows for driving finite element models with realistic motions of each structure. Therefore, the models generated using the new methodology described in this work could be used to perform realistic, patient-specific finite element analysis to observe the insult to the median nerve resulting from wrist extension and flexion, and/or hand and finger loading. FEA would provide a quantification of the insults to the median nerve that were identified in this work as the wrist flexed or as the hand and fingers were loaded. More importantly, FEA could quantify the mechanical stresses induced in the nerve as a result of impingement from neighboring structures.

# APPENDIX. FLOW CHARTS AND DATA TABLES

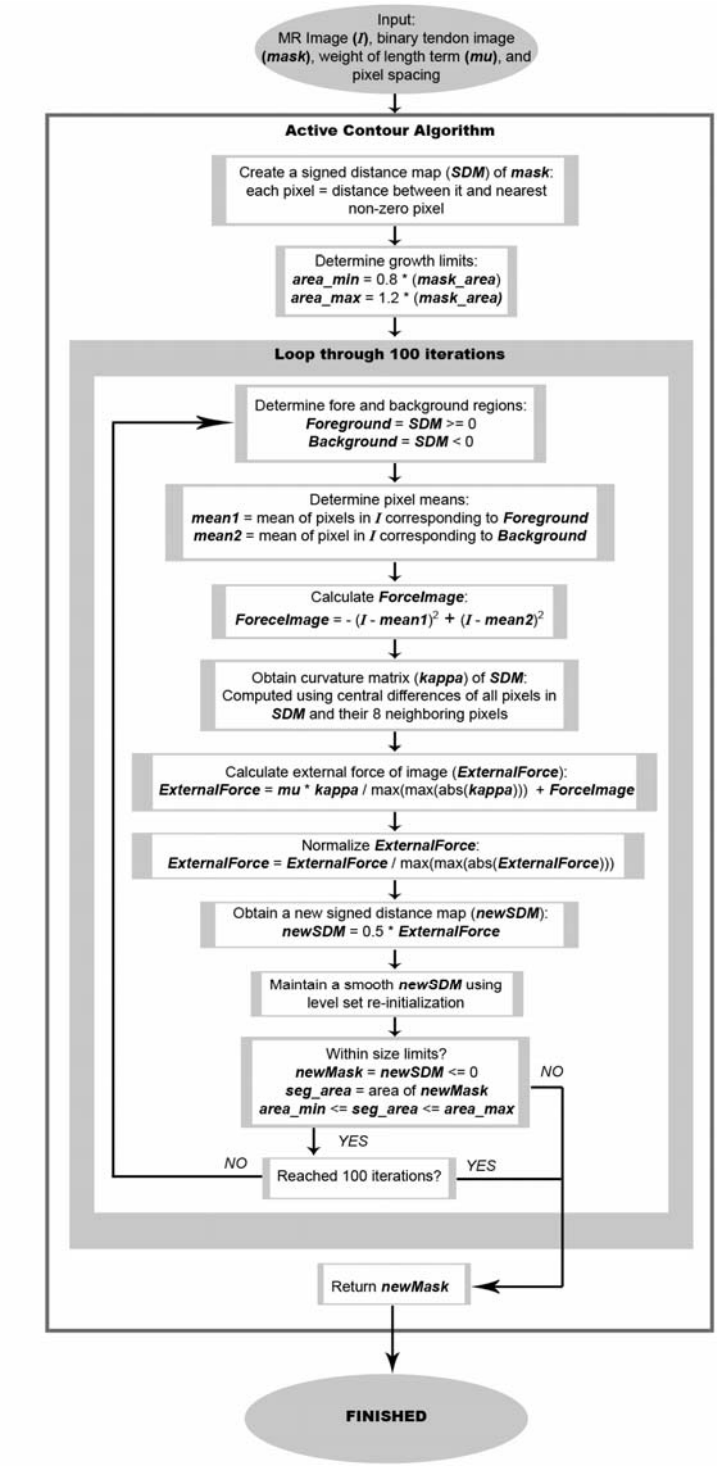


Figure A-1. Flowchart detailing the steps of the active contour growing algorithm.

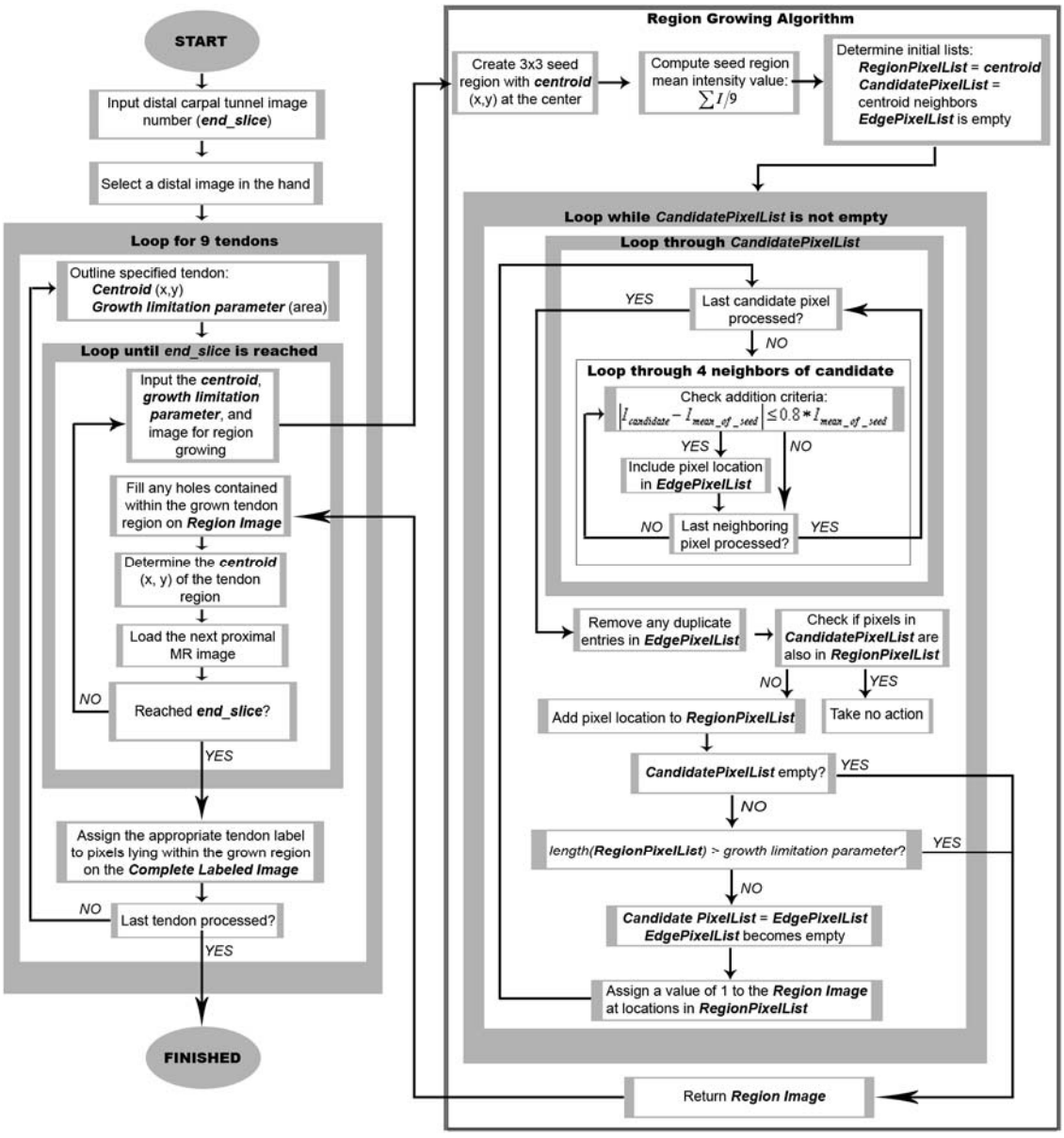


Figure A-2. Flowchart detailing the steps of the tendon identification algorithm.[79]

Table A-1. Percent change in structure cross-sectional areas from the pisiform to the hook of the hamate for the CTS patient group.

| | | | | NERVE | TUNNEL | THUMB | INDEX | | LONG | | FOURTH | | LITTLE | |
|---|---|---|---|---|---|---|---|---|---|---|---|---|---|---|
| Patient | Wrist Position | Finger Position | Activity | | | | Sup | Deep | Sup | Deep | Sup | Deep | Sup | Deep |
| CTS - 1 | Neu | S | NL | -20 | -14 | 3 | -20 | -13 | -1 | 5 | -8 | 4 | -30 | 23 |
| CTS - 1 | Neu | S | FP | 4 | -5 | 11 | 0 | -2 | -1 | 12 | -1 | 14 | -44 | 15 |
| CTS - 1 | Neu | G | SG | -14 | -17 | 13 | -8 | -5 | -10 | -13 | -10 | -6 | -65 | 2 |
| CTS - 1 | Neu | G | IP | -31 | -16 | 13 | -12 | 6 | -3 | -13 | -10 | -7 | -47 | -9 |
| CTS - 1 | 35F | S | NL | -13 | -1 | 8 | -20 | -13 | 0 | 3 | -4 | -5 | -60 | -25 |
| CTS - 1 | 35F | S | FP | -16 | -6 | 17 | -25 | -1 | 31 | 8 | 1 | -6 | -10 | -1 |
| CTS - 1 | 35F | G | SG | -22 | -10 | 2 | -15 | -8 | -8 | -29 | -8 | -17 | -25 | 11 |
| CTS - 1 | 35F | G | IP | -15 | -3 | 8 | 21 | -15 | -5 | -11 | -8 | 0 | 12 | -6 |
| CTS - 2 | Neu | S | NL | -46 | -25 | 23 | -18 | 11 | 6 | -21 | -11 | 21 | -49 | 8 |
| CTS - 2 | Neu | G | IP | -39 | -26 | 8 | 22 | -8 | 43 | 23 | -15 | 50 | -31 | -9 |
| CTS - 2 | 35F | S | NL | 29 | -5 | 15 | 3 | -12 | -12 | 74 | 4 | -9 | -28 | -11 |
| CTS - 2 | 35F | S | FP | 101 | -4 | 10 | -9 | -15 | -4 | 11 | -30 | -20 | -39 | 6 |
| CTS - 2 | 35F | G | SG | 4 | -10 | -11 | -12 | 0 | 14 | 3 | 11 | -4 | -26 | -6 |
| CTS - 2 | 35F | G | IP | 39 | -6 | -14 | 24 | -10 | 67 | 77 | 49 | 154 | -22 | -16 |
| CTS - 3 | Neu | S | NL | -43 | -23 | 10 | 18 | 4 | 1 | 17 | -3 | 29 | -30 | -5 |
| CTS - 3 | Neu | S | FP | -21 | -10 | -12 | -34 | -21 | 24 | -20 | -11 | 20 | 11 | -13 |
| CTS - 3 | Neu | G | SG | -8 | -20 | -18 | -22 | 12 | -3 | -12 | -26 | -22 | -54 | -7 |
| CTS - 3 | Neu | G | IP | -38 | 0 | 27 | 2 | 0 | 18 | -16 | -13 | -22 | -20 | 21 |
| CTS - 3 | 35F | S | NL | -17 | -15 | 0 | -5 | 3 | 4 | 8 | -10 | 15 | -5 | 9 |
| CTS - 4 | Neu | S | NL | -15 | -10 | 9 | -2 | -1 | 1 | 20 | -13 | 12 | -46 | -10 |
| CTS - 4 | Neu | S | FP | -14 | -10 | 3 | 14 | 1 | -5 | -10 | -20 | -7 | -26 | 22 |
| CTS - 4 | Neu | G | SG | -3 | -8 | 3 | 8 | -4 | 6 | -19 | 8 | -16 | -40 | 27 |
| CTS - 4 | Neu | G | IP | -5 | -6 | 5 | -1 | -3 | -16 | 0 | -19 | -11 | -36 | -13 |
| CTS - 4 | 35F | S | NL | 3 | -9 | -8 | -13 | -10 | -16 | 1 | -9 | 38 | -53 | -7 |
| CTS - 4 | 35F | S | FP | -33 | -2 | -2 | -11 | 21 | 18 | 3 | 4 | 10 | -38 | -14 |
| CTS - 4 | 35F | G | SG | -24 | -6 | -8 | -20 | -3 | -1 | -35 | -11 | 1 | -36 | -7 |
| CTS - 5 | Neu | S | NL | -31 | -18 | 7 | 20 | 4 | 8 | 11 | 0 | -2 | -19 | 12 |
| CTS - 5 | Neu | S | FP | -15 | -9 | 0 | 28 | 0 | 16 | 21 | -4 | -3 | -1 | 49 |
| CTS - 5 | Neu | G | SG | -21 | -16 | 0 | -13 | -6 | -3 | -16 | 0 | 23 | -2 | -10 |
| CTS - 5 | Neu | G | IP | -12 | -1 | -4 | 5 | -7 | 7 | 6 | 13 | 0 | -51 | 21 |
| CTS - 5 | 35F | S | NL | -24 | -8 | -10 | -1 | -3 | 16 | 15 | -9 | 10 | -8 | 20 |
| CTS - 5 | 35F | S | FP | 5 | -7 | -5 | -5 | -9 | 13 | 19 | -23 | 39 | 10 | 53 |
| CTS - 5 | 35F | G | SG | -26 | -18 | -6 | -19 | -1 | 12 | 2 | -29 | 14 | -25 | -13 |
| CTS - 6 | Neu | S | NL | 15 | -7 | -7 | -14 | -11 | 2 | 12 | 14 | 21 | -19 | -18 |
| CTS - 6 | Neu | S | FP | -16 | -12 | 12 | 1 | -7 | 12 | 3 | -13 | 11 | -16 | -9 |
| CTS - 6 | Neu | G | SG | -25 | -1 | 18 | 3 | 1 | 13 | -15 | 8 | 15 | 20 | 19 |
| CTS - 6 | 35F | S | NL | -9 | -9 | -4 | -4 | -18 | 9 | 15 | -4 | 5 | -12 | -4 |
| CTS - 6 | 35F | S | FP | 6 | -5 | 10 | -16 | -34 | 2 | -1 | 1 | 2 | -24 | -5 |
| CTS - 6 | 35F | G | SG | -11 | -7 | 18 | 3 | -6 | -7 | 0 | 5 | 2 | 13 | -21 |
| CTS - 6 | 35F | G | IP | 2 | -9 | 15 | 2 | -7 | 16 | 7 | 19 | 7 | -18 | -5 |
| CTS - 7 | Neu | S | NL | -4 | 9 | 25 | 12 | 12 | 1 | 10 | -26 | 4 | -15 | -9 |
| CTS - 7 | Neu | S | FP | 0 | 5 | 7 | -3 | 5 | 0 | 19 | -48 | 8 | -37 | -10 |
| CTS - 7 | Neu | G | SG | 19 | -1 | -1 | 6 | -24 | 18 | 2 | -59 | -7 | -27 | -8 |
| CTS - 7 | Neu | G | IP | -16 | 6 | 16 | -25 | -23 | -12 | 6 | -33 | -27 | -37 | -20 |
| CTS - 7 | 35F | S | NL | -28 | -17 | -13 | -10 | -2 | -8 | 28 | 6 | 5 | -35 | -12 |
| CTS - 7 | 35F | S | FP | 13 | -14 | -1 | -15 | -1 | -15 | 3 | -8 | -2 | 0 | -8 |
| CTS - 7 | 35F | G | SG | -16 | -12 | 6 | -2 | -25 | -11 | -16 | 5 | -12 | -20 | -12 |
| CTS - 7 | 35F | G | IP | -16 | -2 | 3 | -6 | -13 | -4 | 17 | -13 | -5 | -26 | -10 |

A positive percent increase in the cross-sectional area indicates the structure became larger moving from the proximal end (pisiform) to the distal end (hook of the hamate) of the tunnel. Abbreviations: Wrists were either in 35 degrees of flexion (35F) or 0 degrees of flexion (Neu), and fingers were either straight (S) or gripped (G) loosely. Activities were either none (NL), flat press (FP), squeeze grip (SG), or index-thumb pinch (IP).

Table A-2. Percent change in structure cross-sectional areas from the pisiform to the hook of the hamate for the normal subject group.

| | | | | NERVE | TUNNEL | THUMB | INDEX | | LONG | | FOURTH | | LITTLE | |
|---|---|---|---|---|---|---|---|---|---|---|---|---|---|---|
| Patient | Wrist Position | Finger Position | Activity | | | | Sup | Deep | Sup | Deep | Sup | Deep | Sup | Deep |
| Norm - 1 | Neu | S | NL | -30 | -8 | 1 | 2 | -15 | -3 | 9 | 16 | 17 | 10 | -2 |
| Norm - 1 | Neu | S | FP | 20 | -10 | 0 | 0 | -26 | -3 | 5 | -23 | -26 | -13 | -19 |
| Norm - 1 | Neu | G | SG | 22 | -16 | 23 | 27 | 1 | -10 | -12 | -1 | 3 | 38 | 1 |
| Norm - 1 | Neu | G | IP | 42 | -18 | 11 | 2 | -3 | -3 | -16 | -6 | -13 | 19 | -5 |
| Norm - 1 | 35F | S | NL | 27 | -7 | 1 | -21 | -12 | -6 | 27 | -1 | 23 | 5 | 16 |
| Norm - 1 | 35F | S | FP | 35 | -2 | 7 | 10 | -10 | 8 | 8 | 5 | 3 | 2 | 17 |
| Norm - 1 | 35F | G | SG | 50 | -1 | 2 | -10 | -11 | -11 | -5 | -17 | -9 | 24 | 29 |
| Norm - 1 | 35F | G | IP | -23 | -5 | 8 | 32 | 2 | 2 | 39 | -10 | 12 | -19 | 13 |
| Norm - 2 | Neu | S | NL | -20 | -6 | -9 | -9 | -1 | 7 | -6 | 10 | 16 | -33 | 0 |
| Norm - 2 | Neu | S | FP | 6 | -6 | -3 | -2 | -5 | 5 | 6 | 2 | 23 | -8 | 35 |
| Norm - 2 | Neu | G | SG | -13 | -6 | 8 | -2 | -3 | -6 | -45 | 1 | 3 | -25 | 11 |
| Norm - 2 | Neu | G | IP | -9 | -13 | 13 | -5 | 13 | -18 | -28 | -3 | -33 | -43 | -24 |
| Norm - 2 | 35F | S | NL | 4 | 4 | 0 | 17 | 2 | 0 | 7 | 4 | 35 | -34 | 20 |
| Norm - 2 | 35F | S | FP | 30 | 7 | -18 | -16 | 3 | -17 | 37 | 14 | -6 | -50 | -9 |
| Norm - 2 | 35F | G | SG | -5 | -9 | -26 | -14 | -17 | 21 | -40 | -12 | -2 | 266 | 10 |
| Norm - 2 | 35F | G | IP | -25 | -5 | -11 | -6 | 7 | 5 | -36 | 32 | -3 | 462 | 23 |
| Norm - 3 | Neu | S | NL | 36 | -10 | -8 | 21 | -3 | 9 | 7 | 15 | 14 | 31 | -6 |
| Norm - 3 | Neu | S | FP | -5 | -13 | -9 | 0 | -2 | 13 | 8 | 18 | 8 | 1 | 27 |
| Norm - 3 | Neu | G | SG | -5 | 15 | 16 | 27 | 79 | 63 | 6 | 9 | -3 | 40 | -14 |
| Norm - 3 | Neu | G | IP | -23 | 0 | -9 | 3 | 8 | 14 | -19 | 1 | -3 | -14 | 9 |
| Norm - 3 | 35F | S | NL | -17 | -12 | -9 | -20 | -16 | -1 | 0 | 7 | -6 | -17 | 10 |
| Norm - 3 | 35F | S | FP | 19 | -14 | -19 | 1 | -27 | -6 | 9 | -22 | 0 | 4 | 9 |
| Norm - 3 | 35F | G | SG | -11 | -6 | -24 | -2 | -5 | 1 | -8 | 18 | -9 | 24 | -1 |
| Norm - 3 | 35F | G | IP | 3 | 2 | 0 | -8 | 17 | -5 | -11 | 12 | -19 | 31 | 3 |
| Norm - 4 | Neu | S | NL | 18 | -3 | 26 | 4 | 5 | 10 | 12 | -4 | 29 | -4 | 21 |
| Norm - 4 | Neu | S | FP | 11 | 0 | 10 | -4 | 3 | 12 | 4 | -10 | 15 | -37 | 24 |
| Norm - 4 | Neu | G | SG | 4 | -5 | -1 | 4 | -17 | 15 | -31 | -3 | 1 | -13 | 13 |
| Norm - 4 | Neu | G | IP | 13 | -4 | 3 | -8 | -5 | 2 | -26 | -14 | -2 | -12 | 17 |
| Norm - 4 | 35F | S | NL | -14 | -13 | 3 | -8 | 0 | -2 | 8 | -3 | 27 | 1 | -9 |
| Norm - 4 | 35F | S | FP | -33 | -8 | 1 | -23 | -30 | 3 | -11 | 0 | 1 | -1 | -5 |
| Norm - 4 | 35F | G | SG | 15 | -1 | -18 | -5 | -16 | -4 | -23 | 16 | 42 | 65 | 30 |
| Norm - 4 | 35F | G | IP | -19 | -11 | -7 | -4 | -6 | -6 | -8 | 0 | -2 | 17 | 11 |
| Norm - 5 | Neu | S | NL | -10 | -4 | 3 | 2 | -4 | -2 | 40 | 14 | 3 | -17 | -1 |
| Norm - 5 | Neu | S | FP | 18 | 1 | 2 | 3 | -8 | 5 | 9 | -6 | 1 | -36 | 15 |
| Norm - 5 | Neu | G | SG | 41 | 3 | 6 | -5 | -10 | 5 | -8 | -18 | -1 | -51 | -8 |
| Norm - 5 | Neu | G | IP | -5 | -4 | -7 | -14 | -8 | -2 | 1 | -19 | -1 | -35 | -22 |
| Norm - 5 | 35F | S | NL | 4 | -3 | -8 | 1 | 12 | 0 | 7 | -5 | 11 | -5 | -4 |
| Norm - 5 | 35F | S | FP | -29 | -8 | -13 | 10 | 13 | 1 | -1 | -6 | -4 | 7 | 0 |
| Norm - 5 | 35F | G | SG | -2 | -14 | -9 | -3 | -8 | -1 | 14 | -26 | 6 | -3 | -10 |
| Norm - 5 | 35F | G | IP | 4 | 3 | -3 | 6 | 0 | 15 | 17 | 10 | 35 | 2 | -3 |

A positive percent increase in the cross-sectional area indicates the structure became larger moving from the proximal end (pisiform) to the distal end (hook of the hamate) of the tunnel. Abbreviations: Wrists were either in 35 degrees of flexion (35F) or 0 degrees of flexion (Neu), and fingers were either straight (S) or gripped (G) loosely. Activities were either none (NL), flat press (FP), squeeze grip (SG), or index-thumb pinch (IP).

Table A-3. Percent change in flattening ratio from the pisiform to the hook of the hamate for the CTS patient group.

| | | | | NERVE | TUNNEL | THUMB | INDEX | | LONG | | FOURTH | | LITTLE | |
|---|---|---|---|---|---|---|---|---|---|---|---|---|---|---|
| Patient | Wrist Position | Finger Position | Activity | | | | Sup | Deep | Sup | Deep | Sup | Deep | Sup | Deep |
| CTS - 1 | Neu | S | NL | -32 | 3 | -11 | -22 | 0 | -8 | -14 | -5 | 8 | 5 | -22 |
| CTS - 1 | Neu | S | FP | -1 | -7 | 1 | -7 | -16 | 8 | -2 | 19 | 10 | 16 | 18 |
| CTS - 1 | Neu | G | SG | 4 | 1 | -18 | 16 | 42 | -30 | -21 | -7 | 38 | -7 | 2 |
| CTS - 1 | Neu | G | IP | 48 | -3 | 24 | -21 | -9 | 36 | -14 | -8 | 20 | -9 | 9 |
| CTS - 1 | 35F | S | NL | 56 | 7 | 0 | 11 | -2 | -17 | 0 | -12 | 30 | -19 | 71 |
| CTS - 1 | 35F | S | FP | 25 | 7 | 6 | 37 | 16 | -15 | -5 | -8 | 13 | 10 | 49 |
| CTS - 1 | 35F | G | SG | 23 | 6 | 26 | -3 | -28 | -18 | -1 | -24 | 24 | -8 | 3 |
| CTS - 1 | 35F | G | IP | 42 | 3 | -7 | -13 | -17 | -8 | 7 | -11 | 17 | -12 | 11 |
| CTS - 2 | Neu | S | NL | 95 | 14 | -1 | 51 | -21 | -2 | -55 | -29 | 5 | 110 | 1 |
| CTS - 2 | Neu | G | IP | 39 | 6 | 23 | 111 | 25 | 39 | -46 | 4 | -17 | 89 | 83 |
| CTS - 2 | 35F | S | NL | -14 | -12 | -35 | 0 | 23 | 19 | -16 | 33 | -18 | -61 | 3 |
| CTS - 2 | 35F | S | FP | -11 | -13 | -39 | -13 | 20 | 8 | -3 | 14 | -1 | -17 | 46 |
| CTS - 2 | 35F | G | SG | -29 | -11 | 12 | 30 | 21 | 36 | 15 | -19 | 20 | -34 | 11 |
| CTS - 2 | 35F | G | IP | 5 | -5 | -30 | -32 | -9 | -31 | 8 | -43 | 30 | -39 | 18 |
| CTS - 3 | Neu | S | NL | 115 | 9 | -18 | 53 | -17 | -1 | -28 | -10 | 58 | 11 | 85 |
| CTS - 3 | Neu | S | FP | -25 | -8 | 10 | -27 | -19 | -19 | -25 | -8 | -6 | -26 | 76 |
| CTS - 3 | Neu | G | SG | 7 | 6 | -21 | -13 | -39 | 4 | -37 | -1 | -1 | 31 | 13 |
| CTS - 3 | Neu | G | IP | 58 | 8 | 32 | -16 | 4 | 10 | 9 | -19 | -3 | 26 | 18 |
| CTS - 3 | 35F | S | NL | 63 | 5 | -19 | -15 | 11 | -19 | -3 | 3 | 10 | 14 | 22 |
| CTS - 4 | Neu | S | NL | 48 | 1 | 31 | 6 | 19 | -9 | -22 | 12 | 23 | -6 | 17 |
| CTS - 4 | Neu | S | FP | -5 | 0 | 26 | -8 | -8 | 1 | -21 | 12 | -27 | -10 | -27 |
| CTS - 4 | Neu | G | SG | 5 | 2 | -4 | 9 | -19 | 9 | -26 | 1 | 0 | 30 | 4 |
| CTS - 4 | Neu | G | IP | 11 | -5 | -2 | -5 | -9 | 10 | -21 | 4 | -14 | 5 | 13 |
| CTS - 4 | 35F | S | NL | 43 | 8 | 6 | -24 | -24 | 10 | -10 | -11 | 14 | 62 | -4 |
| CTS - 4 | 35F | S | FP | 68 | -8 | 26 | -5 | 16 | 1 | -14 | 57 | 4 | -6 | 94 |
| CTS - 4 | 35F | G | SG | 70 | -3 | 50 | -24 | -21 | -16 | -4 | -5 | 1 | -41 | -29 |
| CTS - 5 | Neu | S | NL | 40 | 17 | -28 | 25 | -8 | -21 | -27 | 8 | -4 | 78 | -38 |
| CTS - 5 | Neu | S | FP | -3 | -8 | 16 | -29 | -34 | -32 | -32 | -6 | 24 | -15 | -18 |
| CTS - 5 | Neu | G | SG | 6 | -5 | -11 | 11 | -1 | -15 | -26 | -1 | -1 | 46 | 5 |
| CTS - 5 | Neu | G | IP | 53 | -6 | -5 | -6 | -28 | -11 | 10 | -13 | -5 | 7 | 1 |
| CTS - 5 | 35F | S | NL | 17 | 12 | 6 | -6 | 15 | -14 | -25 | 1 | 6 | 7 | 25 |
| CTS - 5 | 35F | S | FP | 10 | 4 | 21 | 19 | 37 | 6 | -12 | 2 | -17 | 27 | -21 |
| CTS - 5 | 35F | G | SG | -9 | 18 | 37 | 41 | 21 | -34 | 1 | 4 | 10 | -18 | -24 |
| CTS - 6 | Neu | S | NL | 2 | 11 | -18 | -2 | 29 | 11 | 10 | 12 | 1 | 14 | 37 |
| CTS - 6 | Neu | S | FP | -12 | 7 | -1 | -29 | 38 | 9 | -10 | 0 | -5 | 6 | 18 |
| CTS - 6 | Neu | G | SG | -14 | 12 | -11 | -20 | 1 | 7 | -3 | 1 | -16 | -10 | -16 |
| CTS - 6 | 35F | S | NL | -3 | 5 | -28 | 3 | 21 | 3 | 19 | 1 | -6 | -16 | 42 |
| CTS - 6 | 35F | S | FP | -41 | 15 | -16 | -12 | -27 | -11 | 10 | 10 | -12 | 2 | -18 |
| CTS - 6 | 35F | G | SG | 19 | 7 | -23 | 24 | -16 | 45 | -9 | 38 | 2 | -24 | 13 |
| CTS - 6 | 35F | G | IP | 10 | 5 | -17 | -9 | -7 | 5 | 4 | -4 | 36 | 26 | -15 |
| CTS - 7 | Neu | S | NL | -13 | -1 | -21 | -5 | 19 | 14 | 13 | -4 | 1 | 8 | 41 |
| CTS - 7 | Neu | S | FP | -8 | 4 | 25 | 7 | 0 | -7 | -8 | 13 | 27 | 2 | -40 |
| CTS - 7 | Neu | G | SG | -30 | -13 | 21 | 20 | -13 | -9 | 4 | -17 | -4 | 30 | -5 |
| CTS - 7 | Neu | G | IP | 8 | -4 | 1 | -8 | -12 | -11 | 3 | -14 | -6 | -3 | 6 |
| CTS - 7 | 35F | S | NL | -1 | 3 | -28 | 17 | -12 | 1 | -8 | -3 | 12 | 54 | -8 |
| CTS - 7 | 35F | S | FP | 10 | 2 | -20 | 35 | -35 | 25 | 5 | 16 | -9 | -23 | -5 |
| CTS - 7 | 35F | G | SG | 14 | 10 | 9 | -15 | 14 | -2 | 4 | 19 | -8 | -12 | 25 |
| CTS - 7 | 35F | G | IP | -7 | 5 | 2 | 7 | 50 | 1 | -13 | -20 | -3 | -13 | -4 |

A positive percent increase in the flattening ratio indicates the structure became flatter moving from the proximal end (pisiform) to the distal end (hook of the hamate) of the tunnel. Abbreviations: Wrists were either in 35 degrees of flexion (35F) or 0 degrees of flexion (Neu), and fingers were either straight (S) or gripped (G) loosely. Activities were either none (NL), flat press (FP), squeeze grip (SG), or index-thumb pinch (IP).

Table A-4. Percent change in flattening ratio from the pisiform to the hook of the hamate for the normal subject group.

| | | | | NERVE | TUNNEL | THUMB | INDEX | | LONG | | FOURTH | | LITTLE | |
|---|---|---|---|---|---|---|---|---|---|---|---|---|---|---|
| Patient | Wrist Position | Finger Position | Activity | | | | Sup | Deep | Sup | Deep | Sup | Deep | Sup | Deep |
| Norm - 1 | Neu | S | NL | 20 | 0 | 24 | 41 | 14 | 2 | 8 | 42 | 14 | 38 | -11 |
| Norm - 1 | Neu | S | FP | -8 | -12 | 30 | -13 | 27 | -6 | 20 | -10 | 10 | 41 | 9 |
| Norm - 1 | Neu | G | SG | -49 | 4 | -14 | 15 | 21 | 36 | -8 | 49 | -3 | -7 | 15 |
| Norm - 1 | Neu | G | IP | -69 | 10 | -7 | 8 | 2 | 12 | -42 | -3 | -17 | 6 | 16 |
| Norm - 1 | 35F | S | NL | 42 | 7 | 39 | 23 | 31 | 6 | -7 | 54 | 30 | -21 | -3 |
| Norm - 1 | 35F | S | FP | 11 | -5 | 32 | 7 | 0 | 13 | -33 | 45 | 28 | -8 | 18 |
| Norm - 1 | 35F | G | SG | 41 | -6 | -1 | -24 | -9 | 10 | 5 | 22 | 55 | 3 | 64 |
| Norm - 1 | 35F | G | IP | 58 | -3 | -1 | 15 | -26 | 24 | -17 | 26 | -7 | -57 | 23 |
| Norm - 2 | Neu | S | NL | 8 | 6 | -7 | -17 | 23 | -18 | -14 | 19 | 13 | 7 | 47 |
| Norm - 2 | Neu | S | FP | -22 | 14 | 25 | -23 | 18 | 1 | -17 | 30 | -4 | -17 | 31 |
| Norm - 2 | Neu | G | SG | 0 | 7 | -15 | -15 | -13 | 21 | -13 | 0 | -22 | 42 | -15 |
| Norm - 2 | Neu | G | IP | -10 | 10 | 12 | -9 | 1 | -25 | -8 | 11 | 6 | 12 | -21 |
| Norm - 2 | 35F | S | NL | -27 | 18 | 35 | 19 | 12 | 23 | -2 | 0 | -23 | -43 | 17 |
| Norm - 2 | 35F | S | FP | -14 | 15 | 16 | 18 | -6 | 34 | 1 | 1 | -6 | -31 | 39 |
| Norm - 2 | 35F | G | SG | -25 | 11 | -33 | 34 | 18 | 16 | -1 | 18 | 42 | -42 | 49 |
| Norm - 2 | 35F | G | IP | 29 | 6 | -11 | 4 | -21 | -21 | -7 | -4 | 77 | -31 | 41 |
| Norm - 3 | Neu | S | NL | -4 | 10 | -4 | -33 | 23 | -25 | 15 | -10 | 0 | -4 | 41 |
| Norm - 3 | Neu | S | FP | -1 | 4 | 6 | -9 | 1 | -16 | 13 | -15 | 11 | 17 | 39 |
| Norm - 3 | Neu | G | SG | -9 | 15 | 30 | -10 | 25 | -35 | 19 | 17 | -33 | -28 | 16 |
| Norm - 3 | Neu | G | IP | 42 | 14 | 65 | 44 | 7 | 10 | 24 | 56 | -39 | 17 | -27 |
| Norm - 3 | 35F | S | NL | 22 | 32 | -8 | 26 | -19 | -12 | -15 | -17 | -35 | -10 | 5 |
| Norm - 3 | 35F | S | FP | -9 | 16 | -30 | 7 | -2 | 25 | 30 | -1 | -10 | 19 | 17 |
| Norm - 3 | 35F | G | SG | 35 | 2 | 23 | -10 | -24 | 5 | 5 | 23 | -21 | -4 | -13 |
| Norm - 3 | 35F | G | IP | 14 | 16 | 12 | -23 | -7 | 18 | -7 | -35 | -21 | -13 | 3 |
| Norm - 4 | Neu | S | NL | -20 | 6 | -10 | -5 | 11 | -2 | -28 | -3 | -14 | -15 | -13 |
| Norm - 4 | Neu | S | FP | -18 | -3 | 15 | 10 | -20 | -25 | 19 | 3 | 6 | -4 | 14 |
| Norm - 4 | Neu | G | SG | -13 | 2 | 0 | 76 | -1 | -8 | -12 | 4 | -44 | 20 | 0 |
| Norm - 4 | Neu | G | IP | -33 | -1 | -10 | 11 | -2 | -7 | 3 | 4 | -27 | 54 | -7 |
| Norm - 4 | 35F | S | NL | -17 | 8 | -4 | 9 | 1 | 4 | -20 | -8 | -5 | -3 | 17 |
| Norm - 4 | 35F | S | FP | 40 | 5 | -30 | 23 | -8 | -8 | 0 | 7 | 43 | -5 | 28 |
| Norm - 4 | 35F | G | SG | 82 | 18 | -12 | -3 | 23 | 7 | 12 | -18 | -2 | -45 | -16 |
| Norm - 4 | 35F | G | IP | 60 | 25 | -22 | 23 | -26 | -10 | 25 | -15 | -26 | 35 | 27 |
| Norm - 5 | Neu | S | NL | 0 | 23 | -33 | -3 | 46 | 8 | 17 | -1 | -2 | 50 | 20 |
| Norm - 5 | Neu | S | FP | -8 | 7 | -25 | 19 | 30 | -7 | 20 | 13 | -9 | 20 | 19 |
| Norm - 5 | Neu | G | SG | -31 | -11 | 32 | 45 | -14 | -9 | -25 | 18 | 28 | 54 | 5 |
| Norm - 5 | Neu | G | IP | 43 | -7 | 19 | -5 | 2 | -20 | 46 | 15 | 8 | 73 | 7 |
| Norm - 5 | 35F | S | NL | -35 | 19 | 11 | -21 | 20 | 2 | -13 | 18 | -12 | -14 | -12 |
| Norm - 5 | 35F | S | FP | 6 | 12 | 20 | -33 | 13 | -33 | -5 | 11 | -15 | 16 | -10 |
| Norm - 5 | 35F | G | SG | 72 | 8 | 2 | -18 | -7 | -11 | 20 | 7 | 10 | -9 | -1 |
| Norm - 5 | 35F | G | IP | -34 | 14 | -20 | 16 | -11 | 10 | 24 | 10 | 6 | -41 | 7 |

A positive percent increase in the flattening ratio indicates the structure became flatter moving from the proximal end (pisiform) to the distal end (hook of the hamate) of the tunnel. Abbreviations: Wrists were either in 35 degrees of flexion (35F) or 0 degrees of flexion (Neu), and fingers were either straight (S) or gripped (G) loosely. Activities were either none (NL), flat press (FP), squeeze grip (SG), or index-thumb pinch (IP).

Table A-5. Nerve adjacency at the level of the pisiform for the CTS patient group.

| | | | | | TUNNEL | THUMB | INDEX | | LONG | | FOURTH | | LITTLE | |
|---|---|---|---|---|---|---|---|---|---|---|---|---|---|---|
| Patient | Wrist Position | Finger Position | Activity | % Adjacency | | | Sup | Deep | Sup | Deep | Sup | Deep | Sup | Deep |
| CTS - 1 | Neu | S | NL | 64 | 29 | 15 | 0 | 0 | 19 | 0 | 0 | 0 | 0 | 0 |
| CTS - 1 | Neu | S | FP | 63 | 0 | 36 | 19 | 7 | 0 | 0 | 0 | 0 | 0 | 0 |
| CTS - 1 | Neu | G | SG | 49 | 35 | 0 | 0 | 0 | 14 | 0 | 0 | 0 | 0 | 0 |
| CTS - 1 | Neu | G | IP | 65 | 38 | 19 | 0 | 0 | 8 | 0 | 0 | 0 | 0 | 0 |
| CTS - 1 | 35F | S | NL | 72 | 28 | 24 | 0 | 21 | 0 | 0 | 0 | 0 | 0 | 0 |
| CTS - 1 | 35F | S | FP | 69 | 25 | 25 | 0 | 19 | 0 | 0 | 0 | 0 | 0 | 0 |
| CTS - 1 | 35F | G | SG | 64 | 25 | 25 | 3 | 11 | 0 | 0 | 0 | 0 | 0 | 0 |
| CTS - 1 | 35F | G | IP | 51 | 33 | 18 | 0 | 0 | 0 | 0 | 0 | 0 | 0 | 0 |
| CTS - 2 | Neu | S | NL | 15 | 15 | 0 | 0 | 0 | 0 | 0 | 0 | 0 | 0 | 0 |
| CTS - 2 | Neu | G | IP | 57 | 35 | 0 | 0 | 0 | 22 | 0 | 0 | 0 | 0 | 0 |
| CTS - 2 | 35F | S | NL | 56 | 19 | 17 | 0 | 19 | 0 | 0 | 0 | 0 | 0 | 0 |
| CTS - 2 | 35F | S | FP | 17 | 0 | 7 | 0 | 10 | 0 | 0 | 0 | 0 | 0 | 0 |
| CTS - 2 | 35F | G | SG | 74 | 35 | 19 | 13 | 7 | 0 | 0 | 0 | 0 | 0 | 0 |
| CTS - 2 | 35F | G | IP | 25 | 0 | 24 | 0 | 1 | 0 | 0 | 0 | 0 | 0 | 0 |
| CTS - 3 | Neu | S | NL | 47 | 32 | 0 | 0 | 0 | 15 | 0 | 0 | 0 | 0 | 0 |
| CTS - 3 | Neu | S | FP | 72 | 31 | 8 | 10 | 0 | 24 | 0 | 0 | 0 | 0 | 0 |
| CTS - 3 | Neu | G | SG | 49 | 39 | 0 | 0 | 0 | 0 | 0 | 10 | 0 | 0 | 0 |
| CTS - 3 | Neu | G | IP | 53 | 32 | 0 | 0 | 0 | 1 | 0 | 19 | 0 | 0 | 0 |
| CTS - 3 | 35F | S | NL | 58 | 28 | 0 | 0 | 0 | 4 | 0 | 19 | 0 | 7 | 0 |
| CTS - 4 | Neu | S | NL | 24 | 3 | 3 | 18 | 0 | 0 | 0 | 0 | 0 | 0 | 0 |
| CTS - 4 | Neu | S | FP | 53 | 8 | 29 | 15 | 0 | 0 | 0 | 0 | 0 | 0 | 0 |
| CTS - 4 | Neu | G | SG | 60 | 29 | 0 | 0 | 0 | 24 | 0 | 7 | 0 | 0 | 0 |
| CTS - 4 | Neu | G | IP | 63 | 46 | 0 | 1 | 0 | 15 | 0 | 0 | 0 | 0 | 0 |
| CTS - 4 | 35F | S | NL | 63 | 0 | 32 | 17 | 14 | 0 | 0 | 0 | 0 | 0 | 0 |
| CTS - 4 | 35F | S | FP | 50 | 0 | 26 | 0 | 24 | 0 | 0 | 0 | 0 | 0 | 0 |
| CTS - 4 | 35F | G | SG | 57 | 0 | 31 | 0 | 26 | 0 | 0 | 0 | 0 | 0 | 0 |
| CTS - 5 | Neu | S | NL | 46 | 26 | 0 | 0 | 0 | 19 | 0 | 0 | 0 | 0 | 0 |
| CTS - 5 | Neu | S | FP | 69 | 39 | 0 | 0 | 0 | 31 | 0 | 0 | 0 | 0 | 0 |
| CTS - 5 | Neu | G | SG | 58 | 32 | 0 | 0 | 0 | 26 | 0 | 0 | 0 | 0 | 0 |
| CTS - 5 | Neu | G | IP | 29 | 0 | 3 | 0 | 0 | 26 | 0 | 0 | 0 | 0 | 0 |
| CTS - 5 | 35F | S | NL | 51 | 15 | 0 | 0 | 0 | 24 | 0 | 13 | 0 | 0 | 0 |
| CTS - 5 | 35F | S | FP | 54 | 21 | 0 | 0 | 0 | 21 | 0 | 13 | 0 | 0 | 0 |
| CTS - 5 | 35F | G | SG | 36 | 0 | 0 | 10 | 0 | 10 | 0 | 17 | 0 | 0 | 0 |
| CTS - 6 | Neu | S | NL | 51 | 38 | 0 | 10 | 0 | 4 | 0 | 0 | 0 | 0 | 0 |
| CTS - 6 | Neu | S | FP | 4 | 4 | 0 | 0 | 0 | 0 | 0 | 0 | 0 | 0 | 0 |
| CTS - 6 | Neu | G | SG | 19 | 4 | 0 | 1 | 0 | 14 | 0 | 0 | 0 | 0 | 0 |
| CTS - 6 | 35F | S | NL | 40 | 0 | 21 | 19 | 0 | 0 | 0 | 0 | 0 | 0 | 0 |
| CTS - 6 | 35F | S | FP | 39 | 0 | 26 | 13 | 0 | 0 | 0 | 0 | 0 | 0 | 0 |
| CTS - 6 | 35F | G | SG | 44 | 0 | 19 | 0 | 25 | 0 | 0 | 0 | 0 | 0 | 0 |
| CTS - 6 | 35F | G | IP | 31 | 8 | 22 | 0 | 0 | 0 | 0 | 0 | 0 | 0 | 0 |
| CTS - 7 | Neu | S | NL | 61 | 36 | 4 | 6 | 0 | 15 | 0 | 0 | 0 | 0 | 0 |
| CTS - 7 | Neu | S | FP | 68 | 42 | 3 | 0 | 0 | 15 | 0 | 8 | 0 | 0 | 0 |
| CTS - 7 | Neu | G | SG | 53 | 35 | 7 | 0 | 0 | 11 | 0 | 0 | 0 | 0 | 0 |
| CTS - 7 | Neu | G | IP | 33 | 10 | 0 | 0 | 0 | 24 | 0 | 0 | 0 | 0 | 0 |
| CTS - 7 | 35F | S | NL | 72 | 29 | 0 | 0 | 0 | 13 | 11 | 17 | 0 | 3 | 0 |
| CTS - 7 | 35F | S | FP | 63 | 0 | 0 | 0 | 15 | 21 | 13 | 14 | 0 | 0 | 0 |
| CTS - 7 | 35F | G | SG | 68 | 0 | 0 | 0 | 14 | 24 | 11 | 19 | 0 | 0 | 0 |
| CTS - 7 | 35F | G | IP | 69 | 0 | 0 | 0 | 11 | 21 | 18 | 19 | 0 | 0 | 0 |

The first four columns identify the subject, wrist angle, finger position, and loading activity (if one was used). The next column identifies the total percentage of the nerve boundary that is adjacent to tendons and the carpal tunnel boundary. Abbreviations: Wrists were either in 35 degrees of flexion (35F) or neutral (Neu), and fingers were either straight (S) or gripped (G) loosely. Activities were either none (NL), flat press (FP), squeeze grip (SG), or index-thumb pinch (IP).

Table A-6. Nerve adjacency at the level of the pisiform for the normal subject group.

| | | | | | TUNNEL | THUMB | INDEX | | LONG | | FOURTH | | LITTLE | |
|---|---|---|---|---|---|---|---|---|---|---|---|---|---|---|
| Patient | Wrist Position | Finger Position | Activity | % Adjacency | | | Sup | Deep | Sup | Deep | Sup | Deep | Sup | Deep |
| Norm - 1 | Neu | S | NL | 49 | 33 | 0 | 0 | 0 | 15 | 0 | 0 | 0 | 0 | 0 |
| Norm - 1 | Neu | S | FP | 60 | 0 | 0 | 14 | 17 | 0 | 7 | 22 | 0 | 0 | 0 |
| Norm - 1 | Neu | G | SG | 61 | 24 | 18 | 19 | 0 | 0 | 0 | 0 | 0 | 0 | 0 |
| Norm - 1 | Neu | G | IP | 63 | 0 | 38 | 22 | 3 | 0 | 0 | 0 | 0 | 0 | 0 |
| Norm - 1 | 35F | S | NL | 49 | 0 | 0 | 17 | 6 | 19 | 0 | 7 | 0 | 0 | 0 |
| Norm - 1 | 35F | S | FP | 38 | 0 | 0 | 10 | 1 | 10 | 0 | 17 | 0 | 0 | 0 |
| Norm - 1 | 35F | G | SG | 78 | 28 | 26 | 24 | 0 | 0 | 0 | 0 | 0 | 0 | 0 |
| Norm - 1 | 35F | G | IP | 36 | 19 | 17 | 0 | 0 | 0 | 0 | 0 | 0 | 0 | 0 |
| Norm - 2 | Neu | S | NL | 58 | 29 | 0 | 18 | 0 | 11 | 0 | 0 | 0 | 0 | 0 |
| Norm - 2 | Neu | S | FP | 68 | 46 | 0 | 11 | 0 | 11 | 0 | 0 | 0 | 0 | 0 |
| Norm - 2 | Neu | G | SG | 53 | 35 | 0 | 0 | 0 | 18 | 0 | 0 | 0 | 0 | 0 |
| Norm - 2 | Neu | G | IP | 71 | 39 | 0 | 4 | 0 | 28 | 0 | 0 | 0 | 0 | 0 |
| Norm - 2 | 35F | S | NL | 69 | 39 | 15 | 15 | 0 | 0 | 0 | 0 | 0 | 0 | 0 |
| Norm - 2 | 35F | S | FP | 85 | 44 | 11 | 11 | 18 | 0 | 0 | 0 | 0 | 0 | 0 |
| Norm - 2 | 35F | G | SG | 90 | 43 | 18 | 14 | 15 | 0 | 0 | 0 | 0 | 0 | 0 |
| Norm - 2 | 35F | G | IP | 61 | 24 | 0 | 11 | 0 | 0 | 0 | 21 | 0 | 6 | 0 |
| Norm - 3 | Neu | S | NL | 46 | 18 | 0 | 0 | 0 | 28 | 0 | 0 | 0 | 0 | 0 |
| Norm - 3 | Neu | S | FP | 31 | 0 | 0 | 0 | 7 | 14 | 0 | 10 | 0 | 0 | 0 |
| Norm - 3 | Neu | G | SG | 79 | 42 | 0 | 0 | 0 | 0 | 0 | 22 | 0 | 15 | 0 |
| Norm - 3 | Neu | G | IP | 53 | 26 | 0 | 0 | 0 | 17 | 0 | 10 | 0 | 0 | 0 |
| Norm - 3 | 35F | S | NL | 54 | 0 | 22 | 7 | 25 | 0 | 0 | 0 | 0 | 0 | 0 |
| Norm - 3 | 35F | S | FP | 65 | 0 | 38 | 0 | 14 | 0 | 14 | 0 | 0 | 0 | 0 |
| Norm - 3 | 35F | G | SG | 74 | 25 | 18 | 0 | 13 | 0 | 18 | 0 | 0 | 0 | 0 |
| Norm - 3 | 35F | G | IP | 61 | 21 | 14 | 0 | 0 | 0 | 26 | 0 | 0 | 0 | 0 |
| Norm - 4 | Neu | S | NL | 72 | 29 | 6 | 10 | 0 | 28 | 0 | 0 | 0 | 0 | 0 |
| Norm - 4 | Neu | S | FP | 72 | 42 | 7 | 0 | 0 | 24 | 0 | 0 | 0 | 0 | 0 |
| Norm - 4 | Neu | G | SG | 72 | 40 | 0 | 13 | 0 | 6 | 0 | 14 | 0 | 0 | 0 |
| Norm - 4 | Neu | G | IP | 81 | 43 | 6 | 3 | 0 | 25 | 0 | 4 | 0 | 0 | 0 |
| Norm - 4 | 35F | S | NL | 56 | 13 | 25 | 15 | 3 | 0 | 0 | 0 | 0 | 0 | 0 |
| Norm - 4 | 35F | S | FP | 15 | 0 | 15 | 0 | 0 | 0 | 0 | 0 | 0 | 0 | 0 |
| Norm - 4 | 35F | G | SG | 29 | 1 | 15 | 0 | 13 | 0 | 0 | 0 | 0 | 0 | 0 |
| Norm - 4 | 35F | G | IP | 22 | 0 | 13 | 0 | 10 | 0 | 0 | 0 | 0 | 0 | 0 |
| Norm - 5 | Neu | S | NL | 50 | 24 | 0 | 7 | 0 | 18 | 0 | 1 | 0 | 0 | 0 |
| Norm - 5 | Neu | S | FP | 29 | 0 | 0 | 7 | 4 | 4 | 0 | 14 | 0 | 0 | 0 |
| Norm - 5 | Neu | G | SG | 65 | 31 | 0 | 15 | 0 | 19 | 0 | 0 | 0 | 0 | 0 |
| Norm - 5 | Neu | G | IP | 63 | 33 | 0 | 0 | 0 | 15 | 0 | 14 | 0 | 0 | 0 |
| Norm - 5 | 35F | S | NL | 42 | 0 | 0 | 7 | 14 | 11 | 0 | 10 | 0 | 0 | 0 |
| Norm - 5 | 35F | S | FP | 46 | 0 | 0 | 0 | 21 | 0 | 25 | 0 | 0 | 0 | 0 |
| Norm - 5 | 35F | G | SG | 50 | 0 | 24 | 26 | 0 | 0 | 0 | 0 | 0 | 0 | 0 |
| Norm - 5 | 35F | G | IP | 32 | 0 | 24 | 0 | 8 | 0 | 0 | 0 | 0 | 0 | 0 |

The first four columns identify the subject, wrist angle, finger position, and loading activity (if one was used). The next column identifies the total percentage of the nerve boundary that is adjacent to tendons and the carpal tunnel boundary. Abbreviations: Wrists were either in 35 degrees of flexion (35F) or 0 degrees of flexion (Neu), and fingers were either straight (S) or gripped (G) loosely. Activities were either none (NL), flat press (FP), squeeze grip (SG), or index-thumb pinch (IP).

Table A-7. Nerve adjacency at the level of the hook of the hamate for the CTS patient group.

| | | | | | TUNNEL | THUMB | INDEX | | LONG | | FOURTH | | LITTLE | |
|---|---|---|---|---|---|---|---|---|---|---|---|---|---|---|
| Patient | Wrist Position | Finger Position | Activity | % Adjacency | | | Sup | Deep | Sup | Deep | Sup | Deep | Sup | Deep |
| CTS - 1 | Neu | S | NL | 81 | 29 | 26 | 11 | 0 | 14 | 0 | 0 | 0 | 0 | 0 |
| CTS - 1 | Neu | S | FP | 75 | 13 | 36 | 14 | 13 | 0 | 0 | 0 | 0 | 0 | 0 |
| CTS - 1 | Neu | G | SG | 79 | 36 | 18 | 0 | 0 | 25 | 0 | 0 | 0 | 0 | 0 |
| CTS - 1 | Neu | G | IP | 72 | 28 | 26 | 18 | 0 | 0 | 0 | 0 | 0 | 0 | 0 |
| CTS - 1 | 35F | S | NL | 76 | 38 | 18 | 0 | 21 | 0 | 0 | 0 | 0 | 0 | 0 |
| CTS - 1 | 35F | S | FP | 76 | 40 | 15 | 0 | 21 | 0 | 0 | 0 | 0 | 0 | 0 |
| CTS - 1 | 35F | G | SG | 71 | 38 | 18 | 1 | 14 | 0 | 0 | 0 | 0 | 0 | 0 |
| CTS - 1 | 35F | G | IP | 46 | 31 | 15 | 0 | 0 | 0 | 0 | 0 | 0 | 0 | 0 |
| CTS - 2 | Neu | S | NL | 33 | 3 | 0 | 0 | 0 | 31 | 0 | 0 | 0 | 0 | 0 |
| CTS - 2 | Neu | G | IP | 58 | 24 | 0 | 15 | 19 | 0 | 0 | 0 | 0 | 0 | 0 |
| CTS - 2 | 35F | S | NL | 53 | 26 | 0 | 0 | 26 | 0 | 0 | 0 | 0 | 0 | 0 |
| CTS - 2 | 35F | S | FP | 43 | 29 | 0 | 0 | 14 | 0 | 0 | 0 | 0 | 0 | 0 |
| CTS - 2 | 35F | G | SG | 56 | 26 | 11 | 4 | 14 | 0 | 0 | 0 | 0 | 0 | 0 |
| CTS - 2 | 35F | G | IP | 36 | 14 | 22 | 0 | 0 | 0 | 0 | 0 | 0 | 0 | 0 |
| CTS - 3 | Neu | S | NL | 64 | 25 | 7 | 1 | 0 | 31 | 0 | 0 | 0 | 0 | 0 |
| CTS - 3 | Neu | S | FP | 76 | 28 | 19 | 18 | 0 | 11 | 0 | 0 | 0 | 0 | 0 |
| CTS - 3 | Neu | G | SG | 71 | 32 | 13 | 0 | 0 | 26 | 0 | 0 | 0 | 0 | 0 |
| CTS - 3 | Neu | G | IP | 69 | 26 | 0 | 0 | 0 | 25 | 0 | 18 | 0 | 0 | 0 |
| CTS - 3 | 35F | S | NL | 85 | 43 | 0 | 0 | 0 | 31 | 0 | 8 | 0 | 3 | 0 |
| CTS - 4 | Neu | S | NL | 35 | 0 | 13 | 22 | 0 | 0 | 0 | 0 | 0 | 0 | 0 |
| CTS - 4 | Neu | S | FP | 69 | 6 | 33 | 15 | 15 | 0 | 0 | 0 | 0 | 0 | 0 |
| CTS - 4 | Neu | G | SG | 69 | 31 | 0 | 8 | 0 | 25 | 0 | 6 | 0 | 0 | 0 |
| CTS - 4 | Neu | G | IP | 67 | 40 | 0 | 4 | 0 | 22 | 0 | 0 | 0 | 0 | 0 |
| CTS - 4 | 35F | S | NL | 78 | 14 | 31 | 11 | 22 | 0 | 0 | 0 | 0 | 0 | 0 |
| CTS - 4 | 35F | S | FP | 67 | 11 | 32 | 0 | 24 | 0 | 0 | 0 | 0 | 0 | 0 |
| CTS - 4 | 35F | G | SG | 58 | 0 | 35 | 0 | 24 | 0 | 0 | 0 | 0 | 0 | 0 |
| CTS - 5 | Neu | S | NL | 65 | 35 | 1 | 6 | 0 | 24 | 0 | 0 | 0 | 0 | 0 |
| CTS - 5 | Neu | S | FP | 71 | 39 | 0 | 11 | 0 | 21 | 0 | 0 | 0 | 0 | 0 |
| CTS - 5 | Neu | G | SG | 68 | 26 | 11 | 6 | 0 | 25 | 0 | 0 | 0 | 0 | 0 |
| CTS - 5 | Neu | G | IP | 36 | 0 | 8 | 0 | 0 | 28 | 0 | 0 | 0 | 0 | 0 |
| CTS - 5 | 35F | S | NL | 54 | 11 | 0 | 0 | 0 | 26 | 0 | 17 | 0 | 0 | 0 |
| CTS - 5 | 35F | S | FP | 51 | 4 | 0 | 8 | 0 | 19 | 0 | 19 | 0 | 0 | 0 |
| CTS - 5 | 35F | G | SG | 58 | 8 | 0 | 19 | 0 | 10 | 0 | 21 | 0 | 0 | 0 |
| CTS - 6 | Neu | S | NL | 57 | 38 | 0 | 17 | 0 | 3 | 0 | 0 | 0 | 0 | 0 |
| CTS - 6 | Neu | S | FP | 38 | 32 | 0 | 0 | 0 | 6 | 0 | 0 | 0 | 0 | 0 |
| CTS - 6 | Neu | G | SG | 74 | 40 | 0 | 7 | 0 | 26 | 0 | 0 | 0 | 0 | 0 |
| CTS - 6 | 35F | S | NL | 46 | 8 | 15 | 22 | 0 | 0 | 0 | 0 | 0 | 0 | 0 |
| CTS - 6 | 35F | S | FP | 39 | 0 | 25 | 14 | 0 | 0 | 0 | 0 | 0 | 0 | 0 |
| CTS - 6 | 35F | G | SG | 61 | 3 | 28 | 0 | 31 | 0 | 0 | 0 | 0 | 0 | 0 |
| CTS - 6 | 35F | G | IP | 47 | 8 | 19 | 0 | 19 | 0 | 0 | 0 | 0 | 0 | 0 |
| CTS - 7 | Neu | S | NL | 78 | 43 | 8 | 14 | 0 | 13 | 0 | 0 | 0 | 0 | 0 |
| CTS - 7 | Neu | S | FP | 68 | 36 | 0 | 0 | 0 | 19 | 0 | 13 | 0 | 0 | 0 |
| CTS - 7 | Neu | G | SG | 72 | 42 | 14 | 0 | 0 | 17 | 0 | 0 | 0 | 0 | 0 |
| CTS - 7 | Neu | G | IP | 63 | 28 | 6 | 10 | 0 | 19 | 0 | 0 | 0 | 0 | 0 |
| CTS - 7 | 35F | S | NL | 82 | 33 | 0 | 0 | 0 | 11 | 14 | 18 | 0 | 6 | 0 |
| CTS - 7 | 35F | S | FP | 68 | 0 | 11 | 0 | 14 | 17 | 18 | 8 | 0 | 0 | 0 |
| CTS - 7 | 35F | G | SG | 76 | 8 | 0 | 0 | 13 | 24 | 13 | 19 | 0 | 0 | 0 |
| CTS - 7 | 35F | G | IP | 79 | 0 | 0 | 0 | 13 | 24 | 24 | 19 | 0 | 0 | 0 |

The first four columns identify the subject, wrist angle, finger position, and loading activity (if one was used). The next column identifies the total percentage of the nerve boundary that is adjacent to tendons and the carpal tunnel boundary. Abbreviations: Wrists were either in 35 degrees of flexion (35F) or 0 degrees of flexion (Neu), and fingers were either straight (S) or gripped (G) loosely. Activities were either none (NL), flat press (FP), squeeze grip (SG), or index-thumb pinch (IP).

Table A-8. Nerve adjacency at the level of the hook of the hamate for the normal group.

| | | | | | TUNNEL | THUMB | INDEX | | LONG | | FOURTH | | LITTLE | |
|---|---|---|---|---|---|---|---|---|---|---|---|---|---|---|
| Patient | Wrist Position | Finger Position | Activity | % Adjacency | | | Sup | Deep | Sup | Deep | Sup | Deep | Sup | Deep |
| Norm - 1 | Neu | S | NL | 57 | 25 | 0 | 0 | 0 | 24 | 0 | 8 | 0 | 0 | 0 |
| Norm - 1 | Neu | S | FP | 50 | 8 | 0 | 10 | 0 | 15 | 0 | 17 | 0 | 0 | 0 |
| Norm - 1 | Neu | G | SG | 72 | 28 | 22 | 0 | 22 | 0 | 0 | 0 | 0 | 0 | 0 |
| Norm - 1 | Neu | G | IP | 56 | 22 | 19 | 0 | 14 | 0 | 0 | 0 | 0 | 0 | 0 |
| Norm - 1 | 35F | S | NL | 53 | 0 | 0 | 13 | 4 | 22 | 0 | 14 | 0 | 0 | 0 |
| Norm - 1 | 35F | S | FP | 44 | 0 | 0 | 13 | 7 | 10 | 0 | 14 | 0 | 1 | 0 |
| Norm - 1 | 35F | G | SG | 58 | 38 | 1 | 19 | 0 | 0 | 0 | 0 | 0 | 0 | 0 |
| Norm - 1 | 35F | G | IP | 44 | 17 | 13 | 15 | 0 | 0 | 0 | 0 | 0 | 0 | 0 |
| Norm - 2 | Neu | S | NL | 67 | 35 | 3 | 22 | 0 | 7 | 0 | 0 | 0 | 0 | 0 |
| Norm - 2 | Neu | S | FP | 82 | 46 | 13 | 17 | 0 | 7 | 0 | 0 | 0 | 0 | 0 |
| Norm - 2 | Neu | G | SG | 68 | 40 | 4 | 0 | 0 | 22 | 0 | 1 | 0 | 0 | 0 |
| Norm - 2 | Neu | G | IP | 90 | 46 | 6 | 11 | 0 | 22 | 0 | 6 | 0 | 0 | 0 |
| Norm - 2 | 35F | S | NL | 79 | 42 | 19 | 18 | 0 | 0 | 0 | 0 | 0 | 0 | 0 |
| Norm - 2 | 35F | S | FP | 68 | 42 | 0 | 11 | 15 | 0 | 0 | 0 | 0 | 0 | 0 |
| Norm - 2 | 35F | G | SG | 93 | 50 | 15 | 14 | 14 | 0 | 0 | 0 | 0 | 0 | 0 |
| Norm - 2 | 35F | G | IP | 82 | 35 | 0 | 15 | 0 | 0 | 0 | 22 | 0 | 10 | 0 |
| Norm - 3 | Neu | S | NL | 71 | 35 | 0 | 0 | 0 | 25 | 0 | 11 | 0 | 0 | 0 |
| Norm - 3 | Neu | S | FP | 24 | 0 | 0 | 0 | 0 | 14 | 0 | 10 | 0 | 0 | 0 |
| Norm - 3 | Neu | G | SG | 71 | 32 | 0 | 10 | 0 | 0 | 0 | 29 | 0 | 0 | 0 |
| Norm - 3 | Neu | G | IP | 64 | 26 | 4 | 0 | 0 | 26 | 0 | 7 | 0 | 0 | 0 |
| Norm - 3 | 35F | S | NL | 75 | 28 | 15 | 11 | 21 | 0 | 0 | 0 | 0 | 0 | 0 |
| Norm - 3 | 35F | S | FP | 72 | 24 | 17 | 0 | 13 | 0 | 19 | 0 | 0 | 0 | 0 |
| Norm - 3 | 35F | G | SG | 71 | 40 | 14 | 0 | 17 | 0 | 0 | 0 | 0 | 0 | 0 |
| Norm - 3 | 35F | G | IP | 65 | 28 | 10 | 0 | 7 | 0 | 21 | 0 | 0 | 0 | 0 |
| Norm - 4 | Neu | S | NL | 53 | 6 | 10 | 17 | 0 | 21 | 0 | 0 | 0 | 0 | 0 |
| Norm - 4 | Neu | S | FP | 74 | 31 | 8 | 1 | 0 | 28 | 0 | 6 | 0 | 0 | 0 |
| Norm - 4 | Neu | G | SG | 86 | 42 | 0 | 14 | 0 | 18 | 0 | 13 | 0 | 0 | 0 |
| Norm - 4 | Neu | G | IP | 67 | 21 | 8 | 7 | 0 | 25 | 0 | 6 | 0 | 0 | 0 |
| Norm - 4 | 35F | S | NL | 36 | 0 | 19 | 17 | 0 | 0 | 0 | 0 | 0 | 0 | 0 |
| Norm - 4 | 35F | S | FP | 40 | 0 | 18 | 0 | 22 | 0 | 0 | 0 | 0 | 0 | 0 |
| Norm - 4 | 35F | G | SG | 54 | 29 | 10 | 0 | 15 | 0 | 0 | 0 | 0 | 0 | 0 |
| Norm - 4 | 35F | G | IP | 25 | 0 | 10 | 0 | 15 | 0 | 0 | 0 | 0 | 0 | 0 |
| Norm - 5 | Neu | S | NL | 50 | 21 | 0 | 0 | 0 | 18 | 0 | 11 | 0 | 0 | 0 |
| Norm - 5 | Neu | S | FP | 40 | 18 | 0 | 0 | 0 | 7 | 7 | 8 | 0 | 0 | 0 |
| Norm - 5 | Neu | G | SG | 36 | 6 | 0 | 0 | 0 | 21 | 0 | 10 | 0 | 0 | 0 |
| Norm - 5 | Neu | G | IP | 39 | 0 | 0 | 0 | 0 | 21 | 0 | 18 | 0 | 0 | 0 |
| Norm - 5 | 35F | S | NL | 31 | 0 | 0 | 4 | 15 | 1 | 10 | 0 | 0 | 0 | 0 |
| Norm - 5 | 35F | S | FP | 29 | 0 | 0 | 0 | 13 | 0 | 17 | 0 | 0 | 0 | 0 |
| Norm - 5 | 35F | G | SG | 53 | 0 | 25 | 28 | 0 | 0 | 0 | 0 | 0 | 0 | 0 |
| Norm - 5 | 35F | G | IP | 57 | 14 | 25 | 0 | 18 | 0 | 0 | 0 | 0 | 0 | 0 |

The first four columns identify the subject, wrist angle, finger position, and loading activity (if one was used). The next column identifies the total percentage of the nerve boundary that is adjacent to tendons and the carpal tunnel boundary. Abbreviations: Wrists were either in 35 degrees of flexion (35F) or 0 degrees of flexion (Neu), and fingers were either straight (S) or gripped (G) loosely. Activities were either none (NL), flat press (FP), squeeze grip (SG), or index-thumb pinch (IP).

Table A-9. Location of structures adjacent to the nerve at the level of the pisiform for the CTS patient group.

| | | | | | | INDEX | | LONG | | FOURTH | | LITTLE | |
|---|---|---|---|---|---|---|---|---|---|---|---|---|---|
| Patient | Wrist Position | Finger Position | Activity | TUNNEL | THUMB | Sup | Deep | Sup | Deep | Sup | Deep | Sup | Deep |
| CTS - 1 | Neu | S | NL | V | DR | -- | -- | DU | -- | -- | -- | -- | -- |
| CTS - 1 | Neu | S | FP | -- | R | U | DU | -- | -- | -- | -- | -- | -- |
| CTS - 1 | Neu | G | SG | V | -- | -- | -- | D | -- | -- | -- | -- | -- |
| CTS - 1 | Neu | G | IP | V | -- | -- | -- | U | -- | -- | -- | -- | -- |
| CTS - 1 | 35F | S | NL | D | VR | -- | U | -- | -- | -- | -- | -- | -- |
| CTS - 1 | 35F | S | FP | D | VR | -- | DU | -- | -- | -- | -- | -- | -- |
| CTS - 1 | 35F | G | SG | D | VR | VU | U | -- | -- | -- | -- | -- | -- |
| CTS - 1 | 35F | G | IP | DR | V | -- | -- | -- | -- | -- | -- | -- | -- |
| CTS - 2 | Neu | S | NL | V | -- | -- | -- | -- | -- | -- | -- | -- | -- |
| CTS - 2 | Neu | G | IP | V | -- | -- | -- | DU | -- | -- | -- | -- | -- |
| CTS - 2 | 35F | S | NL | D | R | -- | U | -- | -- | -- | -- | -- | -- |
| CTS - 2 | 35F | S | FP | -- | R | -- | VU | -- | -- | -- | -- | -- | -- |
| CTS - 2 | 35F | G | SG | R | D | VU | U | -- | -- | -- | -- | -- | -- |
| CTS - 2 | 35F | G | IP | -- | R | -- | -- | -- | -- | -- | -- | -- | -- |
| CTS - 3 | Neu | S | NL | V | -- | -- | -- | DR | -- | -- | -- | -- | -- |
| CTS - 3 | Neu | S | FP | V | R | DR | -- | D | -- | -- | -- | -- | -- |
| CTS - 3 | Neu | G | SG | V | -- | -- | -- | -- | -- | -- | -- | -- | -- |
| CTS - 3 | Neu | G | IP | V | -- | -- | -- | R | -- | -- | -- | -- | -- |
| CTS - 3 | 35F | S | NL | V | -- | -- | -- | R | -- | D | -- | DU | -- |
| CTS - 4 | Neu | S | NL | VU | DR | D | -- | -- | -- | -- | -- | -- | -- |
| CTS - 4 | Neu | S | FP | V | R | U | -- | -- | -- | -- | -- | -- | -- |
| CTS - 4 | Neu | G | SG | V | -- | -- | -- | D | -- | DU | -- | -- | -- |
| CTS - 4 | Neu | G | IP | V | -- | -- | -- | DU | -- | -- | -- | -- | -- |
| CTS - 4 | 35F | S | NL | -- | R | UV | U | -- | -- | -- | -- | -- | -- |
| CTS - 4 | 35F | S | FP | -- | R | -- | U | -- | -- | -- | -- | -- | -- |
| CTS - 4 | 35F | G | SG | -- | DR | -- | VU | -- | -- | -- | -- | -- | -- |
| CTS - 5 | Neu | S | NL | V | -- | -- | -- | D | -- | -- | -- | -- | -- |
| CTS - 5 | Neu | S | FP | V | -- | -- | -- | D | -- | -- | -- | -- | -- |
| CTS - 5 | Neu | G | SG | V | -- | -- | -- | D | -- | -- | -- | -- | -- |
| CTS - 5 | Neu | G | IP | -- | DR | -- | -- | D | -- | -- | -- | -- | -- |
| CTS - 5 | 35F | S | NL | V | -- | -- | -- | R | -- | DU | -- | -- | -- |
| CTS - 5 | 35F | S | FP | V | -- | -- | -- | R | -- | D | -- | -- | -- |
| CTS - 5 | 35F | G | SG | -- | -- | R | -- | DR | -- | DU | -- | -- | -- |
| CTS - 6 | Neu | S | NL | V | -- | DR | -- | D | -- | -- | -- | -- | -- |
| CTS - 6 | Neu | S | FP | V | -- | -- | -- | -- | -- | -- | -- | -- | -- |
| CTS - 6 | Neu | G | SG | U | -- | DR | -- | D | -- | -- | -- | -- | -- |
| CTS - 6 | 35F | S | NL | -- | R | U | -- | -- | -- | -- | -- | -- | -- |
| CTS - 6 | 35F | S | FP | -- | R | U | -- | -- | -- | -- | -- | -- | -- |
| CTS - 6 | 35F | G | SG | -- | R | -- | U | -- | -- | -- | -- | -- | -- |
| CTS - 6 | 35F | G | IP | D | VR | -- | -- | -- | -- | -- | -- | -- | -- |
| CTS - 7 | Neu | S | NL | V | DR | D | -- | DU | -- | -- | -- | -- | -- |
| CTS - 7 | Neu | S | FP | V | R | -- | -- | DR | -- | DU | -- | -- | -- |
| CTS - 7 | Neu | G | SG | V | R | -- | -- | D | -- | -- | -- | -- | -- |
| CTS - 7 | Neu | G | IP | V | -- | -- | -- | D | -- | -- | -- | -- | -- |
| CTS - 7 | 35F | S | NL | VU | -- | -- | -- | VR | DR | D | -- | DU | -- |
| CTS - 7 | 35F | S | FP | -- | -- | -- | DR | VR | DU | VU | -- | -- | -- |
| CTS - 7 | 35F | G | SG | -- | -- | -- | DR | R | DU | U | -- | -- | -- |
| CTS - 7 | 35F | G | IP | -- | -- | -- | DR | VR | D | U | -- | -- | -- |

Abbreviations: Wrists were either in 35 degrees of flexion (35F) or 0 degrees of flexion (Neu), and fingers were either straight (S) or gripped (G) loosely. Activities were either none (NL), flat press (FP), squeeze grip (SG), or index-thumb pinch (IP). Locations are specified as radial (R), ulnar (U), dorsal (D), volar (V), or a combination of two directions.

Table A-10. Location of structures adjacent to the nerve at the level of the pisiform for the normal subject group.

| | | | | | | INDEX | | LONG | | FOURTH | | LITTLE | |
|---|---|---|---|---|---|---|---|---|---|---|---|---|---|
| Patient | Wrist Position | Finger Position | Activity | TUNNEL | THUMB | Sup | Deep | Sup | Deep | Sup | Deep | Sup | Deep |
| Norm - 1 | Neu | S | NL | V | -- | -- | -- | DR | -- | -- | -- | -- | -- |
| Norm - 1 | Neu | S | FP | -- | -- | R | DR | -- | DU | UV | -- | -- | -- |
| Norm - 1 | Neu | G | SG | V | DR | DU | -- | -- | -- | -- | -- | -- | -- |
| Norm - 1 | Neu | G | IP | -- | R | U | -- | -- | -- | -- | -- | -- | -- |
| Norm - 1 | 35F | S | NL | -- | -- | R | DR | VR | -- | VU | -- | -- | -- |
| Norm - 1 | 35F | S | FP | -- | -- | R | DR | VR | -- | VU | -- | -- | -- |
| Norm - 1 | 35F | G | SG | D | VR | U | -- | -- | -- | -- | -- | -- | -- |
| Norm - 1 | 35F | G | IP | DR | V | -- | -- | -- | -- | -- | -- | -- | -- |
| Norm - 2 | Neu | S | NL | V | -- | D | -- | DU | -- | -- | -- | -- | -- |
| Norm - 2 | Neu | S | FP | VR | -- | DU | -- | U | -- | -- | -- | -- | -- |
| Norm - 2 | Neu | G | SG | V | -- | -- | -- | D | -- | -- | -- | -- | -- |
| Norm - 2 | Neu | G | IP | V | -- | -- | -- | DU | -- | -- | -- | -- | -- |
| Norm - 2 | 35F | S | NL | VR | -- | VU | -- | -- | -- | -- | -- | -- | -- |
| Norm - 2 | 35F | S | FP | R | -- | V | -- | -- | -- | -- | -- | -- | -- |
| Norm - 2 | 35F | G | SG | R | D | VU | U | -- | -- | -- | -- | -- | -- |
| Norm - 2 | 35F | G | IP | VU | -- | R | -- | -- | -- | D | -- | DU | -- |
| Norm - 3 | Neu | S | NL | V | -- | -- | -- | DR | -- | -- | -- | -- | -- |
| Norm - 3 | Neu | S | FP | -- | -- | -- | D | R | -- | U | -- | -- | -- |
| Norm - 3 | Neu | G | SG | V | -- | -- | -- | -- | -- | R | -- | DU | -- |
| Norm - 3 | Neu | G | IP | V | -- | -- | -- | R | -- | DU | -- | -- | -- |
| Norm - 3 | 35F | S | NL | -- | R | V | U | -- | -- | -- | -- | -- | -- |
| Norm - 3 | 35F | S | FP | -- | R | -- | V | -- | DU | -- | -- | -- | -- |
| Norm - 3 | 35F | G | SG | R | DU | -- | VR | -- | VU | -- | -- | -- | -- |
| Norm - 3 | 35F | G | IP | D | VR | -- | -- | -- | VU | -- | -- | -- | -- |
| Norm - 4 | Neu | S | NL | V | DR | D | -- | DU | -- | -- | -- | -- | -- |
| Norm - 4 | Neu | S | FP | V | DR | -- | -- | D | -- | -- | -- | -- | -- |
| Norm - 4 | Neu | G | SG | V | -- | R | -- | DR | -- | DU | -- | -- | -- |
| Norm - 4 | Neu | G | IP | V | R | DR | -- | R | -- | U | -- | -- | -- |
| Norm - 4 | 35F | S | NL | VR | D | VU | DU | -- | -- | -- | -- | -- | -- |
| Norm - 4 | 35F | S | FP | -- | DU | -- | -- | -- | -- | -- | -- | -- | -- |
| Norm - 4 | 35F | G | SG | DR | VR | -- | VU | -- | -- | -- | -- | -- | -- |
| Norm - 4 | 35F | G | IP | -- | V | -- | VU | -- | -- | -- | -- | -- | -- |
| Norm - 5 | Neu | S | NL | V | -- | DR | -- | R | -- | DU | -- | -- | -- |
| Norm - 5 | Neu | S | FP | -- | -- | DR | D | VR | -- | U | -- | -- | -- |
| Norm - 5 | Neu | G | SG | V | -- | D | -- | DR | -- | -- | -- | -- | -- |
| Norm - 5 | Neu | G | IP | V | -- | -- | -- | R | -- | DU | -- | -- | -- |
| Norm - 5 | 35F | S | NL | -- | -- | VR | DR | V | -- | VU | -- | -- | -- |
| Norm - 5 | 35F | S | FP | -- | -- | -- | R | -- | U | -- | -- | -- | -- |
| Norm - 5 | 35F | G | SG | -- | VR | U | -- | -- | -- | -- | -- | -- | -- |
| Norm - 5 | 35F | G | IP | -- | VR | -- | VU | -- | -- | -- | -- | -- | -- |

Abbreviations: Wrists were either in 35 degrees of flexion (35F) or 0 degrees of flexion (Neu), and fingers were either straight (S) or gripped (G) loosely. Activities were either none (NL), flat press (FP), squeeze grip (SG), or index-thumb pinch (IP). Locations are specified as radial (R), ulnar (U), dorsal (D), volar (V), or a combination of two directions.

Table A-11. Location of structures adjacent to the nerve at the level of the hook of the hamate for the CTS patient group.

| | | | | | | INDEX | | LONG | | FOURTH | | LITTLE | |
|---|---|---|---|---|---|---|---|---|---|---|---|---|---|
| Patient | Wrist Position | Finger Position | Activity | TUNNEL | THUMB | Sup | Deep | Sup | Deep | Sup | Deep | Sup | Deep |
| CTS - 1 | Neu | S | NL | V | R | DU | -- | U | -- | -- | -- | -- | -- |
| CTS - 1 | Neu | S | FP | DR | VR | VU | DU | -- | -- | -- | -- | -- | -- |
| CTS - 1 | Neu | G | SG | V | R | -- | -- | D | -- | -- | -- | -- | -- |
| CTS - 1 | Neu | G | IP | V | R | DU | -- | VU | -- | -- | -- | -- | -- |
| CTS - 1 | 35F | S | NL | R | V | -- | U | -- | -- | -- | -- | -- | -- |
| CTS - 1 | 35F | S | FP | DR | V | -- | VU | -- | -- | -- | -- | -- | -- |
| CTS - 1 | 35F | G | SG | DR | V | VU | U | -- | -- | -- | -- | -- | -- |
| CTS - 1 | 35F | G | IP | DR | V | -- | -- | -- | -- | -- | -- | -- | -- |
| CTS - 2 | Neu | S | NL | V | -- | -- | -- | R | -- | -- | -- | -- | -- |
| CTS - 2 | Neu | G | IP | V | -- | DU | DR | R | -- | -- | -- | -- | -- |
| CTS - 2 | 35F | S | NL | DR | -- | -- | VU | -- | -- | -- | -- | -- | -- |
| CTS - 2 | 35F | S | FP | D | -- | -- | V | -- | -- | -- | -- | -- | -- |
| CTS - 2 | 35F | G | SG | R | D | VU | R | -- | -- | -- | -- | -- | -- |
| CTS - 2 | 35F | G | IP | D | VR | -- | -- | -- | -- | -- | -- | -- | -- |
| CTS - 3 | Neu | S | NL | V | R | DR | -- | D | -- | -- | -- | -- | -- |
| CTS - 3 | Neu | S | FP | V | R | D | -- | DU | -- | -- | -- | -- | -- |
| CTS - 3 | Neu | G | SG | V | R | -- | -- | D | -- | -- | -- | -- | -- |
| CTS - 3 | Neu | G | IP | VU | -- | -- | -- | R | -- | D | -- | -- | -- |
| CTS - 3 | 35F | S | NL | V | -- | -- | -- | DR | -- | D | -- | DU | -- |
| CTS - 4 | Neu | S | NL | -- | R | D | -- | -- | -- | -- | -- | -- | -- |
| CTS - 4 | Neu | S | FP | D | R | VU | DU | -- | -- | -- | -- | -- | -- |
| CTS - 4 | Neu | G | SG | V | -- | DR | -- | D | -- | U | -- | -- | -- |
| CTS - 4 | Neu | G | IP | V | -- | DR | -- | D | -- | -- | -- | -- | -- |
| CTS - 4 | 35F | S | NL | D | R | VU | DU | -- | -- | -- | -- | -- | -- |
| CTS - 4 | 35F | S | FP | D | R | -- | U | -- | -- | -- | -- | -- | -- |
| CTS - 4 | 35F | G | SG | -- | R | -- | U | -- | -- | -- | -- | -- | -- |
| CTS - 5 | Neu | S | NL | V | R | DR | -- | D | -- | -- | -- | -- | -- |
| CTS - 5 | Neu | S | FP | V | -- | D | -- | DU | -- | -- | -- | -- | -- |
| CTS - 5 | Neu | G | SG | V | R | DR | -- | D | -- | -- | -- | -- | -- |
| CTS - 5 | Neu | G | IP | -- | R | -- | -- | D | -- | -- | -- | -- | -- |
| CTS - 5 | 35F | S | NL | V | -- | -- | -- | R | -- | U | -- | -- | -- |
| CTS - 5 | 35F | S | FP | V | -- | DR | -- | R | -- | U | -- | -- | -- |
| CTS - 5 | 35F | G | SG | V | -- | DR | -- | D | -- | DU | -- | -- | -- |
| CTS - 6 | Neu | S | NL | V | -- | DR | -- | DU | -- | -- | -- | -- | -- |
| CTS - 6 | Neu | S | FP | V | -- | -- | -- | D | -- | -- | -- | -- | -- |
| CTS - 6 | Neu | G | SG | V | -- | DR | -- | D | -- | -- | -- | -- | -- |
| CTS - 6 | 35F | S | NL | V | R | U | -- | -- | -- | -- | -- | -- | -- |
| CTS - 6 | 35F | S | FP | -- | R | U | -- | -- | -- | -- | -- | -- | -- |
| CTS - 6 | 35F | G | SG | DR | VR | -- | U | -- | -- | -- | -- | -- | -- |
| CTS - 6 | 35F | G | IP | DR | VR | -- | VU | -- | -- | -- | -- | -- | -- |
| CTS - 7 | Neu | S | NL | V | DR | D | -- | DU | -- | -- | -- | -- | -- |
| CTS - 7 | Neu | S | FP | V | -- | -- | -- | DR | -- | DU | -- | -- | -- |
| CTS - 7 | Neu | G | SG | V | R | -- | -- | D | -- | -- | -- | -- | -- |
| CTS - 7 | Neu | G | IP | V | R | DR | -- | D | -- | -- | -- | -- | -- |
| CTS - 7 | 35F | S | NL | VU | -- | -- | -- | R | DR | D | -- | DU | -- |
| CTS - 7 | 35F | S | FP | -- | D | -- | R | VR | U | VU | -- | -- | -- |
| CTS - 7 | 35F | G | SG | V | -- | -- | DR | VR | D | U | -- | -- | -- |
| CTS - 7 | 35F | G | IP | -- | -- | -- | R | V | D | U | -- | -- | -- |

Abbreviations: Wrists were either in 35 degrees of flexion (35F) or 0 degrees of flexion (Neu), and fingers were either straight (S) or gripped (G) loosely. Activities were either none (NL), flat press (FP), squeeze grip (SG), or index-thumb pinch (IP). Locations are specified as radial (R), ulnar (U), dorsal (D), volar (V), or a combination of two directions.

Table A-12. Location of structures adjacent to the nerve at the level of the hook of the hamate for the normal subject group.

| | | | | | | INDEX | | LONG | | FOURTH | | LITTLE | |
|---|---|---|---|---|---|---|---|---|---|---|---|---|---|
| Patient | Wrist Position | Finger Position | Activity | TUNNEL | THUMB | Sup | Deep | Sup | Deep | Sup | Deep | Sup | Deep |
| Norm - 1 | Neu | S | NL | V | -- | -- | -- | R | -- | U | -- | -- | -- |
| Norm - 1 | Neu | S | FP | V | -- | DR | -- | VR | -- | U | -- | -- | -- |
| Norm - 1 | Neu | G | SG | DR | V | -- | U | -- | -- | -- | -- | -- | -- |
| Norm - 1 | Neu | G | IP | D | VR | -- | VU | -- | -- | -- | -- | -- | -- |
| Norm - 1 | 35F | S | NL | -- | -- | R | DR | V | -- | VU | -- | -- | -- |
| Norm - 1 | 35F | S | FP | -- | -- | VR | DR | V | -- | VU | -- | U | -- |
| Norm - 1 | 35F | G | SG | DR | V | VU | -- | -- | -- | -- | -- | -- | -- |
| Norm - 1 | 35F | G | IP | R | V | U | -- | -- | -- | -- | -- | -- | -- |
| Norm - 2 | Neu | S | NL | V | DR | D | -- | -- | -- | -- | -- | -- | -- |
| Norm - 2 | Neu | S | FP | VR | D | DU | -- | U | -- | -- | -- | -- | -- |
| Norm - 2 | Neu | G | SG | V | -- | -- | -- | D | -- | -- | -- | -- | -- |
| Norm - 2 | Neu | G | IP | V | -- | -- | -- | D | -- | -- | -- | -- | -- |
| Norm - 2 | 35F | S | NL | VR | -- | VU | -- | -- | -- | -- | -- | -- | -- |
| Norm - 2 | 35F | S | FP | R | -- | VU | U | -- | -- | -- | -- | -- | -- |
| Norm - 2 | 35F | G | SG | R | D | VU | U | -- | -- | -- | -- | -- | -- |
| Norm - 2 | 35F | G | IP | U | -- | R | -- | -- | -- | D | -- | DU | -- |
| Norm - 3 | Neu | S | NL | V | -- | -- | -- | DR | -- | U | -- | -- | -- |
| Norm - 3 | Neu | S | FP | -- | -- | -- | -- | R | -- | DU | -- | -- | -- |
| Norm - 3 | Neu | G | SG | V | -- | DR | -- | -- | -- | DU | -- | -- | -- |
| Norm - 3 | Neu | G | IP | V | R | -- | -- | DR | -- | DU | -- | -- | -- |
| Norm - 3 | 35F | S | NL | DR | VR | V | DU | -- | -- | -- | -- | -- | -- |
| Norm - 3 | 35F | S | FP | D | R | -- | V | -- | U | -- | -- | -- | -- |
| Norm - 3 | 35F | G | SG | DR | DU | -- | VR | -- | -- | -- | -- | -- | -- |
| Norm - 3 | 35F | G | IP | D | VR | -- | V | -- | VU | -- | -- | -- | -- |
| Norm - 4 | Neu | S | NL | V | DR | D | -- | DU | -- | -- | -- | -- | -- |
| Norm - 4 | Neu | S | FP | V | R | DR | -- | D | -- | U | -- | -- | -- |
| Norm - 4 | Neu | G | SG | V | -- | R | -- | D | -- | DU | -- | -- | -- |
| Norm - 4 | Neu | G | IP | V | R | DR | -- | D | -- | DU | -- | -- | -- |
| Norm - 4 | 35F | S | NL | -- | D | U | -- | -- | -- | -- | -- | -- | -- |
| Norm - 4 | 35F | S | FP | -- | DU | -- | VU | -- | -- | -- | -- | -- | -- |
| Norm - 4 | 35F | G | SG | DR | V | -- | VU | -- | -- | -- | -- | -- | -- |
| Norm - 4 | 35F | G | IP | -- | V | -- | VU | -- | -- | -- | -- | -- | -- |
| Norm - 5 | Neu | S | NL | V | -- | -- | -- | R | -- | DU | -- | -- | -- |
| Norm - 5 | Neu | S | FP | V | -- | -- | -- | VR | D | U | -- | -- | -- |
| Norm - 5 | Neu | G | SG | V | -- | -- | -- | R | -- | U | -- | -- | -- |
| Norm - 5 | Neu | G | IP | -- | -- | -- | -- | R | -- | U | -- | -- | -- |
| Norm - 5 | 35F | S | NL | -- | -- | VR | R | V | U | -- | -- | -- | -- |
| Norm - 5 | 35F | S | FP | -- | -- | -- | VR | -- | U | -- | -- | -- | -- |
| Norm - 5 | 35F | G | SG | -- | V | U | -- | -- | -- | -- | -- | -- | -- |
| Norm - 5 | 35F | G | IP | DR | VR | -- | VU | -- | -- | -- | -- | -- | -- |

Abbreviations: Wrists were either in 35 degrees of flexion (35F) or 0 degrees of flexion (Neu), and fingers were either straight (S) or gripped (G) loosely. Activities were either none (NL), flat press (FP), squeeze grip (SG), or index-thumb pinch (IP). Locations are specified as radial (R), ulnar (U), dorsal (D), volar (V), or a combination of two directions.

Table A-13. Shape number chains at the level of the pisiform for the CTS patient group.

| Patient | Wrist Position | Finger Position | Activity | |
|---|---|---|---|---|
| CTS - 1 | Neu | S | NL | 1 1 1 2 1 1 0 0 1 1 1 1 2 0 1 3 0 0 0 0 0 2 |
| CTS - 1 | Neu | S | FP | 0 1 0 0 -1 3 3 2 2 0 0 0 0 0 0 0 4 2 0 1 0 1 |
| CTS - 1 | Neu | G | SG | -1 1 1 1 2 0 1 0 1 1 1 1 1 0 1 1 1 1 1 0 1 0 0 2 |
| CTS - 1 | Neu | G | IP | -1 1 1 2 2 1 0 1 0 1 1 0 1 1 3 1 0 -1 -1 1 3 1 1 |
| CTS - 1 | 35F | S | NL | 1 0 0 1 4 1 -1 0 -1 1 1 1 1 1 1 1 1 1 1 1 1 1 1 |
| CTS - 1 | 35F | S | FP | 0 1 0 0 1 1 4 1 0 0 0 -1 0 2 0 1 2 0 1 2 1 1 1 |
| CTS - 1 | 35F | G | SG | 0 0 0 0 0 0 0 2 4 0 0 0 0 0 1 2 1 1 1 1 0 1 1 1 1 |
| CTS - 1 | 35F | G | IP | 0 1 0 0 0 4 0 -1 0 1 1 1 1 1 1 0 1 1 1 0 1 1 1 1 1 |
| CTS - 2 | Neu | S | NL | 1 2 -1 2 1 0 1 0 1 1 1 1 1 2 2 0 0 0 1 1 1 0 1 |
| CTS - 2 | Neu | G | IP | 0 -1 0 -1 0 0 3 0 1 1 1 2 -1 1 0 1 0 1 1 0 0 1 2 1 1 0 0 0 4 |
| CTS - 2 | 35F | S | NL | 2 0 2 1 1 1 0 0 0 1 0 2 1 0 2 1 1 0 0 0 0 2 |
| CTS - 2 | 35F | S | FP | 1 1 1 1 2 0 0 1 2 2 1 1 1 1 1 2 |
| CTS - 2 | 35F | G | SG | 0 2 1 0 1 3 1 1 0 0 0 0 1 0 1 1 4 1 -1 0 1 0 0 0 |
| CTS - 2 | 35F | G | IP | 0 3 1 0 1 2 1 1 1 0 0 1 3 1 1 0 2 0 0 1 1 |
| CTS - 3 | Neu | S | NL | 3 1 0 1 0 0 0 1 0 1 1 0 1 0 2 0 1 0 1 0 1 1 1 0 0 1 2 |
| CTS - 3 | Neu | S | FP | 2 0 1 1 0 0 0 1 0 1 2 2 1 1 1 1 3 0 0 -1 0 0 0 2 4 |
| CTS - 3 | Neu | G | SG | 1 2 1 0 0 1 1 0 2 4 1 0 0 0 0 0 1 1 2 |
| CTS - 3 | Neu | G | IP | 1 3 1 0 1 0 0 0 2 1 0 1 1 0 2 1 1 1 1 0 1 0 1 |
| CTS - 3 | 35F | S | NL | 2 1 1 0 0 0 1 0 1 1 1 2 2 1 0 0 0 0 0 1 1 2 1 |
| CTS - 4 | Neu | S | NL | 1 1 2 1 1 0 0 0 0 1 2 1 2 2 1 1 0 0 0 1 0 2 |
| CTS - 4 | Neu | S | FP | 0 0 1 0 1 0 1 2 1 2 2 0 0 -1 0 0 0 1 2 1 2 1 1 0 0 0 |
| CTS - 4 | Neu | G | SG | 1 1 1 0 1 0 0 0 0 0 1 1 1 1 2 2 1 0 0 0 0 0 0 0 1 0 0 1 1 2 |
| CTS - 4 | Neu | G | IP | 2 2 1 0 0 0 0 0 0 0 0 0 0 0 1 3 1 1 1 1 0 0 0 0 0 0 0 1 1 2 |
| CTS - 4 | 35F | S | NL | 0 1 1 0 0 1 2 3 2 0 0 0 0 0 1 2 3 1 0 2 1 1 1 |
| CTS - 4 | 35F | S | FP | 1 0 1 1 0 1 1 2 2 0 0 -1 0 1 2 2 0 0 3 0 1 1 |
| CTS - 4 | 35F | G | SG | 1 0 0 0 0 0 0 1 3 2 0 1 1 0 1 0 1 0 0 0 1 3 3 |
| CTS - 5 | Neu | S | NL | 1 1 1 -1 1 1 1 2 2 1 1 0 0 0 0 0 0 0 1 2 1 0 1 0 1 |
| CTS - 5 | Neu | S | FP | 1 0 0 0 0 0 0 0 0 0 -1 1 1 2 1 1 1 1 1 1 0 0 0 0 0 1 0 1 0 0 0 2 1 0 2 |
| CTS - 5 | Neu | G | SG | 0 0 1 1 -1 0 -1 0 0 -1 1 2 1 1 2 1 1 1 0 1 0 1 0 0 0 0 0 1 1 0 1 1 1 1 |
| CTS - 5 | Neu | G | IP | 1 0 0 0 0 -1 0 3 1 1 1 2 1 0 0 0 0 0 0 1 1 1 1 1 2 1 |
| CTS - 5 | 35F | S | NL | 2 1 1 2 2 1 0 0 0 1 1 2 1 1 1 0 0 1 0 0 1 2 0 0 0 0 0 1 |
| CTS - 5 | 35F | S | FP | 0 0 0 0 0 0 1 0 3 2 0 1 1 1 1 0 1 0 1 1 -1 4 |
| CTS - 5 | 35F | G | SG | 0 0 0 1 0 -1 1 1 1 -1 2 1 1 0 0 3 1 0 1 0 0 0 0 0 0 0 0 2 1 -1 1 0 2 3 |
| CTS - 6 | Neu | S | NL | 2 1 1 0 0 0 0 0 0 0 1 1 1 3 1 1 1 1 0 0 0 0 0 0 0 1 3 |
| CTS - 6 | Neu | S | FP | 2 2 1 0 0 0 1 0 0 0 1 0 2 3 2 1 1 0 0 0 0 0 0 0 0 0 0 1 1 2 |
| CTS - 6 | Neu | G | SG | 2 2 1 0 0 0 0 0 1 0 1 1 1 2 1 2 1 0 0 0 0 0 0 0 0 1 1 2 |
| CTS - 6 | 35F | S | NL | 0 0 0 0 -1 0 1 1 2 3 1 1 1 0 1 0 0 0 0 0 0 2 2 2 2 1 0 |
| CTS - 6 | 35F | S | FP | 0 0 0 0 0 0 0 0 0 0 0 3 2 2 1 0 0 0 0 0 0 0 0 1 1 3 2 1 1 |
| CTS - 6 | 35F | G | SG | 1 0 0 0 0 0 0 0 1 4 1 1 0 1 0 1 0 1 0 0 0 1 1 3 1 |
| CTS - 6 | 35F | G | IP | 1 0 0 0 1 2 3 1 -1 0 0 -1 2 1 0 0 0 2 2 2 0 0 1 |
| CTS - 7 | Neu | S | NL | 2 1 1 0 0 0 0 0 0 0 0 0 0 0 1 1 1 1 2 1 1 1 0 0 1 0 0 0 0 0 0 0 0 1 1 2 |
| CTS - 7 | Neu | S | FP | 2 1 1 0 0 0 0 0 1 0 0 0 0 1 1 1 1 1 1 1 1 1 1 1 0 0 0 0 0 1 0 0 0 1 0 0 0 2 |
| CTS - 7 | Neu | G | SG | 1 1 2 1 1 0 1 0 0 0 0 0 0 0 0 0 1 0 0 0 1 1 1 2 1 0 1 0 0 0 1 0 0 0 0 0 0 0 1 0 1 |
| CTS - 7 | Neu | G | IP | 1 2 2 1 0 1 0 1 -1 1 0 1 0 0 0 1 1 1 1 1 2 1 1 1 1 1 0 0 1 0 0 0 1 1 1 |
| CTS - 7 | 35F | S | NL | 0 2 1 1 0 0 0 0 0 0 0 0 0 1 2 1 2 1 -1 0 1 0 0 0 0 0 1 2 0 0 0 -1 2 2 |
| CTS - 7 | 35F | S | FP | 0 0 1 0 0 0 2 2 2 1 1 0 0 -1 0 0 1 1 1 1 1 1 0 1 1 1 0 0 1 |
| CTS - 7 | 35F | G | SG | 1 0 0 -1 1 1 1 1 1 1 1 1 0 0 -1 0 0 1 1 2 0 0 2 1 1 1 1 0 |
| CTS - 7 | 35F | G | IP | -1 1 1 1 1 0 2 2 1 -1 -1 0 -1 1 3 1 0 0 2 1 2 0 1 1 1 1 |

Abbreviations: Wrists were either in 35 degrees of flexion (35F) or 0 degrees of flexion (Neu), and fingers were either straight (S) or gripped (G) loosely. Activities were either none (NL), flat press (FP), squeeze grip (SG), or index-thumb pinch (IP).

Table A-14. Shape number chains at the level of the pisiform for the normal subject group.

| Patient | Wrist Position | Finger Position | Activity | |
|---|---|---|---|---|
| Norm - 1 | Neu | S | NL | 0 1 1 1 0 1 1 1 0 1 0 2 2 1 1 0 0 0 0 0 2 0 1 1 |
| Norm - 1 | Neu | S | FP | 1 0 0 0 2 2 2 0 1 0 1 0 0 1 0 1 2 1 1 1 1 |
| Norm - 1 | Neu | G | SG | 0 0 -1 0 0 1 1 1 2 2 1 1 1 0 2 -1 -1 0 0 0 3 4 2 |
| Norm - 1 | Neu | G | IP | 0 0 0 0 0 1 1 1 2 0 2 3 1 0 0 0 0 0 0 1 2 2 3 1 0 1 |
| Norm - 1 | 35F | S | NL | 1 1 1 3 0 0 0 3 0 0 2 2 1 1 1 0 1 |
| Norm - 1 | 35F | S | FP | 0 0 0 1 0 1 3 1 2 1 1 1 0 1 2 0 1 2 1 1 |
| Norm - 1 | 35F | G | SG | 0 0 0 0 0 -1 0 1 2 2 1 0 1 1 2 2 2 -1 0 0 0 0 1 -1 8 |
| Norm - 1 | 35F | G | IP | 1 2 1 0 0 0 2 1 1 1 0 1 1 1 1 1 1 1 1 1 0 0 1 |
| Norm - 2 | Neu | S | NL | 3 2 0 0 0 0 0 1 0 1 1 1 1 3 2 0 0 0 0 0 0 0 1 2 |
| Norm - 2 | Neu | S | FP | 2 2 1 1 1 0 0 0 0 0 1 0 0 0 1 1 2 2 1 0 1 0 0 0 0 0 0 0 0 1 |
| Norm - 2 | Neu | G | SG | 2 1 1 1 0 0 0 0 0 0 0 1 0 1 1 2 1 1 1 0 0 1 0 0 0 0 0 1 1 0 2 |
| Norm - 2 | Neu | G | IP | 1 2 1 1 1 1 0 0 0 0 0 0 0 1 1 1 1 2 1 1 0 0 0 1 1 0 0 0 0 0 0 2 1 |
| Norm - 2 | 35F | S | NL | 0 1 0 0 1 1 1 1 3 1 0 0 0 0 0 0 0 1 1 1 1 1 1 1 1 0 1 |
| Norm - 2 | 35F | S | FP | 0 0 0 2 1 -1 2 3 1 0 1 0 0 1 0 0 1 1 1 2 1 1 1 1 1 |
| Norm - 2 | 35F | G | SG | 0 0 0 0 0 2 2 2 1 0 0 0 0 0 0 0 0 0 2 2 1 1 0 1 0 1 0 0 1 |
| Norm - 2 | 35F | G | IP | 0 0 1 1 0 2 1 1 0 1 0 1 1 1 1 1 0 0 0 3 0 0 0 1 2 1 1 |
| Norm - 3 | Neu | S | NL | 0 1 1 2 0 0 0 0 1 2 3 1 0 1 1 0 1 0 0 4 |
| Norm - 3 | Neu | S | FP | 1 1 1 1 1 1 0 1 0 0 0 3 3 0 1 0 0 0 1 1 1 1 2 |
| Norm - 3 | Neu | G | SG | 2 1 0 0 2 -1 0 0 0 0 4 2 2 1 1 0 0 0 0 1 0 1 1 1 |
| Norm - 3 | Neu | G | IP | 1 1 0 1 1 0 0 -1 3 2 2 1 0 0 0 0 0 1 1 1 3 |
| Norm - 3 | 35F | S | NL | 0 1 0 2 1 1 1 1 1 1 0 0 0 0 1 2 2 1 2 0 -1 0 0 0 0 1 1 1 |
| Norm - 3 | 35F | S | FP | 1 3 1 2 0 0 -1 0 1 -1 2 3 1 2 0 0 1 0 1 1 0 0 0 1 |
| Norm - 3 | 35F | G | SG | 1 0 1 -1 0 4 0 1 0 0 0 0 0 1 0 1 3 3 -1 -1 0 2 0 1 1 1 0 3 |
| Norm - 3 | 35F | G | IP | 1 1 1 1 1 0 0 1 0 0 0 1 1 1 -1 0 2 4 1 0 0 0 0 0 1 1 0 1 |
| Norm - 4 | Neu | S | NL | 1 2 2 0 1 0 0 0 1 1 0 1 2 2 2 0 2 0 0 0 0 0 1 3 |
| Norm - 4 | Neu | S | FP | 2 1 2 0 0 0 0 0 0 0 1 1 1 3 2 0 1 0 1 0 0 0 1 0 0 1 2 |
| Norm - 4 | Neu | G | SG | 1 2 1 1 0 1 0 0 1 1 1 2 2 0 1 2 0 1 0 0 1 0 1 1 1 |
| Norm - 4 | Neu | G | IP | 2 0 0 0 0 0 2 1 1 2 2 0 -1 -1 0 2 1 4 |
| Norm - 4 | 35F | S | NL | 1 2 0 0 0 2 2 1 0 0 1 0 1 1 1 2 2 0 0 0 -1 0 0 1 3 |
| Norm - 4 | 35F | S | FP | 0 0 0 0 1 1 1 0 1 1 1 1 0 0 0 0 1 0 0 0 1 1 0 1 1 1 1 1 |
| Norm - 4 | 35F | G | SG | 1 0 1 0 1 1 4 0 0 0 0 1 1 2 0 1 1 1 0 1 1 1 1 1 |
| Norm - 4 | 35F | G | IP | 0 0 2 3 1 -1 0 1 1 0 1 1 1 1 0 0 1 1 1 1 2 |
| Norm - 5 | Neu | S | NL | 1 2 1 0 0 0 1 0 1 2 2 0 0 0 1 2 1 1 0 0 0 1 |
| Norm - 5 | Neu | S | FP | 1 1 1 1 1 1 1 1 1 2 1 1 1 1 1 1 0 1 1 1 1 2 |
| Norm - 5 | Neu | G | SG | 0 3 1 0 0 0 3 1 1 2 0 3 |
| Norm - 5 | Neu | G | IP | 2 1 2 0 0 1 0 1 1 2 2 1 0 0 0 1 1 2 0 1 0 1 |
| Norm - 5 | 35F | S | NL | 0 1 0 0 0 0 3 3 0 0 1 1 0 0 0 0 1 2 2 1 1 0 1 |
| Norm - 5 | 35F | S | FP | 0 0 1 1 3 1 1 1 1 0 1 0 0 2 1 1 2 1 1 1 1 0 0 |
| Norm - 5 | 35F | G | SG | 1 0 0 1 3 0 0 0 1 2 1 2 1 0 0 1 2 2 2 |
| Norm - 5 | 35F | G | IP | 0 0 0 2 4 0 0 0 0 0 1 1 1 2 1 1 0 2 1 1 1 1 0 |

Abbreviations: Wrists were either in 35 degrees of flexion (35F) or 0 degrees of flexion (Neu), and fingers were either straight (S) or gripped (G) loosely. Activities were either none (NL), flat press (FP), squeeze grip (SG), or index-thumb pinch (IP).

Table A-15. Shape number chains at the level of the hook of the hamate for the CTS patient group.

| Patient | Wrist Position | Finger Position | Activity | |
|---|---|---|---|---|
| CTS - 1 | Neu | S | NL | 0 1 2 1 1 0 1 1 3 0 0 0 1 3 1 0 1 0 0 1 |
| CTS - 1 | Neu | S | FP | 1 0 0 7 0 0 0 0 0 -1 0 4 1 2 1 1 1 0 0 0 1 |
| CTS - 1 | Neu | G | SG | 1 0 1 2 1 0 1 1 0 1 2 0 0 1 2 1 1 0 0 0 1 2 |
| CTS - 1 | Neu | G | IP | -1 0 -1 0 1 1 1 2 1 1 0 3 2 -1 0 -1 0 0 2 4 1 2 |
| CTS - 1 | 35F | S | NL | 0 0 0 0 0 4 0 0 -1 3 3 1 0 0 0 0 1 1 1 2 2 1 1 |
| CTS - 1 | 35F | S | FP | 1 0 0 0 0 0 3 0 -1 4 2 0 0 0 0 1 1 2 1 3 |
| CTS - 1 | 35F | G | SG | 0 1 0 0 4 -2 0 1 4 0 0 0 0 0 0 1 1 3 2 1 1 |
| CTS - 1 | 35F | G | IP | 0 0 0 0 0 2 1 0 4 2 1 0 0 0 1 1 1 0 1 1 1 2 1 |
| CTS - 2 | Neu | S | NL | -1 0 1 0 2 3 1 1 0 0 -1 0 1 1 1 2 3 0 1 0 1 1 |
| CTS - 2 | Neu | G | IP | -1 -2 -1 0 -1 3 4 1 0 0 0 1 0 1 1 1 0 0 1 1 2 2 0 0 1 0 3 |
| CTS - 2 | 35F | S | NL | 1 1 1 1 1 1 1 1 0 1 0 1 1 1 1 2 0 0 0 0 1 |
| CTS - 2 | 35F | S | FP | 1 1 1 1 1 0 1 1 1 1 1 2 0 1 0 1 1 2 1 1 1 |
| CTS - 2 | 35F | G | SG | 2 2 1 0 1 1 2 1 1 1 0 0 0 0 2 2 2 2 1 0 -1 0 1 |
| CTS - 2 | 35F | G | IP | 1 1 1 0 1 1 1 1 1 1 0 -1 0 1 3 2 2 0 -1 0 0 1 |
| CTS - 3 | Neu | S | NL | 1 1 1 1 0 0 1 0 1 1 1 1 1 3 2 1 -1 0 0 0 0 0 1 1 4 |
| CTS - 3 | Neu | S | FP | 3 1 0 0 0 0 1 1 2 1 0 0 3 -1 -2 0 0 2 1 0 3 |
| CTS - 3 | Neu | G | SG | 2 2 0 1 0 0 0 1 1 0 0 1 2 2 3 0 -1 0 -1 0 1 0 1 2 |
| CTS - 3 | Neu | G | IP | 2 0 1 -1 0 1 0 4 2 2 0 0 -2 0 1 4 1 0 0 4 |
| CTS - 3 | 35F | S | NL | 2 1 0 0 0 0 0 0 0 0 1 2 4 2 -1 0 0 -1 -1 0 0 3 0 0 0 4 |
| CTS - 4 | Neu | S | NL | 2 1 1 0 0 0 0 1 -1 2 3 1 1 1 1 0 0 -1 0 1 1 1 3 |
| CTS - 4 | Neu | S | FP | 0 -1 1 2 3 2 1 0 0 0 0 0 0 -1 2 2 2 1 2 1 1 -1 0 1 2 |
| CTS - 4 | Neu | G | SG | 1 1 1 2 -2 2 0 0 0 0 0 0 0 1 2 1 2 1 1 0 0 2 -1 1 -1 -1 0 0 2 3 |
| CTS - 4 | Neu | G | IP | 2 0 1 0 1 0 0 0 1 0 0 0 0 1 2 4 1 1 0 0 0 1 0 0 -1 0 0 0 1 1 4 |
| CTS - 4 | 35F | S | NL | 0 0 0 1 4 1 2 0 0 0 0 0 0 0 1 1 1 2 1 0 1 0 0 0 0 |
| CTS - 4 | 35F | S | FP | 0 -1 -1 1 1 2 3 2 0 0 0 0 0 1 1 1 1 2 2 2 |
| CTS - 4 | 35F | G | SG | -1 1 0 -1 0 -1 2 3 1 2 2 1 0 0 0 0 0 1 0 2 2 2 2 |
| CTS - 5 | Neu | S | NL | 2 0 0 0 0 -1 1 2 0 3 2 1 0 2 1 0 0 1 1 2 1 4 |
| CTS - 5 | Neu | S | FP | 0 1 0 0 -1 0 2 1 0 0 1 1 1 1 1 1 1 1 1 0 0 0 0 0 0 0 0 0 0 1 1 3 1 1 |
| CTS - 5 | Neu | G | SG | 2 1 0 0 0 -1 0 1 0 0 2 -1 2 2 1 -1 0 2 1 2 -1 0 1 0 0 0 0 0 1 0 1 1 1 2 |
| CTS - 5 | Neu | G | IP | 0 1 0 -1 0 -1 0 0 1 0 1 2 0 1 2 2 1 0 0 0 0 0 0 0 0 0 0 1 1 2 3 1 0 1 |
| CTS - 5 | 35F | S | NL | 0 1 0 1 2 1 2 1 0 0 0 0 0 0 1 3 1 -1 1 1 1 1 0 1 1 |
| CTS - 5 | 35F | S | FP | 2 1 1 1 1 0 1 1 1 1 -1 0 0 0 3 2 1 1 1 1 1 0 0 0 0 0 1 1 |
| CTS - 5 | 35F | G | SG | -1 2 0 0 -1 1 2 1 1 1 0 0 0 0 1 0 2 2 1 0 1 0 0 0 0 0 0 1 2 0 2 |
| CTS - 6 | Neu | S | NL | 2 0 0 1 0 0 0 0 0 0 0 0 1 1 3 3 1 1 0 -1 0 0 0 0 0 0 1 1 4 |
| CTS - 6 | Neu | S | FP | 1 1 1 0 0 0 0 0 0 0 0 2 2 2 2 1 0 0 0 0 0 1 1 3 2 |
| CTS - 6 | Neu | G | SG | 1 1 0 1 0 0 0 0 0 0 1 2 2 2 1 0 2 0 -1 -1 -1 -1 3 3 1 |
| CTS - 6 | 35F | S | NL | 2 2 1 1 1 1 0 0 -1 0 1 1 1 1 3 1 2 1 0 0 -1 -1 0 0 1 1 |
| CTS - 6 | 35F | S | FP | 0 0 0 0 0 1 4 3 0 0 0 0 0 0 1 1 1 1 1 3 2 1 0 0 |
| CTS - 6 | 35F | G | SG | 0 0 0 -1 0 0 0 0 0 1 2 3 3 0 0 0 0 -1 -1 0 1 1 1 1 1 1 2 2 1 |
| CTS - 6 | 35F | G | IP | 0 0 0 0 1 0 1 3 2 2 0 0 -1 -1 0 1 1 1 1 1 1 1 2 1 2 |
| CTS - 7 | Neu | S | NL | 1 1 1 1 0 0 0 0 0 0 1 0 1 2 1 1 1 1 0 1 1 0 1 -1 1 0 0 0 0 1 2 2 |
| CTS - 7 | Neu | S | FP | 1 1 0 0 0 0 0 0 0 0 1 -1 2 2 0 0 0 4 1 0 -1 0 -1 0 1 1 1 0 1 2 -1 0 0 3 |
| CTS - 7 | Neu | G | SG | 0 1 1 2 0 1 0 1 0 0 0 1 1 0 1 1 2 2 0 0 -1 3 1 0 0 1 0 -2 2 1 2 1 |
| CTS - 7 | Neu | G | IP | 1 1 2 0 0 0 0 0 0 0 1 1 2 0 1 1 2 1 1 0 1 0 0 -1 0 0 0 3 1 2 |
| CTS - 7 | 35F | S | NL | 1 0 1 0 0 0 0 1 0 1 4 0 -1 -1 1 1 0 0 1 1 2 0 -1 0 1 3 1 |
| CTS - 7 | 35F | S | FP | 0 1 1 2 2 0 0 0 1 0 0 0 1 0 0 1 1 1 2 1 1 1 -1 0 -1 -1 1 2 |
| CTS - 7 | 35F | G | SG | 0 0 -1 0 2 2 2 2 1 1 0 -1 0 0 0 0 1 2 1 1 2 1 0 1 0 2 |
| CTS - 7 | 35F | G | IP | 2 1 4 -1 0 0 -1 4 0 0 1 3 2 0 -1 1 2 1 2 0 1 |

Abbreviations: Wrists were either in 35 degrees of flexion (35F) or 0 degrees of flexion (Neu), and fingers were either straight (S) or gripped (G) loosely. Activities were either none (NL), flat press (FP), squeeze grip (SG), or index-thumb pinch (IP).

Table A-16. Shape number chains at the level of the hook of the hamate for the normal subject group.

| Patient | Wrist Position | Finger Position | Activity | |
|---|---|---|---|---|
| Norm - 1 | Neu | S | NL | 0 0 2 1 1 0 2 2 2 1 0 0 0 1 1 2 2 1 1 |
| Norm - 1 | Neu | S | FP | 0 0 0 1 1 2 1 0 1 1 1 0 0 0 1 0 0 1 2 1 2 1 1 1 |
| Norm - 1 | Neu | G | SG | 0 0 0 0 0 1 4 0 -1 -1 4 1 0 1 0 0 1 1 3 2 1 |
| Norm - 1 | Neu | G | IP | 1 0 0 0 1 3 2 0 0 -1 2 2 1 1 0 1 0 1 1 2 2 |
| Norm - 1 | 35F | S | NL | 1 0 0 2 4 0 -1 0 -1 2 2 -1 1 2 3 1 1 1 0 1 1 |
| Norm - 1 | 35F | S | FP | 1 1 1 1 1 2 3 0 0 0 0 1 1 1 1 2 1 1 1 0 1 0 0 |
| Norm - 1 | 35F | G | SG | 0 1 0 0 0 -1 3 2 1 2 2 0 1 1 0 0 0 2 2 3 2 |
| Norm - 1 | 35F | G | IP | 0 0 0 0 0 2 2 -2 3 1 1 1 0 1 1 1 0 1 2 1 2 |
| Norm - 2 | Neu | S | NL | 3 2 0 0 0 0 0 0 1 1 2 2 2 1 1 1 1 0 -1 1 0 1 1 |
| Norm - 2 | Neu | S | FP | 2 2 1 0 0 0 0 0 0 1 1 1 1 1 1 1 1 1 0 0 0 0 0 0 1 1 |
| Norm - 2 | Neu | G | SG | 1 1 2 2 0 1 0 0 0 0 0 1 1 1 1 1 2 1 1 1 0 0 -1 0 -1 1 2 2 |
| Norm - 2 | Neu | G | IP | 1 1 1 1 0 0 0 1 0 0 0 0 0 1 1 1 1 1 1 1 -1 1 2 0 0 -1 0 0 -1 3 1 |
| Norm - 2 | 35F | S | NL | 1 0 0 0 0 1 2 1 0 1 0 1 0 0 1 1 1 2 1 0 0 1 0 1 1 1 |
| Norm - 2 | 35F | S | FP | 1 1 -1 2 2 1 1 0 0 0 0 0 0 1 1 1 1 0 1 0 1 1 0 1 0 -1 1 1 |
| Norm - 2 | 35F | G | SG | 0 0 0 3 2 1 1 0 1 0 1 1 1 1 0 1 1 3 1 -1 1 2 0 1 1 0 1 |
| Norm - 2 | 35F | G | IP | 2 1 0 1 0 1 0 1 1 3 1 0 -1 1 1 2 0 1 0 2 0 1 1 |
| Norm - 3 | Neu | S | NL | 1 1 1 1 0 1 2 -1 0 0 0 1 2 2 2 0 0 1 0 0 0 0 1 2 1 |
| Norm - 3 | Neu | S | FP | 1 1 1 1 0 1 1 1 1 0 -1 4 2 1 0 0 0 0 0 0 1 2 2 |
| Norm - 3 | Neu | G | SG | 2 0 0 0 -1 -1 0 -1 0 2 1 2 1 1 1 0 2 1 1 0 0 0 0 0 0 2 2 3 |
| Norm - 3 | Neu | G | IP | 1 1 0 2 0 0 0 0 -1 0 4 2 1 1 1 0 0 0 0 1 1 3 |
| Norm - 3 | 35F | S | NL | 0 3 2 1 1 0 0 0 1 1 2 1 0 0 -1 0 3 0 1 1 1 0 0 0 0 0 0 2 |
| Norm - 3 | 35F | S | FP | 0 2 1 2 1 1 -1 1 0 1 1 1 -1 0 -1 0 4 1 1 0 1 0 1 0 1 1 |
| Norm - 3 | 35F | G | SG | 2 0 0 2 1 0 0 0 0 0 0 0 0 1 1 3 3 0 0 -1 0 1 1 0 0 1 0 3 |
| Norm - 3 | 35F | G | IP | 0 2 2 2 0 1 0 0 0 0 0 0 0 1 1 0 1 2 2 0 1 0 0 0 0 0 0 1 |
| Norm - 4 | Neu | S | NL | 1 2 2 0 0 0 0 0 0 1 0 0 1 2 0 4 0 0 0 1 1 0 0 0 1 2 |
| Norm - 4 | Neu | S | FP | 1 1 1 1 0 1 0 0 1 0 1 1 1 1 1 1 3 1 1 -1 0 -1 0 0 0 3 1 1 |
| Norm - 4 | Neu | G | SG | 1 1 1 0 0 0 0 1 1 0 1 1 1 2 0 0 3 0 0 -1 1 1 2 1 1 0 0 1 |
| Norm - 4 | Neu | G | IP | 2 1 1 0 1 0 1 2 2 2 1 2 0 0 0 -1 3 1 2 |
| Norm - 4 | 35F | S | NL | 2 -1 0 -1 0 2 2 1 1 1 1 1 1 0 1 3 1 0 -1 0 1 4 |
| Norm - 4 | 35F | S | FP | 0 1 1 0 0 0 -1 1 2 3 1 1 0 0 0 0 0 0 0 1 1 2 2 0 0 1 1 |
| Norm - 4 | 35F | G | SG | 0 0 0 0 0 0 0 1 3 -1 2 2 1 0 1 0 0 0 0 0 0 1 2 2 1 1 0 1 |
| Norm - 4 | 35F | G | IP | 0 0 1 0 0 1 1 1 2 2 1 0 1 0 0 1 1 2 1 1 1 0 |
| Norm - 5 | Neu | S | NL | 2 1 0 1 0 1 2 2 1 1 0 0 0 1 2 1 0 0 0 1 1 1 |
| Norm - 5 | Neu | S | FP | 1 1 1 0 1 1 1 1 1 1 1 1 1 1 1 1 1 1 0 1 1 1 2 |
| Norm - 5 | Neu | G | SG | 1 1 1 0 0 2 4 0 -1 1 2 2 1 2 |
| Norm - 5 | Neu | G | IP | 0 0 0 0 1 1 0 2 2 1 0 0 0 0 0 1 2 1 1 1 1 1 1 1 |
| Norm - 5 | 35F | S | NL | 2 2 1 1 1 1 1 1 0 1 1 1 2 1 1 0 0 0 1 |
| Norm - 5 | 35F | S | FP | 1 2 2 1 1 1 0 0 1 1 0 0 1 0 1 2 1 1 1 1 0 0 0 0 1 |
| Norm - 5 | 35F | G | SG | 0 0 0 0 -1 2 4 1 0 0 1 1 1 1 1 1 0 2 2 2 1 |
| Norm - 5 | 35F | G | IP | 0 0 0 0 1 2 2 -1 0 0 1 2 2 1 1 0 1 1 1 1 1 1 |

Abbreviations: Wrists were either in 35 degrees of flexion (35F) or 0 degrees of flexion (Neu), and fingers were either straight (S) or gripped (G) loosely. Activities were either none (NL), flat press (FP), squeeze grip (SG), or index-thumb pinch (IP).

# REFERENCES

1. Buchberger W. Radiologic imaging of the carpal tunnel. Eur J Radiol 1997 Sep;25(2):112-7.

2. Rotman MB, Donovan JP. Practical anatomy of the carpal tunnel. Hand Clin 2002 May;18(2):219-30.

3. Hochman MG, Zilberfarb JL. Nerves in a pinch: Imaging of nerve compression syndromes. Radiol Clin North Am 2004 Jan;42(1):221-45.

4. Aroori S, Spence RA. Carpal tunnel syndrome. Ulster Med J 2008 Jan;77(1):6-17.

5. D'Arcy C, McGee S. Does this patient have carpal tunnel syndrome? JAMA 2000;283(23):3110.

6. Neal S, Fields KB. Peripheral nerve entrapment and injury in the upper extremity. Am Fam Physician 2010 Jan 15;81(2):147-55.

7. Ashworth NL. Carpal Tunnel Syndrome; 2008. Available from: emedicine.medscape.com.

8. Fuller DA. Carpal Tunnel Syndrome; 2009. Available from: emedicine.medscape.com.

9. Phalen GS. The carpal-tunnel syndrome. seventeen years' experience in diagnosis and treatment of six hundred fifty-four hands. J Bone Joint Surg Am 1966 Mar;48(2):211-28.

10. Jarvik JG, Yuen E, Kliot M. Diagnosis of carpal tunnel syndrome: Electrodiagnostic and MR imaging evaluation. Neuroimaging Clin N Am 2004 Feb;14(1):93,102, viii.

11. Roquelaure Y, Ha C, Nicolas G, Pelier-Cady MC, Mariot C, Descatha A, Leclerc A, Raimbeau G, Goldberg M, Imbernon E. Attributable risk of carpal tunnel syndrome according to industry and occupation in a general population. Arthritis Rheum 2008 Sep 15;59(9):1341-8.

12. Keogh JP, Nuwayhid I, Gordon JL, Gucer PW. The impact of occupational injury on injured worker and family: Outcomes of upper extremity cumulative trauma disorders in maryland workers. Am J Ind Med 2000 Nov;38(5):498-506.

13. Foley M, Silverstein B, Polissar N. The economic burden of carpal tunnel syndrome: Long-term earnings of CTS claimants in washington state. Am J Ind Med 2007 Mar;50(3):155-72.

14. NINDS. Carpal Tunnel Syndrome Fact Sheet; 2009.

15. BLS. Nonfatal occupational injuries and illnesses requiring days away from work for state government and local government workers, 2008. Bureau of Labor Statistics; 2010.

16. Jarvik JG, Yuen E, Haynor DR, Bradley CM, Fulton-Kehoe D, Smith-Weller T, Wu R, Kliot M, Kraft G, Wang L, Erlich V, Heagerty PJ, Franklin GM. MR nerve imaging in a prospective cohort of patients with suspected carpal tunnel syndrome. Neurology 2002 Jun 11;58(11):1597-602.

17. AAOS. Clinical practice guideline on the diagnosis of carpal tunnel syndrome. American Academy of Orthopaedic Surgeons; 2007.

18. Witt JC, Hentz JG, Stevens JC. Carpal tunnel syndrome with normal nerve conduction studies. Muscle Nerve 2004 Apr;29(4):515-22.

19. Cobb TK, Bond JR, Cooney WP, Metcalf BJ. Assessment of the ratio of carpal contents to carpal tunnel volume in patients with carpal tunnel syndrome: A preliminary report. J Hand Surg [Am] 1997 Jul;22(4):635-9.

20. Slutsky DJ. Use of nerve conduction studies and the pressure-specified sensory device in the diagnosis of carpal tunnel syndrome. J Hand Surg Eur Vol 2009 Feb;34(1):60-5.

21. AAOS. Clinical practice guideline on the treatment of carpal tunnel syndrome. Rosemont, IL: American Academy of Orthopaedic Surgeons; 2008.

22. Jarvik JG, Comstock BA, Kliot M, Turner JA, Chan L, Heagerty PJ, Hollingworth W, Kerrigan CL, Deyo RA. Surgery versus non-surgical therapy for carpal tunnel syndrome: A randomised parallel-group trial. Lancet 2009 Sep 26;374(9695):1074-81.

23. Agee JM, McCarroll HR,Jr, Tortosa RD, Berry DA, Szabo RM, Peimer CA. Endoscopic release of the carpal tunnel: A randomized prospective multicenter study. J Hand Surg Am 1992 Nov;17(6):987-95.

24. Chow JC. The chow technique of endoscopic release of the carpal ligament for carpal tunnel syndrome: Four years of clinical results. Arthroscopy 1993;9(3):301-14.

25. Scholten R, Mink van der Molen, A, Uitdehaag B, Bouter L, de Vet H. Surgical treatment options for carpal tunnel syndrome CochraneDatabase of SystematicReviews 2007(4).

26. Adams BD. Endoscopic carpal tunnel release. J Am Acad Orthop Surg 1994 May;2(3):179-84.

27. Brown RA, Gelberman RH, Seiler JG,3rd, Abrahamsson SO, Weiland AJ, Urbaniak JR, Schoenfeld DA, Furcolo D. Carpal tunnel release. A prospective, randomized assessment of open and endoscopic methods. J Bone Joint Surg Am 1993 Sep;75(9):1265-75.

28. Rab M, Grunbeck M, Beck H, Haslik W, Schrogendorfer K, Schiefer H, Mittlbock M, Frey M. Intra-individual comparison between open and 2-portal endoscopic release in clinically matched bilateral carpal syndrome. Journal of Plastic, Reconstructive, & Aesthetic Surgery 2006(59):730-6.

29. Saw NLB, Jones S, Shepstone L, Meyer M, Chapman PG, Logan AM. Early outcome and cost-effectiveness of endoscopic versus open carpal tunnel release: A randomized prospective trial. J Hand Surg [Br ] 2003;28B(5):444-9.

30. Atroshi I, Larsson GU, Ornstein E, Hofer M, Johnsson R, Ranstam J. Outcomes of endoscopic surgery compared with open surgery for carpal tunnel syndrome among employed patients: Randomised controlled trial. BMJ 2006 Jun 24;332(7556):1473.

31. Palmer AK, Toivonen DA. Complications of endoscopic and open carpal tunnel release. J Hand Surg [Am] 1999 May;24(3):561-5.

32. Jimenez DF, Gibbs SR, Clapper AT. Endoscopic treatment of carpal tunnel syndrome: A critical review. J Neurosurg 1998 May;88(5):817-26.

33. Schmelzer R, Della Rocca G, Caplin D. Endoscopic carpal tunnel release: A review of 753 cases in 486 patients. Plastic and Reconstructive Surgery 2006;117(1).

34. Quaglietta P, Corriero G. Endoscopic carpal tunnel release surgery: Retrospective study of 390 consecutive cases. Acta Neurochir Suppl 2005;92:41-5.

35. Sperka P, Cherry N, Burnham R, Beach J. Impact of compensation on work outcome of carpal tunnel syndrome. Occup Med (Lond) 2008 Oct;58(7):490-5.

36. Horch RE, Allmann KH, Laubenberger J, Langer M, Stark GB. Median nerve compression can be detected by magnetic resonance imaging of the carpal tunnel. Neurosurgery 1997 Jul;41(1):76,82; discussion 82-3.

37. Gelberman RH, Hergenroeder PT, Hargens AR, Lundborg GN, Akeson WH. The carpal tunnel syndrome. A study of carpal canal pressures. J Bone Joint Surg Am 1981 Mar;63(3):380-3.

38. Skie M, Zeiss J, Ebraheim NA, Jackson WT. Carpal tunnel changes and median nerve compression during wrist flexion and extension seen by magnetic resonance imaging. J Hand Surg [Am] 1990 Nov;15(6):934-9.

39. Ko C, Brown TD. A fluid-immersed multi-body contact finite element formulation for median nerve stress in the carpal tunnel. Comput Methods Biomech Biomed Engin 2007 Oct;10(5):343-9.

40. Oneson SR, Scales LM, Erickson SJ, Timins ME. MR imaging of the painful wrist. Radiographics 1996 Sep;16(5):997-1008.

41. Girgis WS, Epstein RE. Magnetic resonance imaging of the hand and wrist. Semin Roentgenol 2000 Jul;35(3):286-96.

42. Yu JS, Habib PA. Normal MR imaging anatomy of the wrist and hand. Radiol Clin North Am 2006 Jul;44(4):569,81, viii.

43. Weiss KL, Beltran J, Shamam OM, Stilla RF, Levey M. High-field MR surface-coil imaging of the hand and wrist. part I. normal anatomy. Radiology 1986 Jul;160(1):143-6.

44. Helms CA, Major NM, Anderson MW, Kaplan PA, Dussault R. Musculoskeletal MRI. Philadelphia, PA: Elsevier; 2009. .

45. Pierre-Jerome C, Smitson RD,Jr, Shah RK, Moncayo V, Abdelnoor M, Terk MR. MRI of the median nerve and median artery in the carpal tunnel: Prevalence of their anatomical variations and clinical significance. Surg Radiol Anat 2009 Dec 22.

46. Beris AE, Lykissas MG, Kontogeorgakos VA, Vekris MD, Korompilias AV. Anatomic variations of the median nerve in carpal tunnel release. Clin Anat 2008 Jun 19;21(6):514-8.

47. GE Healthcare. Clinical Images; 2009. Available from: http://www.gehealthcare.com/usen/mr/open_speed/products/cimages.html.

48. Erickson SJ, Cox IH, Hyde JS, Carrera GF, Strandt JA, Estkowski LD. Effect of tendon orientation on MR imaging signal intensity: A manifestation of the "magic angle" phenomenon. Radiology 1991 Nov;181(2):389-92.

49. Timins ME, O'Connell SE, Erickson SJ, Oneson SR. MR imaging of the wrist: Normal findings that may simulate disease. Radiographics 1996 Sep;16(5):987-95.

50. Chappell KE, Robson MD, Stonebridge-Foster A, Glover A, Allsop JM, Williams AD, Herlihy AH, Moss J, Gishen P, Bydder GM. Magic angle effects in MR neurography. AJNR Am J Neuroradiol 2004 Mar;25(3):431-40.

51. Steinbach LS, Smith DK. MRI of the wrist. Clin Imaging 2000 Sep-Oct;24(5):298-322.

52. Kleindienst A, Hamm B, Lanksch WR. Carpal tunnel syndrome: Staging of median nerve compression by MR imaging. J Magn Reson Imaging 1998 Sep-Oct;8(5):1119-25.

53. Hof JJ, Kliot M, Slimp J, Haynor DR. What's new in MRI of peripheral nerve entrapment? Neurosurg Clin N Am 2008 Oct;19(4):583,95, vi.

54. Zeiss J, Skie M, Ebraheim N, Jackson WT. Anatomic relations between the median nerve and flexor tendons in the carpal tunnel: MR evaluation in normal volunteers. AJR Am J Roentgenol 1989 Sep;153(3):533-6.

55. Howe FA, Saunders DE, Filler AG, McLean MA, Heron C, Brown MM, Griffiths JR. Magnetic resonance neurography of the median nerve. Br J Radiol 1994 Dec;67(804):1169-72.

56. Middleton WD, Kneeland JB, Kellman GM, Cates JD, Sanger JR, Jesmanowicz A, Froncisz W, Hyde JS. MR imaging of the carpal tunnel: Normal anatomy and preliminary findings in the carpal tunnel syndrome. AJR Am J Roentgenol 1987 Feb;148(2):307-16.

57. Mesgarzadeh M, Schneck CD, Bonakdarpour A. Carpal tunnel: MR imaging. part I. normal anatomy. Radiology 1989 Jun;171(3):743-8.

58. Allmann KH, Horch R, Uhl M, Gufler H, Altehoefer C, Stark GB, Langer M. MR imaging of the carpal tunnel. Eur J Radiol 1997 Sep;25(2):141-5.

59. Monagle K, Dai G, Chu A, Burnham RS, Snyder RE. Quantitative MR imaging of carpal tunnel syndrome. AJR Am J Roentgenol 1999 Jun;172(6):1581-6.

60. Yao L, Gai N. Median nerve cross-sectional area and MRI diffusion characteristics: Normative values at the carpal tunnel. Skeletal Radiol 2009 Apr;38(4):355-61.

61. Uchiyama S, Itsubo T, Yasutomi T, Nakagawa H, Kamimura M, Kato H. Quantitative MRI of the wrist and nerve conduction studies in patients with idiopathic carpal tunnel syndrome. J Neurol Neurosurg Psychiatry 2005 Aug;76(8):1103-8.

62. Mesgarzadeh M, Schneck CD, Bonakdarpour A, Mitra A, Conaway D. Carpal tunnel: MR imaging. part II. carpal tunnel syndrome. Radiology 1989 Jun;171(3):749-54.

63. Deryani E, Aki S, Muslumanoglu L, Rozanes I. MR imaging and electrophysiological evaluation in carpal tunnel syndrome. Yonsei Med J 2003 Feb;44(1):27-32.

64. Keir PJ, Bach JM, Rempel DM. Effects of finger posture on carpal tunnel pressure during wrist motion. J Hand Surg Am 1998 Nov;23(6):1004-9.

65. Mogk JP, Keir PJ. The effect of landmarks and bone motion on posture-related changes in carpal tunnel volume. Clin Biomech (Bristol, Avon) 2009 Nov;24(9):708-15.

66. Keberle M, Jenett M, Kenn W, Reiners K, Peter M, Haerten R, Hahn D. Technical advances in ultrasound and MR imaging of carpal tunnel syndrome. Eur Radiol 2000;10(7):1043-50.

67. Mogk JP, Keir PJ. Evaluation of the carpal tunnel based on 3-D reconstruction from MRI. J Biomech 2007;40(10):2222-9.

68. Keir PJ. Magnetic resonance imaging as a research tool for biomechanical studies of the wrist. Semin Musculoskelet Radiol 2001 Sep;5(3):241-50.

69. Widgerow AD, Sacks L, Greenberg D, Becker PJ. Intergroup comparisons of carpal tunnel dimensions. J Hand Surg [Am] 1996 May;21(3):357-9.

70. Bower JA, Stanisz GJ, Keir PJ. An MRI evaluation of carpal tunnel dimensions in healthy wrists: Implications for carpal tunnel syndrome. Clin Biomech (Bristol, Avon) 2006 Oct;21(8):816-25.

71. Yoshioka S, Okuda Y, Tamai K, Hirasawa Y, Koda Y. Changes in carpal tunnel shape during wrist joint motion. MRI evaluation of normal volunteers. J Hand Surg Br 1993 Oct;18(5):620-3.

72. Mogk JP, Keir PJ. Wrist and carpal tunnel size and shape measurements: Effects of posture. Clin Biomech (Bristol, Avon) 2008 Nov;23(9):1112-20.

73. Keir PJ, Wells RP. Changes in geometry of the finger flexor tendons in the carpal tunnel with wrist posture and tendon load: An MRI study on normal wrists. Clin Biomech (Bristol, Avon) 1999 Nov;14(9):635-45.

74. Padua L, LoMonaco M, Gregori B, Valente EM, Padua R, Tonali P. Neurophysiological classification and sensitivity in 500 carpal tunnel syndrome hands. Acta Neurol Scand 1997 Oct;96(4):211-7.

75. Chan TF, Vese LA. Active contours without edges. IEEE Trans Image Process 2001;10(2):266-77.

76. Klain DA. An intuitive derivation of heron's formula. The Mathematical Association of America; 2004.

77. Bribiesca B. Arithmetic operations among shapes using shape numbers. Pattern Recognition 1981;12(2):123.

78. Goetz JE, Thedens DR, Kunze NM, Lawler EA, Brown TD. Day-to-day variability of median nerve location within the carpal tunnel. Clinical Biomechanics 2010;Accepted.

79. Kunze NM, Goetz JE, Thedens DR, Baer TE, Lawler EA, Brown TD. Individual flexor tendon identification within the carpal tunnel: A semi-automated analysis method for serial cross-section magnetic resonance images. Orthopedic Research and Reviews 2009;1:1.